Measuring and modeling of axon membrane properties in motor neuron disorders and normal subjects

Maria Kovalchuk

Measuring and modeling of axon membrane properties in motor neuron disorders and normal subjects

Maria Kovalchuk

Measuring and modeling of axon membrane properties in motor neuron disorders and normal subjects

Meten en modelleren van axonmembraaneigenschappen bij motor neuron aandoeningen en gezonden

(met een samenvatting in het Nederlands)

Proefschrift

ter verkrijging van de graad van doctor aan de Universiteit Utrecht op gezag van de rector magnificus, prof.dr. H.R.B.M Kummeling, ingevolge het besluit van het college voor promoties in het openbaar te verdedigen op donderdag 19 december 2019 des avonds te 6.00 uur

door

Maria Kovalchuk

geboren op 5 oktober 1984
te Moskou, Rusland

Promotor:	Prof. dr. L.H. van den Berg
Copromotoren:	Dr. H. Franssen
	Dr. ir. B.T.H.M. Sleutjes

The last process of reason is to recognize
that there is an infinity of things which transcend it.

Blaise Pascal

CONTENTS

1

Introduction and aims of this thesis

Motor neuron disorders (MNDs) form a heterogenous group of diseases, characterized by upper and/or lower motor neuron involvement with secondary Wallerian degeneration of motor axons.[1] Depending on the level of motor neuron loss, MNDs present with specific types of muscle weakness. Amyotrophic lateral sclerosis (ALS) is the most common motor neuron disease, where both – upper and lower motor neurons, are affected.[2] Special care should be taken to differentiate MNDs from similar clinical characteristics of potentially treatable disorders, especially when suspecting ALS, dramatically influencing life expectancy.[3] Genetical background plays an important role in the pathogenesis of MNDs, being multifactorial and largely unclear.[4,5] MNDs share pathogenic pathways and probably overlap with other neurodegenerative diseases[6,7,8] and even immune-mediated disorders of the peripheral nervous system, such as multifocal motor neuropathy.[9] In multifocal motor neuropathy (MMN) immune-mediated inflammation selectively affects motor fibers, which is clinically presented with slowly progressive, asymmetric distal limb weakness without sensory deficit.[10,11] Electrophysiological hallmark of MMN is the presence of conduction block – failure of proper action potential generation and propagation.[12,13] Conduction block was suggested to be caused by focal demyelination, altered resting membrane-potential, or dysfunction of Na+ channels at the node of Ranvier, but the exact mechanism is unclear.[14] MMN does not affect life expectancy and up to 90% of patients improve in muscle strength after immunoglobulin (Ig) therapy.[15,16] Because of the presence of antibodies against GM1 gangliosides and positive response to Ig MMN is classified as the dysimmune disorder, overlapping with acute motor axonal neuropathy, a form of Guillain-Barré syndrome, although the primary target in MMN is debated.[17,18] In animal models this was shown that anti-GM1 antibodies lead to complement associated disruption of the node of Ranvier complex.[19]

Multiple approaches have been used to broaden the knowledge on the pathogenesis of MNDs and MMN: neurophysiological, immunological, pathological, neuroimaging, experimental model.[20-29] Each of those has limitations, requiring a combination of methods and new techniques to be implemented to explore distinct levels of damaged structures. Threshold tracking technique is a non-invasive, neurophysiological testing, assessing axonal excitability at the site of stimulation.[30,31] This technique provides information on resting membrane potential, sodium-potassium pump and ion currents sustained by voltage-gated ion channels, specifically distributed in the myelinated axon: transient and persistent Na+ channels, fast and slow K+ channels and hyperpolarization-activated cyclic nucleotide-gated channels **(Figure 1)**.[32]

Figure 1. Diagram of a myelinated axon
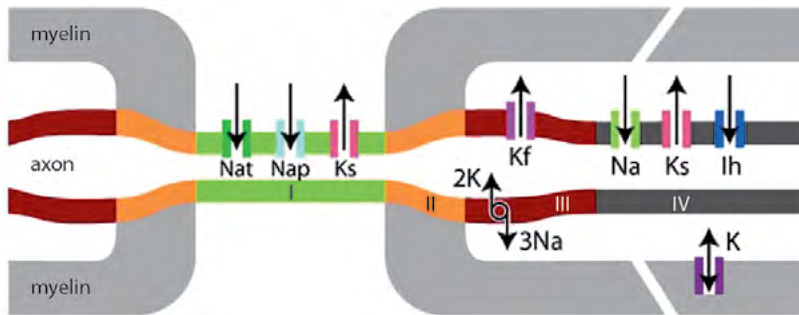
Figure 1 legend. Nat, transient Na+ current; Nap, persistent Na+ current; Ks, slow K+ current; Kf, fast K+ current; Ih, hyperpolarization-activated cation current; the Na+/K+ sodium-potassium pump; I, node of Ranvier; II, paranode; III, juxtaparanode; IV, standard internode.

Excitability properties of the peripheral nerve have previously shown abnormalities both in MMN and ALS.[33-37]

In ALS few excitability abnormalities were demonstrated: (i) sodium-potassium pump hyperactivity, associated with greater fatigue; (ii) changes in persistent sodium conductance and potassium conductance, potentially contributing to axonal hyperexcitability and fasciculation, related to the functional decline and shorter survival.[38-39]

Difference in ion channel presentation of motor and sensory axons could be of relevance in selective motor involvement in MMN and phenomenon of cold paresis, characterized by the aggravation of symptoms in cold and specifically attributed to MMN.[40-43]

The node of Ranvier of motor axons expresses a high density of Na+ channels, which are essential for action potential generation and propagation. Damage to these channels by anti-GM1 antibodies would contribute to conduction block and axonal degeneration in MMN.

Considering that specific ion channels contribute to the pathogenesis of the damaged axons in MMN and ALS, the work described in this thesis aims:

(i) To highlight the phenomenon of conduction block in MMN from the perspective of physiological differences between motor and sensory excitability and by means of computer simulations **(chapters 2 and 3)**.

(ii) To explain pure motor involvement, assess sensory excitability of affected nerves and specify the biophysical abnormalities of motor axons in MMN **(chapter 4)**.

(iii) To determine the involvement of different types of motor axons in MMN **(chapter 5)**.

(iv) To validate excitability testing as a biomarker of hyperexcitability in ALS **(chapter 6)**.

(v) To assess effects of the medication on membrane properties in ALS and MMN **(chapters 6 and 7)**.

(vi) To implement more sophisticated techniques (a) for the assessment of sodium-potassium pump **(chapter 8)**, (b) to reliably investigate ion channel function in single motor units **(chapter 9)** and (c) to specify the temperature requirements for a proper excitability testing **(chapter 10)**.

1

REFERENCES

1. Desai NP, Olney RK, 2009. Neuromuscular diseases. In: Corey-Bloom, J., David, R.B. (Eds.), Clinical Adult Neurology. 3rd ed. Demos Medical Publishing, New York, pp. 307–333.

2. van Es MA, Hardiman O, Chio A, et al. Amyotrophic lateral sclerosis. Lancet 2017;390:2084-2098.

3. Brown RH, Al-Chalabi A. Amyotrophic Lateral Sclerosis. N Engl J Med 2017;377:162-172.

4. van Rheenen W, Shatunov A, Dekker AM, et al. Genome-wide association analyses identify new risk variants and the genetic architecture of amyotrophic lateral sclerosis. Nat Genet. 2016 Sep;48(9):1043-8.

5. Millecamps S, Boillee S, Le Ber I, et al. Phenotype difference between ALS patients with expanded repeats in C9ORF72 and patients with mutations in other ALS related genes. J. Med. Genet. 2012. 49, 258–263.

6. Van Damme P, Veldink JH, van Blitterswijk M, et al. Expanded ATXN2 CAG repeat size in ALS identifies genetic overlap between ALS and SCA2. Neurology. 2011 Jun 14;76(24):2066-72.

7. Burrell JR, Halliday GM, Kril JJ, et al. The frontotemporal dementia-motor neuron disease continuum. Lancet. 2016; 388: 919-931.

8. McLaughlin RL, Schijven D, van Rheenen W, et al. Genetic correlation between amyotrophic lateral sclerosis and schizophrenia. Nat Commun. 2017 Mar 21;8:14774.

9. Vlam L, Piepers S, Sutedja NA, et al. Association of IgM monoclonal gammopathy with progressive muscular atrophy and multifocal motor neuropathy: a case-control study. J Neurol. 2015 Mar;262(3):666-73.

10. Nobile-Orazio E, Cappellari A, Priori A. Multifocal motor neuropathy: current concepts and controversies. Muscle Nerve 2005;31:663– 80.

11. Vlam L, Van der Pol L, Cats EA, et al. Multifocal motor neuropathy: diagnosis, pathogenesis and treatment strategies. Nat Rev Neurol. 2012; 8:48-58.

12. Kaji R. Physiology of conduction block in Multifocal motor neuropathy and other demyelinating neuropathies. Muscle Nerve 27: 285–296, 2003.

13. Van Asseldonk JT, Van Asseldonk JT, Van den Berg, et al. Axon loss is an important determinant of weakness in MMN. J Neurol Neurosurg Psychiatry 2006;77:743-747.

14. Priori A, Bossi B, Ardolino G, et al. Pathophysiological heterogeneity of conduction blocks in multifocal motor neuropathy. Brain. 2005 Jul;128(Pt 7):1642-8.

15. Federico P, Zochodne DW, Hahn AF, et al. Multifocal motor neuropathy improved by IVIg: randomized, double-blind, placebo-controlled study. Neurology. 2000 Nov 14;55(9):1256-62.

16. Léger JM, Viala K, Cancalon F, et al. Intravenous immunoglobulin as short- and long-term therapy of multifocal motor neuropathy: a retrospective study of response to IVIg and of its predictive criteria in 40 patients. J. Neurol. Neurosurg. Psychiatry 79, 93–96 (2008).

17. Léger JM, Chassande B, Musset L, et al. Intravenous immunoglobulin therapy in multifocal motor neuropathy: a double-blind, placebo-controlled study. Brain. 2001;124:145–153.

18. Yuki N. Acute motor axonal neuropathy and multifocal motor neuropathy: more in common than not. Muscle Nerve. 2013 Nov;48(5):693-5.

19. Susuki K, Yuki N, Schafer DP, et al. Dysfunction of nodes of Ranvier: a mechanism for anti-ganglioside antibody-mediated neuropathies. Exp Neurol 2012; 233:534-542.

20. Vucic S, Ziemann U, Eisen A, et al. Transcranial magnetic stimulation and amyotrophic lateral sclerosis: pathophysiological insights. J Neurol Neurosurg Psychiatr. 2013; 84: 1161-1170.

21. Shefner JM, Watson ML, Simionescu L et al. Multipoint incremental motor unit number estimation as an outcome measure in ALS. Neurology. 2011; 77: 235-241.

22. Kiernan MC, Guglielmi JM, Kaji R, et al. Evidence for axonal membrane hyperpolarization in multifocal motor neuropathy with conduction block. Brain 2002;125:664-675.

23. Harschnitz O, van den Berg LH, Johansen LE, et al. Autoantibody pathogenicity in a multifocal motor neuropathy induced pluripotent stem cell-derived model. Ann Neurol. 2016 Jul;80(1):71-88.

24. Bowser R, Turner MR, Shefner J. Biomarkers in amyotrophic lateral sclerosis: opportunities and limitations. Nat Rev Neurol. 2011; 7: 631-638.

25. Corbo M, Abouzahr MK, Latov N, et al. Motor nerve biopsy studies in motor neuropathy and motor neuron disease. Muscle Nerve. 1997 Jan;20(1):15-21.

26. Verstraete E, Veldink JH, Hendrikse J, et al. Structural MRI reveals cortical thinning in amyotrophic lateral sclerosis. J Neurol Neurosurg Psychiatr. 2012; 83: 383-388.

27. Grimm A, Décard BF, Athanasopoulou I, et al. Nerve ultrasound for differentiation between amyotrophic lateral sclerosis and multifocal motor neuropathy. J Neurol 2015; 262:870-880.

28. Sances S, Bruijn LI, Chandran S et al. Modeling ALS with motor neurons derived from human induced pluripotent stem cells. Nat Neurosci. 2016; 16: 542-553.

29. Babin PJ, Goizet C, Raldúa D. Zebrafish models of human motor neuron diseases: advantages and limitations. Prog Neurobiol. 2014; 118: 36-58.

30. Kiernan MC, Burke D, Andersen KV, Bostock H. Multiple measures of axonal excitability: a new approach in clinical testing. Muscle Nerve 2000;23:399–409.

1

31. Burke D, Kiernan MC, Bostock H. Excitability of human axons. Clin Neurophysiol. 2001 Sep;112(9):1575-85.

32. Franssen H, Straver DC. Pathophysiology of immune-mediated demyelinating neuropathies-part I: neuroscience. Muscle Nerve. 2013 Dec;48(6):851-64.

33. Kiernan MC, Guglielmi JM, Kaji R, et al. Evidence for axonal membrane hyperpolarization in multifocal motor neuropathy with conduction block. Brain. 2002 Mar;125(Pt 3):664-75.

34. Kuwabara S, Misawa S. Axonal ionic pathophysiology in human peripheral neuropathy and motor neuron disease. Curr Neurovasc Res. 2004 Oct;1(4):373-9.

35. Vucic S, Krishnan AV, Kiernan MC. Fatigue and activity dependent changes in axonal excitability in amyotrophic lateral sclerosis. J Neurol Neurosurg Psychiatry 2007;78:1202-8.

36. Geevasinga N, Menon P, Howells J, et al. Axonal ion channel dysfunction in c9orf72 familial amyotrophic lateral sclerosis. JAMA Neurol 72, 49-57 2015.

37. Park SB, Kiernan MC, Vucic S. Axonal Excitability in Amyotrophic Lateral Sclerosis: Axonal Excitability in ALS. Neurotherapeutics. 2017 Jan;14(1):78-90.

38. Kanai K., Shibuya K, Sato Y, et al. Motor axonal excitability properties are strong predictors for survival in amyotrophic lateral sclerosis. J Neurol Neurosurg Psychiatry. 2012 Jul;83(7):734-8.

39. Shibuya K., Misawa S, Kimura H., et al. Increased motor axonal persistent sodium currents predict rapid functional declines in amyotrophic lateral sclerosis. Neurol Clin Neurosci 4(2016), 108-11.

40. Neumcke B. Differences in electrophysiological properties of motor and sensory nerve fibers. J Physiol, Paris, 1981; 77:1135-1138.

41. Burke D, Kiernan M, Mogyoros I, Bostock H. Susceptibility to conduction block: differences in the biophysical properties of cutaneous afferents and motor axons. In: Kimura J, Kaji R, editors. Physiology of ALS and related disorders. Amsterdam: Elsevier Science BV; 1997. p 43-53.

42. Kiernan MC, Lin CS, Burke D. Differences in activity-dependent hyperpolarization in human sensory and motor axons. J Physiol. 2004 Jul 1;558(Pt 1):341-9.

43. Straver DC, van Asseldonk JT, Notermans NC, et al. Cold paresis in multifocal motor neuropathy. J Neurol 2011 Feb;258(2):212-7.

2.

Comparing excitability at 37°C with 20°C: differences between motor and sensory axons

MARIA O. KOVALCHUK
HESSEL FRANSSEN
LEONARD VAN SCHELVEN
BOUDEWIJN T.H.M. SLEUTJES

ABSTRACT

Introduction. In some peripheral nervous system disorders cold induces symptoms of muscle weakness without loss of sensation. To understand this selective effect on motor function, it is first necessary to delineate the effects of cooling in motor and sensory axons of healthy subjects.

Methods. In 17 healthy volunteers, we performed excitability and clinical tests of median nerve motor and sensory axons at 37°C and 20°C. Clinical tests consisted of assessing thenar muscle strength, 2-point discrimination and joint position sense of the 3rd finger.

Results. Excitability tests showed that cooling induced opposite changes to hyperpolarizing current in threshold electrotonus (motor: decreased threshold change, sensory: increased threshold change) and I/V-slopes (motor: steepening, sensory: less steep). Clinical tests showed worsening in motor function but no consistent changes in sensory function.

Discussion. Cooling induces changes in motor axons consistent with depolarization and more complicated changes in sensory axons, possibly related to differences in HCN-channel expression.

2

INTRODUCTION

In some peripheral nervous system disorders, including multifocal motor neuropathy (MMN) and Hirayama's disease, cold may induce symptoms of muscle weakness without loss of sensation. Known as cold paresis, this was shown to occur significantly more often in MMN than in other polyneuropathies and lower motor neuron disease[1,2]. The mechanisms of cold paresis and the selective motor involvement in MMN may be related to different antigenic properties of GM1-gangliosides in motor and sensory nerve fibers[3]. These differences were only found for the intramembranous ceramide portion of GM1, however, and not the antigenic sugar portion. Therefore, selective immunological targeting of motor nerve fibers by anti-GM1 antibodies is only possible if it is assumed that the difference in ceramide portion affects the 3D-configuration of the sugar portion[4].

The present study investigated whether differences in ion channel properties between motor and sensory axons might underlie the symptom of cold paresis, because motor axons were shown to have less persistent Na-currents and less hyperpolarization-activated current currents[5,6]. We performed excitability tests of median nerve motor and sensory axons to assess changes in ion channel activity after cooling the nerve from 37°C to 20°C.

METHODS

Subjects

We investigated 17 healthy subjects with a mean age of 32 years (range 22 to 54 years); 7 subjects were men. The subjects had no neurological symptoms and did not take medication. All subjects gave signed informed consent and the investigation was done in accordance to the Declaration of Helsinki and was approved by the local medical ethical committee.

Protocol

We assessed excitability of median nerve motor and sensory axons at the wrist and clinical motor and sensory functions of median nerve fibers to the hand. On the first day the nerve was warmed to 37°C according to the following protocol: warming for 30 minutes, excitability test of motor axons, excitability test of sensory axons, clinical assessment of median nerve motor and sensory functions. On another day the nerve was cooled to 20°C, the protocol consisting of cooling for 45 minutes, excitability test of motor axons, cooling for 15 minutes, excitability test of sensory axons, clinical assessment of median

nerve motor and sensory functions. All healthy controls underwent motor and sensory nerve conduction studies to exclude carpal tunnel syndrome.

Temperature

For excitability testing at 37°C the median nerve was first warmed by wrapping the forearm and hand for 30 minutes in a blanket through which water at 37°C flowed constantly (Cincinatti Sub-zero Norm-O-Temp with Cincinatti Sub-zero maxi-therm lite infant hyper-hypothermia blanket for single patient use)[7]. During excitability testing at 37°C the forearm and hand were kept in the blanket. For excitability testing at 20°C the forearm and hand were first cooled in a bath in which the water temperature of 20°C was kept constant by means of a thermostat valve regulated by a temperature sensor in the bath. During excitability-testing at 20°C, the arm and hand were wrapped in cold packs at 20°C. These warming and cooling protocols were based on previous studies showing that these times were necessary to attain nerve temperatures of 37°C or 20°C[7,8,9]. Skin temperature during excitability testing was continuously monitored by means of a temperature sensor near the stimulating electrode. Since changes in distal motor latency (DML) were shown to more accurately reflect changes in nerve temperature than skin temperature, we also monitored DML every 1.6 seconds during each excitability test. DML was defined as the point where the CMAP deviated from the baseline by 10% of its baseline-to-peak amplitude. The change in DML during testing was obtained by subtracting the means of first three values from the last three.

Excitability tests

Excitability was measured in median nerve motor and sensory axons at the wrist using Viking IV EMG apparatus (Nicolet Biomedical, Inc., Madison, Wisconsin), coupled to a computer (PCI-6221, National instruments) running QTRAC-S software (TROND-NF, version 19-06-2015, Institute of Neurology, Queen Square, London, UK) and an isolated bipolar constant current stimulator (DS5, Digitimer, UK model D185-HB4). The nerve was stimulated at the wrist via non-polarizable surface electrodes (cathode at the wrist; anode 10cm proximal over the radial side of the forearm). For motor excitability, the thenar CMAP was recorded by surface electrodes in belly-tendon montage. For sensory excitability the 3rd digit sensory nerve action potential (SNAP) was recorded by ring electrodes around the proximal and distal interphalangeal joints. Conditioning stimuli were constant currents that either slightly depolarized resting membrane potential, slightly hyperpolarized resting membrane potential, or induced nerve action potentials. Except for assessment of charge-duration properties where 5 different test stimuli were given, threshold changes induced by conditioning stimuli were assessed by test stimuli of 1.0ms duration, both for motor and sensory excitabil-

ity tests. Since most studies used 0.5ms test stimulus duration in sensory excitability testing[10], we also compared sensory excitability indices obtained with 0.5ms and 1.0ms test stimulus duration in a subgroup of 12 subjects. Threshold estimation was done by proportional threshold tracking. Threshold was defined as the test stimulus current needed to produce a target compound muscle action potential (CMAP) or target SNAP of 40% of its maximal amplitude.

Each excitability test measured the following: stimulus response (SR) curve (relation between stimulus current and response amplitude), charge duration (Qt) relation (relation between stimulus charge and default stimulus duration), threshold electrotonus (time course of threshold changes during a slightly depolarizing or hyperpolarizing conditioning current of 100ms duration of 20% or 40% of the current for an unconditioned target response), I/V relation (relation between threshold changes after a 200ms duration conditioning current varying from +50% depolarizing to -100% hyperpolarizing), recovery cycle (threshold changes estimated at various intervals between 2 and 200ms after a supramaximal conditioning stimulus eliciting action potentials).

The following standard parameters were obtained from the TROND NF software: slope of the normalized SR curve, threshold for an unconditioned target response, rheobase (slope of the Qt relation), strength-duration time constant (SDTC; absolute value of the x-intercept of the Qt relation), TEd90-100 (threshold decrease at the end of the 40% depolarizing conditioning stimulus), TEdpeak (maximal threshold decrease during 40% depolarizing conditioning stimulus), S2-accommodation (difference between TEdpeak and TEd90-100), accommodation half-time (time between the onset of the conditioning stimulus and the time point where threshold decrease is halfway between TEdpeak andTEd90-100), TEh90-100 (threshold increase at the end of the 40% hyperpolarizing conditioning stimulus), resting and minimal I/V slope (slope between -10% and +10% conditioning stimuli and smallest slope in the hyperpolarizing part), refractory period (time between conditioning stimulus and return of threshold to baseline), superexcitability (lowest threshold after refractory period), and subexcitability (highest threshold after superexcitability).

As non-standard parameters we also derived fanning (sum of the absolute values of TEd90-100 and TEh90-100) and 30% refractory period (time between conditioning stimulus and return of threshold to 30% above its unconditioned value). For threshold electrotonus, fanning-in was defined as the occurrence of decreased threshold changes during depolarizing as well as hyperpolarizing conditioning currents; fanning-out was defined as the occurrence of increased threshold changes during depolarizing as well as hyperpolarizing conditioning currents.

Clinical tests

Median nerve motor and sensory functions were tested clinically by (i) MRC grading of abductor pollicis brevis muscle strength, (ii) joint position sense of the distal phalangeal joint of the middle finger for 10 random movements, (iii) 2-point discrimination of the distal phalanx of the middle finger by a specially devised caliper (Downs, A-070-01-G); this assesses the minimal distance at which the subject discriminates 2 points, starting from 5mm.

Analysis

As excitability indices were found to be normally distributed, they were compared by the independent t-test. SPSS (version 22; IBM) was used for all analyses. P< 0.05 was considered statistically significant.

RESULTS

Nerve temperature remained constant during each individual excitability test as determined by the minimal changes in DML (Table 1). Skin temperature changed little. Contrary to excitability recording at 37°C, not all excitability indices could be measured at 20°C. In 12 motor and 7 sensory recovery cycles, refractoriness at 20°C had increased such that threshold did not return to baseline so that refractory period, superexcitability and subexcitability could not be measured. In these recovery cycles, fluctuations of threshold above baseline were observed, possibly reflecting depolarizing and hyperpolarizing afterpotentials. Refractoriness at 20°C could, however, be judged by assessing 30% refractory period which was measurable in all, except two, motor nerves. In 3 subjects sensory threshold electrotonus at 20°C showed a sudden decrease in the first 10-20ms after onset of the 40% depolarizing conditioning stimulus threshold, reflecting the induction of nerve action potential by the depolarizing conditioning stimulus; this precluded measurement of TEdpeak, S2-accommodation, accommodation half-time and fanning. Comparison of two test stimulus durations in sensory excitability testing showed the induction of nerve action potential during depolarizing threshold electrotonus in all subjects when test stimulus duration was 0.5ms and in only 3 subjects when test stimulus duration was 1.0ms (Figure 1). A test stimulus duration of 1ms did not induce any tracking problems.

Excitability at 37°C

At 37°C there were significant differences in mean values of excitability-indices between motor and sensory axons (Table 1). In motor axons SDTC was smaller, rheobase greater, TEh90-100 more prominent, fanning more pronounced, S2-accommodation and TEdpeak greater, resting and minimal I/V-slopes less steep, refractory period smaller and superexcitability larger.

2

Table 1. Excitability changes due to cooling in motor and sensory axons.

Variable	Motor		P-value	Sensory		P-value	P-value mot-sens 37°C	P-value mot-sens 20°C
	37°C	20°C		37°C	20°C			
DML decrease (ms)	-0.04	0.14		-0.45	-0.98			
Mean DML (ms)	4.22	8.39		3.31	6.13			
Strength-duration								
SDTC (ms)	0.41 (0.01)	0.51 (0.01)	<0.001	0.59 (0.03)	0.69 (0.03)	0.022	<0.001	<0.001
Rheobase (mA)	2.8 (0.1)	3.2 (0.2)	ns	1.4 (0.1)	1.7 (0.1)	ns	<0.001	<0.001
Threshold electrotonus								
TEdpeak (%)*	65.6 (0.9)	53.4 (1.5)	<0.001	57.6 (1.1)	57.9 (1.9)	ns	<0.001	ns
S2-accommodation (%)*	21.7 (0.8)	9.0 (0.4)	<0.001	16.2 (0.7)	8.2 (0.5)	<0.001	<0.001	ns
Accommodation half-time (ms)*	36.9 (0.9)	52.0 (2.2)	<0.001	35.9 (0.8)	60.6 (2.6)	<0.001	ns	0.019
TEd90-100 (%)*	43.9 (0.8)	44.4 (1.5)	ns	41.4 (1.0)	49.7 (1.6)	<0.001	ns	0.028
TEh90-100 (%)	-114.7 (5.6)	-69.5 (3.2)	<0.001	-84.6 (3.4)	-97.6 (4.5)	0.029	<0.001	<0.001
Fanning (%)*	158.6 (6.3)	113.8 (4.7)	<0.001	126.0 (4.2)	147.3 (6.8)	0.010	<0.001	<0.001
Current-threshold relation								
Resting I/V slope	0.61 (0.01)	0.78 (0.03)	<0.001	0.75 (0.02)	0.64 (0.03)	0.010	<0.001	0.004
Minimal I/V slope	0.23 (0.01)	0.34 (0.02)	<0.001	0.26 (0.01)	0.21 (0.00)	0.003	0.043	<0.001
Recovery cycle								
Superexcitability (%)	-23.2 (1.6)	-	-	-13.3 (2.0)	-	-	0.001	-
Subexcitability (%)	16.34 (1.3)	-	-	13.51 (0.7)	-	-	ns	-
RP (ms)	2.74 (0.06)	-	-	3.52 (0.1)	-	-	<0.001	-
30% RP (ms)*	2.26 (0.03)	14.14 (0.6)	<0.001	2.58 (0.08)	11.27 (0.5)	<0.001	0.002	0.002

Data is given as mean (SEM) for 17 healthy subjects (except where indicated otherwise); SDTC = strength-duration time constant; TEd = depolarizing threshold electrotonus; TEh = hyperpolarizing threshold electrotonus; I/V = current/voltage relation; RP = refractory period; ns = not significant; mot = motor; sens = sensory; "-" = not obtainable at 20°C; * n=14 for TEdpeak, S2-accommodation, accommodation half-time, TEd90-100 and fanning in sensory axons; n=16 for 30% RP in sensory axons at 37°C and n=15 for 30% RP in motor axons at 37°C and 20°C. P-values were derived from t-tests.

Figure 1. Comparison of threshold electrotonus recordings in sensory axons using different test stimulus durations in a single subject at 37°C.
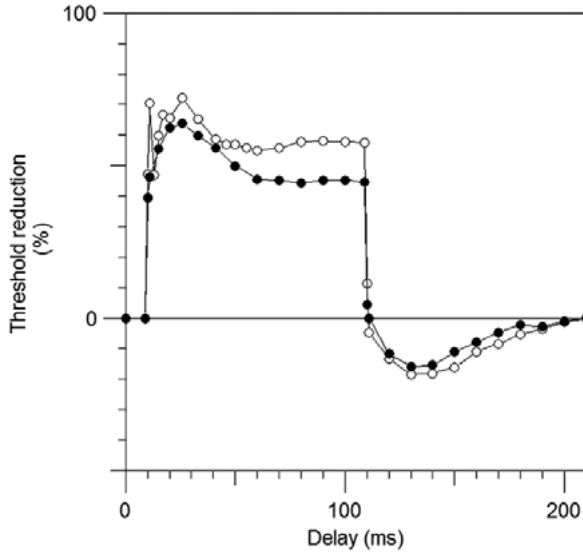
Figure 1 legend. Filled circles: 1ms test stimulus duration. Open circles: 0.5ms test stimulus duration.

Excitability at 20°C versus excitability at 37°C

Cooling resulted in changes in mean excitability values of motor and sensory axons (Table 1, Figure 2). In motor axons cooling resulted in an increase in SDTC and accommodation half-time, less prominent TEh90-100, S2-accommodation and TEdpeak, fanning-in, steepening of resting and minimal I/V slopes, prolongation of 30% refractory period (Figure 2). In sensory axons cooling evoked larger SDTC, more prominent TEd90-100 andTEh90-100, increase of accommodation half-time, decrease of S2-accommodation, fanning-out and prolongation of 30% refractory period; contrary to motor axons, cooling induced a decrease in steepness of current-voltage slopes. All mean excitability variables, except TEdpeak and S2-accommodation, differed significantly between motor and sensory axons at 20°C (Table 1).

Figure 2. Mean excitability recordings of four groups in 17 subjects.
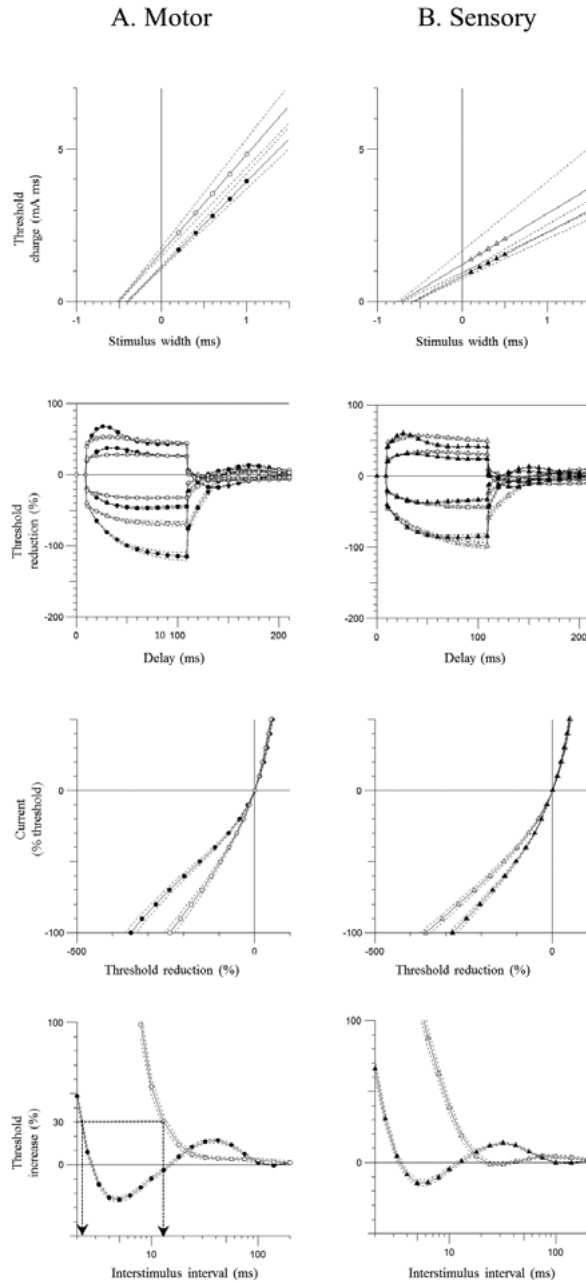
Figure 2 legend. A: Motor 37°C (filled circles) and motor 20°C (open circles); B: Sensory 37°C (filled triangles) and sensory 20 °C (open triangles). Curves are presented as mean and SEM values. The arrow indicates 30% refractory period.

Cooling-induced changes in motor axons versus cooling-induced changes in sensory axons

For some mean values of excitability-indices, cooling-induced changes in motor axons differed significantly from cooling-induced changes in sensory axons **(Tables 1 and 2, Figure 2)**. TEh90-100ms became less prominent in motor axons but more prominent in sensory axons. TEdpeak decreased in motor axons, but no significant changes were found in sensory axons. TEd90-100 became more prominent in sensory axons whereas it did not change in motor axons. Fanning decreased in motor axons but increased in sensory axons. Resting and minimal I/V-slopes became steeper in motor axons but less steep in sensory axons. All mean cooling-induced changes of excitability variables, except SDTC and rheobase, differed significantly between motor and sensory axons **(Table 2)**.

Clinical tests

At 37°C, MRC-grade was 5 in 16 subjects and 4 in 1 subject. Joint position tests showed a 100% right score in all subjects. Two-point discrimination was 1 mm in 1subject, 2 mm in 6 subjects, 3 mm in 7 subjects, 4 mm in 2 subjects and 5 mm in 1 subject.

At 20°C, MRC-grade had decreased from 5 to 4 in 8 subjects and from 5 to 3 in 3 subjects; it remained unchanged in 6 subjects. Joint position sense remained unchanged in all subjects. Two-point discrimination improved in 5 subjects (by 1 mm in 4 subjects and by 2 mm in 1 subject), worsened in 6 subjects (by 1 mm in 5 subjects and by 2 mm in 1 subject) and remained unchanged in the other subjects.

Table 2. Cooling-induced excitability changes in motor versus sensory axons.

Variable	Motor change	Sensory change	P-value
Strength-duration			
SDTC (ms)	0.102 (0.013)	0.108 (0.035)	ns
Rheobase (mA)	0.39 (0.24)	0.23 (0.18)	ns
Threshold electrotonus			
TEdpeak (%)*	13.0 (2.0)	0.7 (1.3)	<0.001
S2-accommodation (%)*	12.71 (0.98)	8.49 (0.81)	0.003
Accommodation half-time (ms)*	15.14 (2.18)	24.41 (2.77)	0.012
TEd90-100 (%)*	0.48 (1.31)	7.79 (1.46)	0.001
TEh90-100 (%)	45.28 (5.11)	12.59 (3.57)	<0.001
Fanning (%)*	44.8 (5.8)	17.8 (4.7)	<0.001
Current-threshold relation			
Resting I/V slope	0.17 (0.03)	0.10 (0.02)	<0.001
Minimal I/V slope	0.11 (0.02)	0.04 (0.01)	<0.001
Recovery cycle			
30% RP (ms)*	12.02 (0.69)	8.64 (0.61)	0.001

Data is given as mean (SEM) for 17 healthy subjects (except where indicated otherwise); SDTC = strength-duration time constant; TEd = depolarizing threshold electrotonus; TEh = hyperpolarizing threshold electrotonus; I/V = current/voltage relation; RP = refractory period; ns = not significant; * n=14 for TEdpeak, S2-accommodation, accommodation half-time, TEd90-100 and fanning in sensory axons; n=13 for 30% RP in motor axons and n=16 for 30% RP in sensory axons. P-values were derived from t-tests.

DISCUSSION

Our investigation showed that cooling induced muscle weakness, no consistent changes in clinical sensory function, and excitability changes that differed between motor and sensory axons. Comparison between motor and sensory axon excitability was possible because our protocol used 1.0ms duration test stimuli for both axon types.

Previous studies showed several differences between motor and sensory axons[10-22]. Studies assessing effects of cooling on excitability showed that the most prominent change was an increase in refractory period both in motor and sensory axons[23,24]. This is expected based on the slowing effect of cooling on ion channel gating. In a previous study, cooling in steps from 37ºC to 25ºC, 20ºC, and 15ºC was shown to induce muscle weakness at 20ºC and 15ºC as well as progressive changes in median nerve motor axon excitability recordings consisting of prolongation of SDTC, fanning-in of threshold electrotonus, steepening of the I/V curve, and increase in refractory period[25]. These changes were

attributed to progressive depolarization of resting membrane potential because they resembled changes during application of a depolarizing DC-current to the nerve and which could be abolished by applying hyperpolarizing DC current[25,26]. The cause of cooling-induced depolarization has not fully been elucidated but contributing factors may be thermal reduction of Na/K pump activity due to several mechanisms[27] and increase in persistent Na-current. Cooling-induced weakness has been attributed to development of block in depolarized axons, effects of cooling on muscle fiber contraction, or both[1,28-31].

The present study showed that cooling results in changes in motor axons resembling those evoked by depolarization of resting membrane potential by DC currents, thereby confirming findings in earlier studies by others and our group[24-26]. The only exception was an increase rather than a decrease in TEd90-100 as would have been expected in true fanning-in; though it was slight and non-significant, it could possibly reflect slower K-channel opening as cooling to 25°C was previously shown to increase accommodation half-time[25]. Due to cooling, 30% refractory period was prolonged with a factor of 6.26 (14.15ms/2.26ms), which matches well with the temperature-dependency of sodium inactivation channel gating (Q_{10} = 2.9) when assuming a nerve temperature drop of 17°C.

In sensory axons, cooling also induced SDTC and refractory period prolongation as well as an increase in TEd90-100. In contrast to the effects on motor axons, however, cooling of sensory axons induced fanning-out of threshold electrotonus and a decrease in resting and minimal I/V-slopes. This suggests that cooling of sensory axons evokes more complicated changes than depolarization. These changes may possibly reflect a combination of decreased slow potassium conductance (explaining the increase in accommodation half-time), decreased Ih (explaining the decrease in I/V slopes) and changes in resting membrane potential.

In the I/V relation, resting slope is usually attributed to transverse axonal conductance, the threshold decrease in the depolarizing part to slow K-channel activation, and the threshold increase in the hyperpolarizing part to Ih activation[24,26,32,33]. Each of these mechanisms likely affects more than one part of the I/V relation, making it difficult to ascribe a change in one of the I/V parts to a single mechanism. Four subtypes of HCN-channels, generating Ih, were found with activation kinetics varying from 30ms to several seconds[34] and different modes of temperature dependence[35-38]. All subtypes were shown in rat peripheral sensory axon terminals with a prevalence of HCN1 and HCN2[39], while data on motor axon HCN-channels expression is lacking. Excitability studies showed more prominent Ih in sensory axons than in motor axons[10,11,20,40]. This difference was explained by a larger maximal conductance and a depolarizing shift in voltage dependence[10]. A more pronounced hyperpolarizing shift of voltage gating in motor axons than sensory axons best explained the excitability differences due to warming in a previous

study[41]. Assuming that the effect of cooling is opposite to that of warming would imply that the depolarizing shift of voltage gating of Ih is larger for motor than sensory axons[41,42]. Our finding that the changes in I/V relation due to cooling differs considerably between motor and sensory axons, may therefore be partially explained by the gating kinetics of different subtypes of the HCN-channels expressed in motor and sensory axons.

Unfortunately, the currently available mathematical models of axonal ion channel properties require considerable adaptation to reliably capture the complicated effects of temperature change on ion channel kinetics and intra-axonal current flows into account. We therefore did not apply modeling to our results since this would have been susceptible to non-physiological parameterization and false results. The clinical motor and sensory tests we used may also have been too simple to detect subtle changes in motor and sensory function and better tests are needed. Moreover, it has been pointed out that it is difficult, if not impossible, to state that given reduction in clinical motor function represents a similar amount of axon dysfunction as the same reduction in clinical sensory function[43].

In conclusion, the present study provides additional evidence for biophysical differences between motor and sensory axons. Our findings may possibly be of relevance in explaining the pure motor involvement and cold paresis in MMN.

REFERENCES

1. R. Kaji. Physiology of conduction block in multifocal motor neuropathy and other demyelinating neuropathies. Muscle Nerve 2003;27:285-96.

2. Straver DC, van Asseldonk JT, Notermans NC, Wokke JH, van den Berg LH, Franssen H. Cold paresis in multifocal motor neuropathy. J Neurol 2011 Feb;258(2):212-7.

3. Ogawa-Goto K, Funamoto N, Abe T, Nagashima K. Different ceramide compositions of gangliosides between human motor and sensory nerves. J Neurochem 1990;55:1486–1493.

4. Franssen H, Straver DC. Pathophysiology of immune-mediated demyelinating neuropathies--Part II: Neurology. Muscle Nerve. 2014 Jan;49(1):4-20.

5. Burke D, Kiernan MC, Bostock H. Excitability of human axons. Clin Neurophysiol. 2001 Sep;112(9):1575-85.

6. Franssen H, Straver DC. Pathophysiology of immune-mediated demyelinating neuropathies-part I: neuroscience. Muscle Nerve. 2013 Dec;48(6):851-64.

7. Franssen H, Wieneke GH. Nerve conduction and temperature: necessary warming time. Muscle Nerve 1994 Mar;17(3):336-44.

8. Geerlings AH, Mechelse K. Temperature and nerve conduction velocity, some practical problems. ElectromyogrClinNeurophysiol1985 May-Jun;25(4):253-9.

9. Drenthen J, Blok JH, Dudok van Heel EB, Visser GH. Limb temperature and nerve conduction velocity during warming with hot water blankets. Journal of Clinical Neurophysiology 2008; 25: 104-10.

10. Howells J, Trevillion L, Bostock H, Burke D. The voltage dependence of I(h) in human myelinated axons. J Physiol 2012 Apr 1;590(7):1625-40.

11. Bostock H, Burke D, Hales JP. Differences in behaviour of sensory and motor axons following release of ischaemia. Brain 1994;117:225-34.

12. Bostock H, Rothwell JC. Latent addition in motor and sensory fibers of human peripheral nerve. J Physiol 1997;498:277-94.

13. Howells J, Bostock H, Burke D. Accommodation to hyperpolarization of human axons assessed in the frequency domain. J Neurophysiol 2016 Aug 1;116(2):322-35.

14. Schwarz JR, Bromm B, Spielmann RP, Weytjens JL. Development of Na inactivation in motor and sensory myelinated nerve fibres of Rana esculenta. Pflugers Arch 1983 Jul;398(2):126-9.

15. Bowe CM, Kocsis JD, Waxman SG. Differences between mammalian ventral and dorsal spinal roots in response to blockade of potassium channels during maturation. Proc R SocLond B Biol Sci. 1985 May 22;224(1236):355-66.

2

16. Vogel W, Schwarz JR. Voltage-clamp studies in axons: macroscopic and single-channel currents. In: Waxman SG, Kocsis JD, Stys PK, editors. The Axon. Oxford: Oxford University Press; 1995. pp. 257-280.

17. Kiernan MC, Mogyoros I, Burke D. Differences in the recovery of excitability in sensory and motor axons of human median nerve. Brain 1996 Aug;119:1099-105.

18. Kiernan MC, Lin CS, Andersen KV, Murray NM, Bostock H. Clinical evaluation of excitability measures in sensory nerve. Muscle Nerve 2001;24(7):883-92.

19. Kiernan MC, Lin CS, Burke D. Differences in activity-dependent hyperpolarization in human sensory and motor axons. J Physiol. 2004 Jul 1;558(Pt 1):341-9.

20. Burke D, Kiernan M, Mogyoros I, Bostock H. Susceptibility to conduction block: differences in the biophysical properties of cutaneous afferents and motor axons. In: Kimura J, Kaji R, editors. Physiology of ALS and related disorders. Amsterdam: Elsevier Science BV; 1997. p 43-53.

21. Lin CS, Kuwabara S, Cappelen-Smith C, Burke D. Responses of human sensory and motor axons to the release of ischaemia and to hyperpolarizing currents. J Physiol. 2002;541(Pt 3):1025-39.

22. Hofmeijer J, Franssen H, Van Schelven LJ, Van Putten MJ. Why are sensory axons more vulnerable for ischemia than motor axons? PLOS-one. 2013 Jun 20;8(6):e67113.

23. Burke D, Mogyoros I, Vagg R, Kiernan MC. Temperature dependence of excitability indices of human cutaneous afferents. Muscle Nerve 1999 Jan;22(1):51-60.

24. Kiernan MC, Cikurel K, Bostock H. Effects of temperature on the excitability properties of human motor axons. Brain. 2001 Apr;124(Pt 4):816-25.

25. Franssen H, Gebbink TA, Wokke JH, van den Berg LH, van Schelven LJ. Is cold paresis related to axonal depolarization? J PeripherNervSyst 2010 Sep;15(3):227-37.

26. Kiernan MC, Bostock H. Effects of membrane polarization and ischaemia on the excitability properties of human motor axons. Brain 2000 Dec;123 Pt 12:2542-51.

27. Kapoor R, Davies M, Blaker PA, Hall SM, Smith KJ. Blockers of sodium and calcium entry protect axons from nitric oxide-mediated degeneration. Ann Neurol 2003;53:174–180.

28. Rack PM, Fox JE. The effects of cold on a partially denervated muscle. J Neurol Neurosurg Psychiatry 1987 Apr;50(4):460-4.

29. Kijima M, Hirayama K, Nakajima Y. Symptomatological and electrophysiological study on cold paresis in juvenile muscular atrophy of distal upper extremity (Hirayama's disease). RinshoShinkeigaku 2002 Sep;42(9):841-8.

30. Taylor BV, Dyck PJ, Engelstad J, Gruener G, Grant I, Dyck PJ. Multifocal motor neuropathy: pathologic alterations at the site of conduction block. J Neuropathol Exp Neurol 2004;63:129–137.

31. van Asseldonk JTH, van den Berg LH, Kalmijn S, van den Berg-Vos RM, Polman CH, Wokke JHJ, et al. Axon loss is an important determinant of weakness in multifocal motor neuropathy. J Neurol Neurosurg Psychiatry 2006;77:743–750.

32. Pape HC. Queer current and pacemaker: the hyperpolarization-activated cation current in neurons. Annu Rev Physiol. 1996;58:299-327.

33. Lin C, Kiernan MC, Burke D, Bostock H. Assessment of nerve excitability properties in peripheral nerve disease. Handbook of Clinical Neurophysiology, Vol. 7. J. Kimura Elsevier B.V. 2006.p. 381-403.

34. Biel M, Wahl-Schott C, Michalakis S, Zong X. Hyperpolarization-activated cation channels: from genes to function. Physiol Rev 2009 Jul;89(3):847-85.

35. Pian P, Bucchi A, Robinson RB, Siegelbaum SA. Regulation of gating and rundown of HCN hyperpolarization-activated channels by exogenous and endogenous PIP2. J Gen Physiol 2006 Nov;128(5):593-604.

36. Pian P, Bucchi A, Decostanzo A, Robinson RB, Siegelbaum SA. Modulation of cyclic nucleotide-regulated HCN channels by PIP(2) and receptors coupled to phospholipase C. Pflugers Arch 2007 Oct;455(1):125-45.

37. Börjesson SI, Elinder F. Structure, function, and modification of the voltage sensor in voltage-gated ion channels. Cell BiochemBiophys 2008;52(3):149-74.

38. Orio P, Madrid R, de la Peña E, Parra A, Meseguer V, Bayliss DA, et al. Characteristics and physiological role of hyperpolarization activated currents in mouse cold thermoreceptors. J Physiol 2009 May 1;587(Pt 9):1961-76.

39. Luo L, Chang L, Brown SM, Ao H, Lee DH, Higuera ES, et al. Role of peripheral hyperpolarization-activated cyclic nucleotide-modulated channel pacemaker channels in acute and chronic pain models in the rat. Neuroscience. 2007 Feb 23;144(4):1477-85.

40. Tomlinson S, Burke D, Hanna M, Koltzenburg M, Bostock H. In vivo assessment of HCN channel current (I(h)) in human motor axons. Muscle Nerve 2010 Feb;41(2):247-56.

41. Howells J, Czesnik D, Trevillion L, Burke D. Excitability and the safety margin in human axons during hyperthermia. J Physiol 2013 Jun 15;591(12):3063-80.

42. Hart G. The kinetics and temperature dependence of the pace-maker current if in sheep Purkinje fibres. J Physiol. 1983 Apr;337, 401-16.

43. Franssen H. Relation between symptoms and pathophysiology in inflammatory neuropathies: Controversies and hypotheses. Neurosci Lett. 2015 Jun 2;596:84-9.

3

Simulating perinodal changes observed in immune-mediated neuropathies – Impact on conduction in a model of myelinated motor and sensory axons

BOUDEWIJN T.H.M. SLEUTJES
MARIA O. KOVALCHUK
NARIC DURMUS
JAN R. BUITENWEG
MICHEL J.A.M. VAN PUTTEN
LEONARD H. VAN DEN BERG
HESSEL FRANSSEN

ABSTRACT

Immune-mediated neuropathies affect myelinated axons, resulting in conduction slowing or block which may affect motor and sensory axons differently. The underlying mechanisms of these neuropathies are not well understood. Using a myelinated axon model, we studied the impact of perinodal changes on conduction. We extended a longitudinal axon model (41 nodes of Ranvier) with biophysical properties unique to human myelinated motor and sensory axons. We simulated effects of temperature and axonal diameter on conduction, and strength-duration properties. Then, we studied effects of impaired nodal sodium channel conductance, paranodal myelin detachment by reducing periaxonal resistance, and their interaction on conduction in the nine middle nodes and enclosed paranodes. Finally, we assessed the impact of reducing the affected region (five nodes) and adding nodal widening. Physiological motor and sensory conduction velocities and changes to axonal diameter and temperature were observed. The sensory axon had a longer strength-duration time constant. Reducing sodium channel conductance and paranodal periaxonal resistance induced progressive conduction slowing. In motor axons conduction block occurred with a 4-fold drop in sodium channel conductance or a 7.7-fold drop in periaxonal resistance. In sensory axons block arose with a 4.8-fold drop in sodium channel conductance or a 9-fold drop in periaxonal resistance. This indicated that motor axons are more vulnerable to develop block. A boundary of block emerged when the two mechanisms interacted. This boundary shifted in opposite directions for a smaller affected region and nodal widening. These differences may contribute to the predominance of motor deficits observed in some immune-mediated neuropathies.

Simulating perinodal changes observed in immune-mediated neuropathies –
Impact on conduction in a model of myelinated motor and sensory axons

35

NEW AND NOTEWORTHY

Immune-mediated neuropathies may affect myelinated motor and sensory axons differently. By the development of a computational model we quantitatively studied the impact of perinodal changes on conduction in motor and sensory axons. Simulations of increasing nodal sodium channel dysfunction and paranodal myelin detachment induced progressive conduction slowing. Sensory axons were more resistant to block than motor axons. This could explain the greater predisposition of motor axons to functional deficits observed in some immune-mediated neuropathies.

3

INTRODUCTION

Immune-mediated polyneuropathies may affect myelinated nerve fibers including the myelin sheath, the node of Ranvier, the adhesion molecules binding the axonal membrane to the Schwann cell membrane, and the axonal membrane itself.[1] These neuropathies include the acute inflammatory demyelinating polyneuropathy (AIDP) and acute motor axonal neuropathy (AMAN) variants of the Guillain-Barré syndrome, chronic inflammatory demyelinating polyneuropathy (CIDP), multifocal motor neuropathy (MMN), and anti-myelin associated (MAG) glycoprotein neuropathy. Developing disease-specific treatments poses a significant challenge as the selective vulnerability of motor or sensory nerve fibers and corresponding downstream mechanisms have not been fully elucidated. As the primary function of myelinated nerve fibers involves efficient transmission of action potentials, their damage will eventually present clinically by loss of muscle strength, loss of sensation, or both. A better understanding of the key mechanisms that hamper impulse transmission via saltatory conduction may potentially help to develop more targeted treatments aimed at prevention of irreversible nerve damage.

Studying the underlying pathology in patients with standard nerve conduction studies may not always provide sufficient detail as conduction slowing and block may originate from the malfunctioning of a variety of components in myelinated nerve fibers.[2,3] Nerve excitability testing is an attractive translational method in which threshold changes, induced by various conditioning stimuli, can be ascribed to changes in ion channel activity at one site of a group of axons. However, detailed aspects of the relation between pathological and heterogeneous pathophysiological disease processes at single axon level cannot be adequately assessed in ex-vivo models such as voltage-clamp experiments.[4] Animal models that accurately mimic human pathology specifically in motor and sensory axons are available for AMAN[5] and to a limited extent for AIDP, but not for CIDP and MMN. Studying computational models of myelinated axons have emerged to pro-

vide a quantitative view on the vital mechanisms for adequate saltatory conduction.[6-14] By systematically investigating pathological processes that cannot be examined otherwise, they may assist in defining avenues for developing disease-specific treatments.

Emerging insights into the pathology of immune-mediated neuropathies have shown specific targeting of molecular complexes that characterize the distinct geometrical domains surrounding the node of Ranvier, including the paranode and juxtaparanode.[15-18] Physiologically, these perinodal domains also have a vital role in saltatory conduction and recovery following action potentials.[9,11,19] Moreover, biophysical differences between motor and sensory axons have often been proposed as potentially contributing to the varied degree of functional impairment in immune-mediated neuropathies.[20] However, the interplay of these biophysical differences and the pathological processes related to immune-mediated neuropathies with the occurrence of conduction block remains yet unclear. This emphasizes the need for a computational model with a sufficient geometrical and biophysical description to systematically study pathological processes and their impact on conduction in motor and sensory axons.

Our study presents an extended longitudinal myelinated axon model, modified from McIntyre et al.[11] by including axonal ion channel properties under the myelin sheath, based on experimental mammalian[21] and human nerve excitability studies.[22-24] Our model allows biophysical characteristics unique to human myelinated motor and sensory axons to be implemented.[25-33] We simulated various physiological conditions, and have shown that these are in agreement with experimental studies. In addition, we explored how saltatory conduction will be affected by some putative mechanisms associated with immune-mediated neuropathies focussing on loss of functioning nodal sodium channels and disruption of the surrounding paranodal seal.[17,18]

METHODS

Model structure and anatomical properties of the myelinated axon model

We applied the double cable structure described by McIntyre et al.[11] As starting point, we used the Matlab implementation of this model as published by Danner et al.[34-36] The model accurately describes the anatomy of a myelinated axon where a successive node-internode configuration consists of a node (1 segment), paranode (1 segment), juxtaparanode (1 segment), standard internode (6 segments), and again a juxtaparanode (1 segment) and paranode (1 segment). Except for the nodal segments, the non-nodal (paranode, juxtaparanode and standard intermode) segments are surrounded by a myelin sheath

Simulating perinodal changes observed in immune-mediated neuropathies –
Impact on conduction in a model of myelinated motor and sensory axons

37

3

in which the periaxonal space was connected to the extracellular space by a myelin capacitance and conductance. Using Kirchoff's first law, each segment k was coupled with the previous segment (k-1) and next segment (k+1), where the non-nodal segments required calculation of the potential across the inner-axonal/periaxonal and periaxonal/extracelullar space. As the nodal segment did not involve the periaxonal space, it included the potential across inner-axonal/extracellular space, which equals the nodal membrane potential.[35] For the longitudinal model, we used a total of 41 nodes of Ranvier separated by 40 internodes. The membrane potential was clamped at its resting membrane potential. Table 1 gives a detailed summary of the morphological and electrical parameters of these segments[11] based on microscopic-anatomical mammalian studies.[21]

Similar to the original model,[11] the node of Ranvier consists of voltage-gated transient and persistent sodium channels, voltage-gated slow potassium channels, a leak channel, and nodal membrane capacitance. Their conductances are given in Table 2 and the gating kinetics in the Appendix.

Table 1. Overview of morphological and electrical parameters of model (obtained from McIntyre et al.[11]).

Morphological parameters			
Nerve fiber	Diameter	10	[μm]
Node-to-node	Distance	1150	[μm]
Node	Length	1	[μm]
	Diameter	3.3	[μm]
Paranode	Length, per segment	3	[μm]
	Diameter	3.3	[μm]
	Periaxonal space width	0.004	[μm]
Juxtaparanode	Length, per segment	46	[μm]
	Diameter	6.9	[μm]
	Periaxonal space width	0.004	[μm]
Standard internode	Length, per segment	175.2	[μm]
	Diameter	6.9	[μm]
	Periaxonal space width	0.004	[μm]
Myelin	c_{myelin}	0.1	[μF/cm²]
	g_{myelin}	0.001	[S/cm²]
	Number of myelin lamella	120	[-]
Longitudinal resistivity	Axoplasmatic,	70	[Ωcm]
	Periaxonal,	70	[Ωcm]

Motor axon - nodal, juxtaparanodal and internodal ion channel conductances.

Table 2. Maximum conductances, specific capacitances and resting membrane potential of motor and sensory axon model.

Node	Parameters	Motor	Sensory[a]	
Transient sodium conductance	$g_{Na,t}$	3.0		[S/cm^2]
Persistent sodium conductance	$g_{Na,p}$	0.01		[S/cm^2]
Slow potassium conductance	g_{Ks}	0.08	0.064	[S/cm^2]
Leak conductance	g_{Lk}	0.007		[S/cm^2]
Nodal capacitance	c_{node}	2		[µF/cm^2]
Paranode				
Paranodal capacitance	c_p	2		[µF/cm^2]
Paranodal conductance	g_p	0.001		[S/cm^2]
Juxtaparanode				
Juxtaparanodal capacitance	c_{jp}	2		[µF/cm^2]
Juxtaparanodal conductance	g_{jp}	0.0001		[S/cm^2]
Fast potassium conductance	g_{Kf}	0.02		[S/cm^2]
Standard internode				
Sodium conductance[c]	$g_{Na,t}$	0.03		[S/cm^2]
Slow potassium conductance[c]	g_{Ks}	0.0027	0.0022	[S/cm^2]
Fast potassium conductance[c]	g_{Kf}	0.0033		[S/cm^2]
Leak conductance	gLk	0.0001		[S/cm^2]
HCN conductance[d]	g_{HCN}	0.0014		[S/cm^2]
Electrogenic pump current[e]	I_{pump}	100		[pA]
Internodal capacitance	c_i	2		[µF/cm^2]
Resting membrane potential[b]	V_{rest}	-84.9	-81.8	[mV]

Unless indicated, parameters were obtained from McIntyre et al.[11] Absolute values were calculated using diameter and length of the regions (Table 1) by assuming circular symmetry.[a] Biophysical differences between motor and sensory axons (see text and Appendix). [b] Resting membrane potentials achieved with the new models (see text). [c] Internodal conductances relative to nodal conductances (see text). [d] Determined to satisfy internodal ionic equilibrium at resting membrane potential. [e] Pump current similar to that previously applied. [14]

To accurately simulate internodal membrane dynamics, the original passive description was modified by implementing juxtaparanodal and internodal voltage-gated fast potassium channels, internodal voltage-gated sodium, slow potassium, and hyperpolarizing-activated nucleotide-gated-cation (HCN) channels. Density of nodal sodium channels is significantly higher (1000-2000/µm^2) than at the internode (<25/µm^2).[21] By taking a physiological ratio of 100 (2000/µm^2 divided by 20/µm^2), the internodal sodium conductance was set at $^1/_{100}$ of the nodal sodium conductance. To reduce complexity, internodal sodium channels in a persistent state were omitted. Since the density of internodal slow potassium channels was suggested to be approximately $^1/_{30}$ of their nodal density, internodal/nodal conductance ratio was set at $^1/_{30}$.[37] Based on the same study, internodal fast potassium conductance was set at $^1/_6$ of juxtaparanodal conductance.[37]

Simulating perinodal changes observed in immune-mediated neuropathies –
Impact on conduction in a model of myelinated motor and sensory axons

39

3

The location of Na$^+$/K$^+$-pumps is still ambiguous. Early work suggested a nodal location but subsequent electrophysiological and staining experiments an internodal location. [21,37] Therefore, an electrogenic pump current was implemented in the internode. Based on the above modifications, a conductance for HCN channels was applied to satisfy internodal ionic equilibrium at the resting membrane potential which was set at -84.9 mV (see Table 2 and Appendix). A schematic view of the new model is shown in Figure 1.

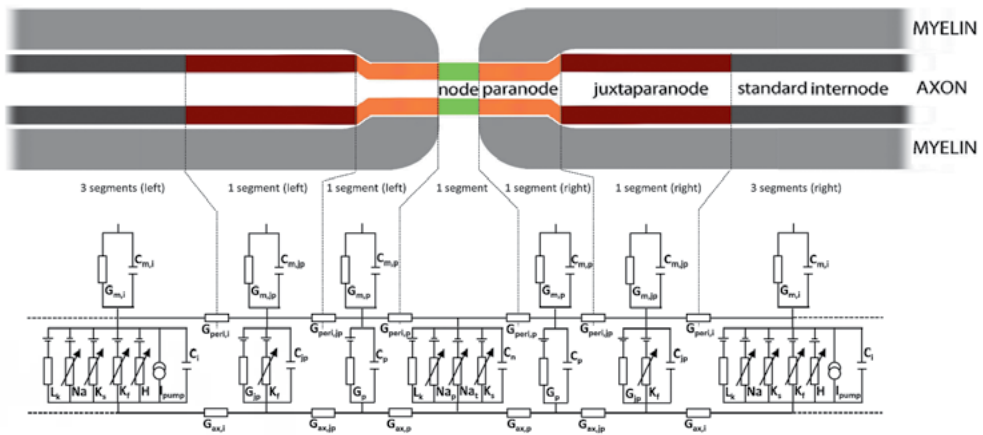**Figure 1.** The longitudinal myelinated axon model.

Figure 1 legend. A schematic view of a myelinated axon (modified from Franssen et al. [38] with permission from © 2013 Wiley Periodicals, Inc) with an electric circuit diagram of the new model showing the nodal, paranodal, juxtaparanodal and internodal regions. The nodal domain (1 segment) contains persistent (Na$_p$) and transient sodium (Na$_t$) channels, slow potassium (K$_s$) and leak (L$_k$) channels, and the nodal capacitance (C$_n$) in the axonal membrane. The paranodal domain (two segments, one left and right) contains, in the axonal membrane, a linear conductance with, in parallel, a capacitance (G$_p$ and C$_p$). The juxtaparanodal domain (two segments, one left and right) contains in the axonal membrane fast potassium channels (K$_f$), and in parallel, a linear conductance (G$_{jp}$) and capacitance (C$_{jp}$). The internodal domain (six segments, three left and right) contains sodium channels (Na$_t$), fast (K$_f$) and slow (K$_s$) potassium channels, a leak (L$_k$) conductance, I$_h$-channels (H), an electrogenic pump (I$_{pump}$), and an internodal capacitance (C$_i$) in the axonal membrane. The myelin sheath is represented by a linear conductance with, in parallel, a capacitance in the paranode (G$_{m,p}$ and C$_{m,p}$), the juxtaparanode (G$_{m,jp}$ and C$_{m,jp}$) and internode (G$_{m,i}$ and C$_{m,i}$) (See Table 2). Longitudinally, the model contains axonal (G$_{ax}$) and periaxonal (G$_{peri}$) resistivities (see Table 2).

Sensory axon – Biophysical differences with respect to motor axon

Sensory axons were suggested to have greater inward rectifying current. [26] Responses to long-lasting hyperpolarization revealed that a major part of this greater current

originates from changes in gating kinetics of HCN channels, which was best modeled by depolarizing their half-activation potential.[22] In our model, this half-activation was depolarized by 6.3 mV. Furthermore, a reduced slow potassium channel expression was hypothesized to contribute to the increased susceptibility of ectopic activity in sensory axons.[22, 40,41] This was modeled by reducing the slow potassium conductance in the sensory axon model by 20% relative to the motor axon. Subsequently, broadening of the sensory action potential due to a reduction in slow potassium channel was compensated by accelerating the activation gate and slowing the inactivation gate of sensory sodium channels (see Appendix).[11,22,42-44] With these biophysical differences, an ionic equilibrium was achieved when setting sensory resting membrane potential at -81.8 mV (see Table 2 and Appendix). Without altering the amount of sodium channels in persistent state, the depolarized membrane potential of 3.1 mV in sensory axons (motor vs. sensory: -84.9 mV vs. -81.8 mV) approximately doubled the persistent sodium current at resting membrane potential, which was also suggested to be an important biophysical difference.[22,27]

Simulation and stimulation settings

Numerical integration of the differential equations was performed within Matlab (R2014b; The MathWorks, Natick, MA) using the SUNDIALS CVode package ([45]; version 2.6.1) with time steps of 10 μsec. To calculate the conduction velocity, first, the derivative of the membrane potential was taken in every node, and from this the time points with maximum gradient were determined. To provide an estimate of conduction velocity, the distance between nodes 11 and 31 was divided by the time interval with maximum gradient at these nodes. The nodal excitation threshold and severity levels of pathological conditions that blocked saltatory conduction were determined using a binary search algorithm based on Hennings et al.[46] These severity levels, expressed as % of normal, were determined with a binary search stop criteria of 0.5% and subsequently rounded down to the integer that induced a block. Similar to a previous study, [47] when the membrane potential reached a target level (0 mV in our simulations) a generated action potential was detected. To avoid boundary effects of the model, results of the simulations were derived from the middle nodes (nodes 11 to 31). Single intracellular stimuli were delivered with a stimulus duration of 1 ms and a fixed stimulus intensity set at three times the excitation threshold at node 11.

Simulating effects of temperature, axon diameter and strength-duration properties

The relation between conduction velocity and myelinated axon diameter was simulated by increasing axon diameter from 10 μm (= default) to 14 μm, and 16 μm. In conjunction, other parameters were also scaled (see Table 1 from[11] including the nodal (3.3 μm, 4.7 μm and 5.5 μm), paranodal (3.3 μm, 4.7 μm and 5.5 μm), juxtaparanodal (6.9 μm, 10.4

Simulating perinodal changes observed in immune-mediated neuropathies –
Impact on conduction in a model of myelinated motor and sensory axons

41

μm and 12.7 μm), standard internodal diameter (6.9 μm, 10.4 μm and 12.7 μm), node-to-node distance (1150 μm, 1400 μm, and 1500 μm), and number of myelin lamellae (120, 140, and 150). The effect of temperature on conduction velocity was modeled by varying temperature from 30°C to 36°C (= default temperature) in steps of 2°C. Rheobase and strength-duration time constant were determined using Weiss's law [29,48] and assessing excitation thresholds at five different stimulus durations (1 ms, 0.8 ms, 0.6 ms, 0.4 ms and 0.2 ms) at the middle node (node 21).

3

Simulating nodal sodium channel disruption and loss of paranodal seal

Several mechanisms in immune-mediated neuropathies have been suggested in which the node of Ranvier and its surrounding structures play an important role.[1] For instance, in MMN half of the patients have high titers of serum antibodies against ganglioside GM1 which is expressed on the axolemma of the nodes of Ranvier and perinodal Schwann cells. Ganglioside GM1 was suggested to contribute to nodal sodium channel clustering and paranodal stabilization. [49-51] Disrupted sodium channel clustering and paranodal myelin detachment at both sides of the nodes may contribute to the development of conduction slowing and eventually block. Simulations were performed to quantify how these mechanisms affect saltatory conduction. Disrupted sodium channel clustering may result in decreased inward sodium current density (reviewed by (Kaji 2003)[52]). In the present study, this was simulated by decreasing maximum transient and persistent sodium channel conductances (Fig. 1 – nodal Na_p and Na_t). Broken paranodal seals were simulated by decreasing the periaxonal resistance across the paranodal region such that juxtaparanodal fast potassium channels also become exposed to the extracellular medium (Fig. 1 – increasing the periaxonal paranodal conductance $G_{peri,p}$ and the juxtaparanodal conductance $G_{peri,jp}$).The resulting effective increase in nodal area was simulated by increasing nodal capacitance (Fig. 1 – C_n). The affected region involved the nine middle nodes (nodes 17 – 25) and the paranodal structures between them.

RESULTS

Validation of motor and sensory axon model

Figure 2 illustrates an action potential in a myelinated motor and a myelinated sensory axon obtained at the middle node (node 21) after applying a single pulse at node 11. The excitation thresholds at node 11 were 577 pA for the motor axon and 403 pA for the sensory axon. The action potential was followed by the physiologically characteristic depolarizing after potential (DAP) and hyperpolarizing after potential (HAP) (zoomed

part in Fig. 2A). Action potential duration (half-way resting and peak potential) was lon-ger for the motor axon (0.34 ms) than for the sensory axon (0.29 ms). With a modeled diameter of 10 µm, the action potential propagation (nodes 11 to 31) was in the physi-ological range with a conduction velocity of 47.9 m/sec for the motor axon (Fig. 3) and 50.0 m/sec for the sensory axon.[53]

Figure 2. Motor and sensory action potential generation.
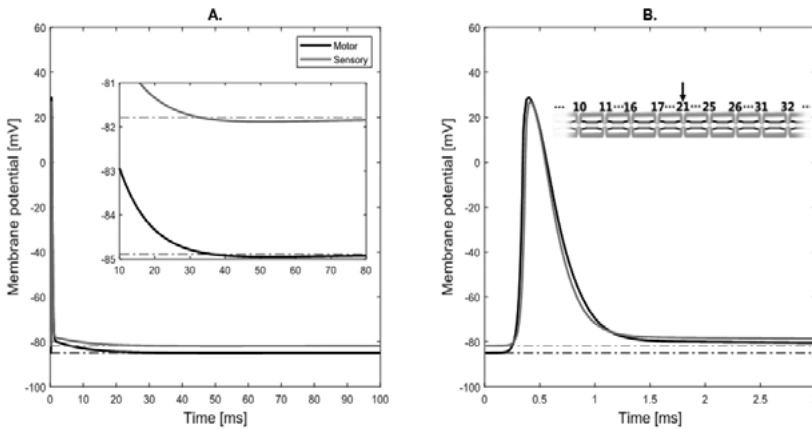

Figure 2 legend. Generated action potential for the motor (black) and sensory (gray) myelinated axon up to 100 ms (A) and up to 3 ms (B) at node 21 after a 1 ms intracellular stimulus pulse of three times the excitation threshold at node 11. In (A), the action potential close to the resting membrane potential is also shown. Dotted lines represent resting membrane potential.

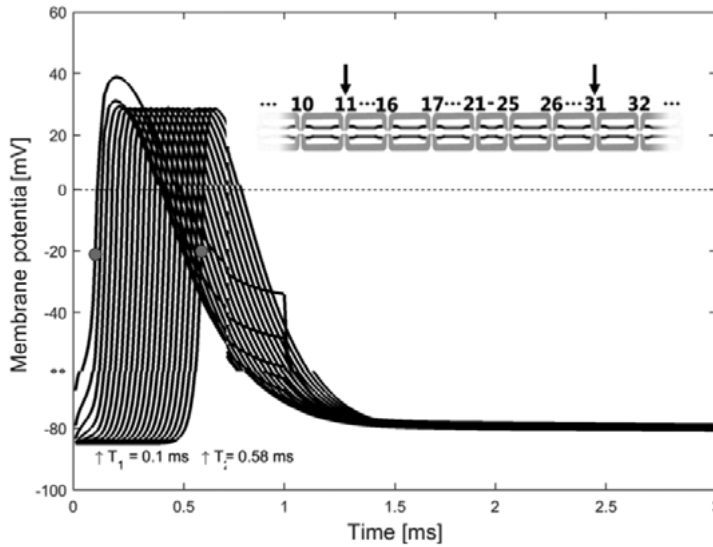**Figure 3.** Motor action potential propagation.

Figure 3 legend. Action potential propagation of the motor myelinated axon model up to 3 ms from node 11 to 31. The dots at node 11 (T_1 = 0.10 ms) and 31 (T_2 = 0.58 ms) define the time points with the highest gradient of membrane potential from which the conduction velocity was derived ([20*1150 µm] / [$T_2 - T_1$] = 47.9 m/sec).

Conduction velocity increased approximately linearly with axon diameter to 70.0 m/sec (14 µm) and 83.3 m/sec (16µm) in motor axons and to 73.7 m/sec (14 µm) and 88.2 m/sec (16 µm) in sensory axons (Fig. 4A). Conduction velocities also increased linearly with temperature (Fig. 4B), the increase being 1.60 m/sec/ °C for the motor and 1.58 m/sec/°C for the sensory axon. Converting to Q_{10} with the conduction velocities at 30°C and 36°C, Q_{10} was 1.45 for the motor axon and 1.43 for the sensory axon, thereby falling within the range of physiologically observed temperature dependence. [54-57]

Figure 4. Effect of axon diameter and temperature on conduction velocity.
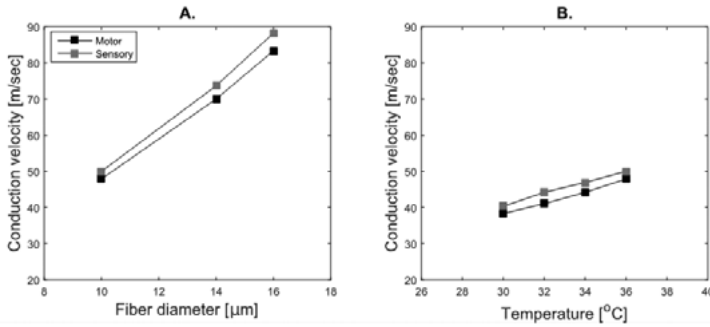

Figure 4 legend. (A) Effect of increase in myelinated fiber diameter - motor (black) and sensory (gray) - on conduction velocity. (B) The relation between temperature and conduction velocity for the motor (black) and sensory (gray) myelinated axon.

Figure 5 illustrates the strength-duration properties for motor and sensory axons determined at the middle node. It must be emphasized that simulations with intracellular stimulation results in a shorter strength-duration time constant (SDTC) compared to experiments with transcutaneous stimulation due to the large nerve/electrode distance.[58] The motor rheobase was 476 pA and the motor SDTC was 205 μs, which closely matches previous modeling studies. [11,48,59] In agreement with experimental studies, the SDTC in the sensory axon (304 μs) was higher and the rheobase was lower (308 pA) compared to the motor axon. This results in a ratio of 1.5 for sensory/motor SDTC (304/205 μs), which matches with experimental observations.[29,60]

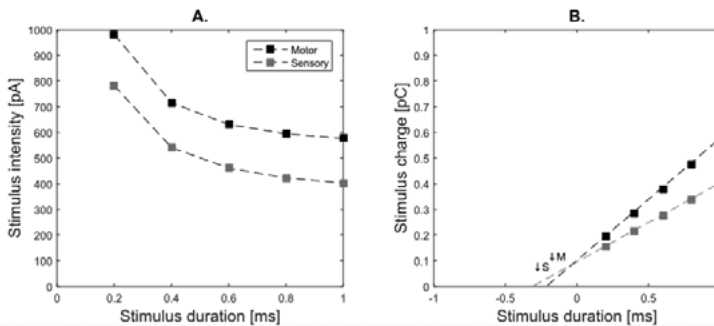**Figure 5.** Motor and sensory strength-duration properties.

Figure 5 legend. (A) Stimulus duration curve for motor (black) and sensory (gray) myelinated axon. In (B) the same result as in (A), but after converting to the charge-duration curve. The vertical arrows indicate the cross-sections with x-axis, which corresponds to the strength-duration time constant (motor = 205 μsec; sensory = 304 μsec).

Simulating perinodal changes observed in immune-mediated neuropathies –
Impact on conduction in a model of myelinated motor and sensory axons

45

3

Disruption of nodal sodium channel clusters in motor and sensory axon

Figure 6 shows motor action potential propagation from node 11 to 31 for a 70% of normal nodal sodium channel conductance (Fig. 6A). A small drop of the maximal membrane potential can be observed at the affected middle nodes with a slowed conduction velocity to 43.4 m/sec. Failure of motor action potential propagation occurred at nodal sodium channel conductance of 25% of normal (4-fold drop, Fig. 6B). To determine the effect of disruption of nodal sodium channel clusters on motor and sensory conduction velocities, nodal sodium channel conductance was reduced from 100% (normal), 70%, 50%, 30% up to conduction block. In sensory axons, action potential propagation failure occurred at a conductance of 21% of normal (4.8-fold drop).

Figure 6. Motor action potential slowing and conduction block due to disrupted nodal sodium channel clusters.
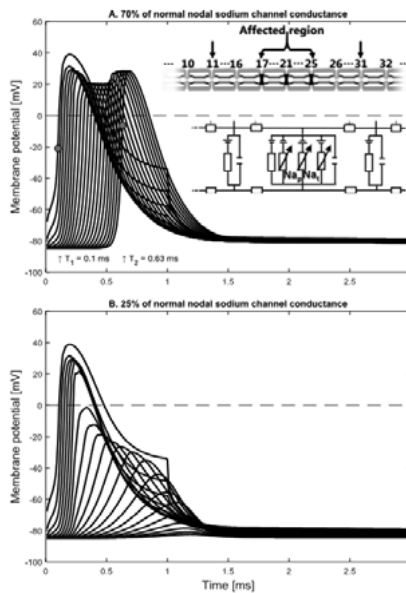
Figure 6 legend. Action potential propagation of the motor myelinated axon model up to 3 ms from node 11 to 31, with (A) 70% of normal nodal sodium channel conductance resulting in a slight drop of the maximum membrane potential around the affected region and conduction slowing ([20*1150 μm] / [$T_2 - T_1$] = 43.4 m / sec), and (B) 25% of normal nodal sodium channel conductance inducing a conduction block when stimulating at node 11 at three times the excitation threshold. Insets in (A) show a schematic view of the myelinated axon with the affected region and the characteristics of the myelinated axon being modeled – the persistent (Na_p) and transient (Na_t) sodium channel conductances.

Decreasing nodal sodium channel conductance induced progressive slowing towards block in the motor and sensory axon with slightly higher conduction velocities and more resistance to conduction block for the sensory axon (Fig. 7).

Figure 7. Relation of motor and sensory conduction slowing towards block with increasing nodal sodium channel cluster disruption.
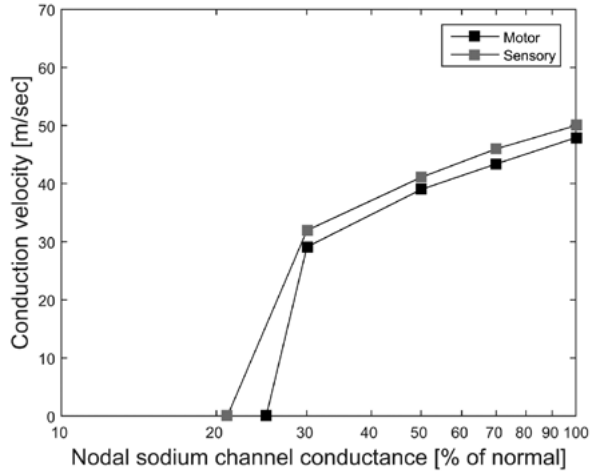
Figure 7 legend. Relation between nodal sodium channel cluster disruption simulated by decreasing the sodium channel conductance from 100% (normal), 70%, 50%, and 30% and decreasing conduction velocities in motor (black) and sensory (gray) axons until conduction block (motor = 25% of normal; sensory = 21% of normal). Note the logarithmic scaling of the x-axis.

Paranodal myelin loop detachment in motor and sensory axon

Detachment of paranodal myelin loops from the axonal membrane in motor and sensory axons was simulated by decreasing the periaxonal resistance to 70%, 50%, 30% and 20% of normal. Motor conduction velocity decreased to 44.2 m/sec (70% of normal), 41.1 m/sec (50% of normal), 35.4 m/sec (30% of normal; Fig. 8A) and 28.0 m/sec (20% of normal) until conduction block occurred at a periaxonal resistance of 13% of normal (Fig. 8B). Sensory conduction velocity decreased to 46.9 m/sec (70% of normal), 44.2 m/sec (50% of normal), 37.7 m/sec (30% of normal) and 30.7 m/sec (20% of normal) until conduction block occurred at a periaxonal resistance of 11% of normal (9-fold drop). Decreasing periaxonal resistance induced progressive slowing towards block in the motor and sensory axon, where the sensory axon had slightly faster conduction velocities and was more resistant to conduction block (Fig. 9).

Simulating perinodal changes observed in immune-mediated neuropathies –
Impact on conduction in a model of myelinated motor and sensory axons

47

Interaction of disrupted nodal sodium channel clusters and paranodal myelin loop detachment

More sophisticated simulations were subsequently performed to the interaction of nodal sodium channel disruption and detachment of paranodal myelin loops on conduction slowing and block. Figure 10A shows that a boundary of block emerges, representing the percentage of normal where this interaction induces conduction block. Outside this boundary (lower left), there is failure of saltatory conduction and within this boundary (upper right of Fig. 10A), saltatory conduction is still maintained, albeit at lower conduction velocities. The sensory axon compared to the motor axon had consistently higher resistance to the emergence of block. Finally, for the motor axon, we completely mapped the conduction velocity distribution within the boundary of block in 2-dimensional (Fig. 10B, top) and projected 3-dimensional representations (Fig. 10B, bottom), which also encompasses the results of Figures 7 and 9.

3

Figure 8. Motor action potential slowing and conduction block due to paranodal myelin loop detachment.
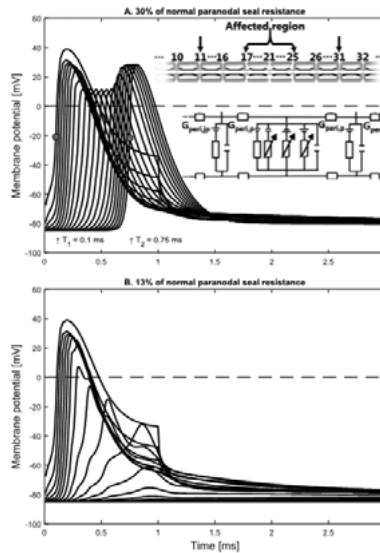
Figure 8 legend. Action potential propagation of the motor myelinated axon model up to 3 ms from node 11 to 31 with (A) 30% of normal paranodal seal resistance resulting in a slight drop of the maximum membrane potential around the affected region and conduction slowing ([20*1150 µm] / [$T_2 - T_1$] = 35.4 m / sec), and (B) 13% of normal paranodal seal resistance inducing a conduction block when stimulating at node 11 at three times the excitation threshold. Insets in (A) show a schematic view of the myelinated axon with the affected region and the characteristics of the myelinated axon being modeled – the periaxonal paranodal ($G_{peri,p}$) and juxtaparanodal conductance ($G_{peri,jp}$)

Figure 9. Relation of motor and sensory conduction slowing towards block with increasing detachment of paranodal myelin loops.

Figure 9 legend. Relation between detachment of paranodal myelin loops simulated by decreasing the paranodal seal resistance from 100% (normal), 70%, 50%, 30%, and 20% of normal and the decreasing conduction velocities in motor (black) and sensory (gray) axons until conduction block (motor = 13% of normal; sensory = 11% of normal). Note the logarithmic scaling of the x-axis.

Simulating perinodal changes observed in immune-mediated neuropathies –
Impact on conduction in a model of myelinated motor and sensory axons

49

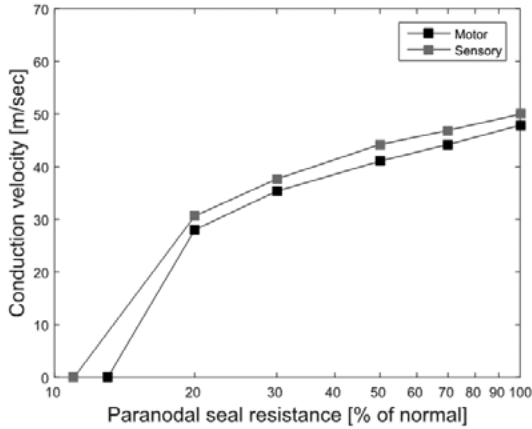**Figure 10.** Emergence of a boundary of block in motor and sensory axon due to the interaction of nodal sodium channel cluster disruption, paranodal myelin loop detachment, and effects of enlarged nodal area and a reduced affected region.
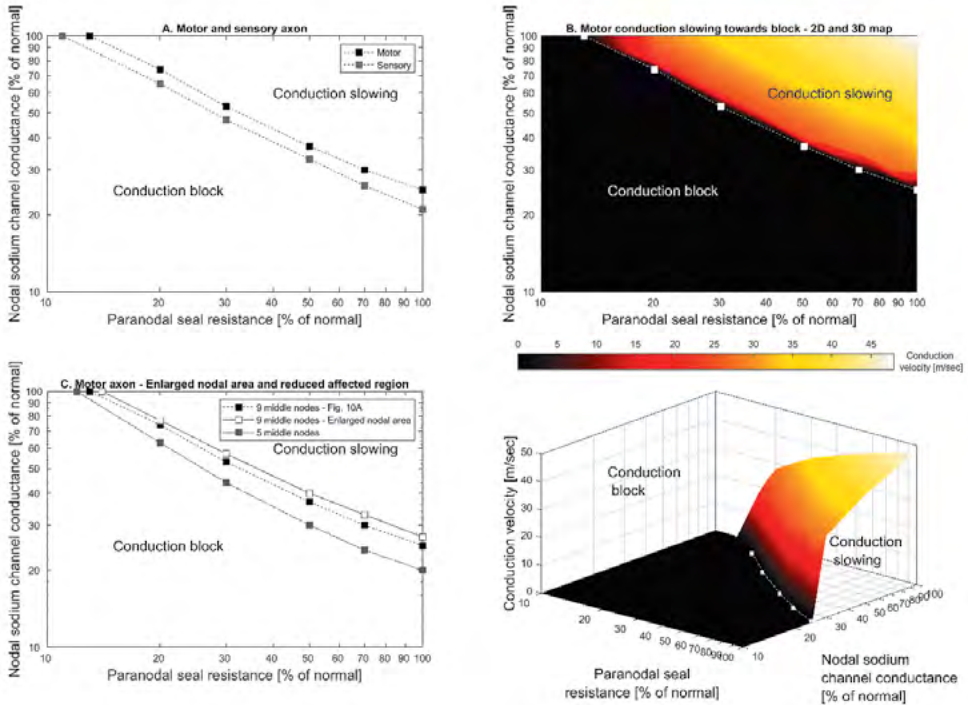
Figure 10 legend. (A) The interaction of nodal sodium channel cluster disruption (as % of normal nodal sodium channel conductance) and paranodal myelin loop detachment (as % of normal paranodal seal resistance) in motor and sensory axon (nine middle nodes) when stimulating at three times the excitation threshold. (B) A 2D (top) and 3D (bottom) map of motor conduction slowing towards block from (A). (C) Boundary of block in motor axon – 9 middle nodes (black solid square – dashed, Fig. 10A), 9 middle nodes with enlarged nodal area (black open square – continues), and 5 middle nodes (gray solid square - dashed). Note the logarithmic scaling of the axes.

Sensitivity of the boundary of block to enlarged nodal area

Depending on various pathophysiological conditions and their severity levels, the boundary of block shifts changing the areas covered by conduction slowing and block. To investigate the sensitivity of this boundary, two additional conditions were simulated in the motor axon. As damage may appear more focally, the affected region was reduced to five nodes (node 19 to 23). Also, paranodal myelin detachment may, as an additional

consequence, effectively enlarge the exposed nodal area. An enlarged nodal area was simulated by increasing the nodal capacitance that reflects widening of nodal length from 1 µm to 3 µm. Figure 10C shows that the two conditions shifts the boundary of block in opposite directions. When only five nodes are affected the area covered by conduction block reduces, while for nodal widening this area increases.

DISCUSSION

In this study we successfully implemented a mathematical model to simulate saltatory conduction along peripheral myelinated motor and sensory axons in circumstances resembling those hypothesized in immune-mediated neuropathies. The simulations with the model generated action potentials followed by the physiological depolarizing and hyperpolarizing afterpotentials. Our model further corresponded with experimental and simulation studies on motor and sensory conduction velocities that scaled linearly with temperature and axonal diameter.[53-55,61,62] Also the motor and sensory strength-duration properties followed the behaviour as observed in human peripheral myelinated nerves.[29,60,63-66] Subsequently, we were able to quantitatively determine that saltatory conduction progressively slows prior to conduction block when inducing pathology associated with immune-mediated neuropathies by focusing on disrupted nodal sodium channel clusters and paranodal detachment.[1,4,15,51] A boundary of block emerged when simulating the interaction of both mechanisms with block occurring outside this boundary and slowing when remaining within this boundary. Simulations provided a link between the biophysical differences characteristic for motor and sensory axons and their varied impact on the emergence of conduction block. This provides quantitative evidence of their differential susceptibility to conduction block,[20] which may also consequently induce a varied degree of functional impairment.

Differences between motor and sensory fibers

The implemented biophysical differences between motor and sensory axons are based on experimental evidence and simulations obtained from human nerve excitability studies.[20,22,26,27] Using these differences, our findings support the studies suggesting that sodium gating kinetics may underlie the narrower sensory action potential compared to motor action potential, [11,22,67] despite the larger persistent sodium current and smaller slow potassium conductance in normal sensory, compared to motor axons. Sensory conduction velocity was also previously found to be slightly higher than the motor nerve conduction velocity.[68] The slopes of the conduction velocity (1.6 m/sec/°C) due to temperature changes were approximately linear and fell within the experimentally observed

Simulating perinodal changes observed in immune-mediated neuropathies –
Impact on conduction in a model of myelinated motor and sensory axons

51

ranges for motor and sensory axons (1.1 m/sec/ºC – 2.3 m/sec/ºC). [54,55,57,61,62,69] Modeled strength-duration properties were in agreement with previous modeled values.[11,48,59] Single intracellular stimuli applied at a node results in shorter simulated strength-duration time constants compared to experiments with large nerve/electrode distance.[58] Uniform stimulation over all nodes and internodes has been suggested to more closely approximate external stimulation with large surface electrodes.[59] It should be further noted that studying single axons[29,66] result in a larger physiological range for strength-duration properties compared to assessing a group of axons. The sensory to motor SDTC ratio of 1.5 (304 / 205 µs) was also in accordance with previous studies.[22,29,60,64,65] Although the excitation threshold depends on many factors, the order of magnitude ($\approx$ 0.1- 1 nA) to generate an action potential resembled that of other modeling results. [14,35,48] With the implemented biophysical differences between motor and sensory axons, our simulations showed that they responded differently to conduction slowing and emergence of block induced by nodal and paranodal dysfunction at various severity levels. Differences in motor and sensory axons are likely not limited to axonal membrane dynamics, but might also include microstructural components. This may further contribute to the varied susceptibility and selectivity of motor and sensory involvement in immune-mediated neuropathies. Although more difficult to elucidate, adequate implementation of these differences may further improve computational models to study immune-mediated neuropathies more specifically.

Emergence of conduction block

Inducing conduction block required considerable blockage of sodium channels (4 to 5-fold) and reducing of the paranodal seal resistance (8 to 9-fold) emphasizing that the safety factor for impulse generation is generally high. Normal axons have a safety factor, defined as the ratio of available/required driving current to excite a node, in the same order of magnitude (about 5 – 7). [70] Our simulations further suggest that the smaller the area (Fig 10B, top) or volume (Fig. 10B, bottom) in the multidimensional diagrams covered by conduction slowing, relative to that of conduction block, the more susceptible the myelinated axon becomes to the occurrence of a conduction block. As a result, additional, either internal or external, perturbations (e.g. membrane hyperpolarization or voluntary activity) that negatively affect the condition is likely to reduce this area or volume and may result in crossing the slowing/block boundary inducing failure of action potential propagation. Being close to this boundary is comparable to a reduced safety factor just above unity, where conduction is still possible, but slower. When it falls below unity by crossing the boundary, conduction failure eventually occurs.[4,38] Interestingly, our findings further indicate that if conduction is still possible at the affected region, the membrane potential recovers outside such a region (Fig 6A and Fig. 8A). This implies that

multifocally affected regions within a myelinated axon do not necessarily lead to block, provided they are separated by sufficient distance. Nevertheless, as long as conduction is preserved, nerve function potentially varies depending on the distant from the affected region, which may explain the excitability studies in patients with MMN showing both abnormal[71] and normal excitability indices outside the affected region.[72] Further experimental evidence of this longitudinal recovery is also present in a study in which a rat myelinated fiber was partly exposed to anti-galactocerebroside serum and internodal conduction time normalized adjacent to the affected region.[73]

Simulating pathology

In various human neuropathies the modeled pathology, including nodal sodium channel abnormalities and paranodal myelin loop detachment, was suggested to be of significant relevance. In CIDP, excitability changes in median nerve motor axons distal to sites with conduction block were consistent with increased current leakage between node and internode; furthermore, sera of these patients were shown to bind to nodal and paranodal regions of teased rat nerve fibers.[71] In anti-MAG neuropathy, electron microscopy of sural nerve biopsy sections revealed loosening of paranodal Schwann cell microvilli.[74] Axonal excitability studies of median nerve motor axons showed decreased threshold changes during the supernormality period of the recovery cycle which were consistent with increased juxtaparanodal fast potassium channel activation due to loss of paranodal sealing.[75] In diabetic neuropathy, latent addition revealed decreased nodal persistent sodium currents; this method allows for separation of changes in strength-duration properties due to passive from those due to active nodal properties.[76] Axonal excitability studies in type 1 diabetes patients without neuropathy showed changes consistent with loss of sodium permeability and decreased fast and slow potassium conductances.[77] Finally, staining of nodal sodium channels was shown to be decreased or lost in a rabbit model of human AMAN.[50]

 Supporting our simulations, an experimental study showed that targeting sodium channels with lidocaine slows conduction, and therefore dysfunction of sodium channels should be considered as a mechanism of slowing, also in absence of block.[78] Similarly, exposure to anti-galactocerebroside antibodies was suggested to disrupt the outermost paranodal myelin loops from the paranodal axon, thus inducing slowing and block.[73] At a microstructural level, abnormalities in various proteins[1] may contribute to altered sodium channel conductance and paranodal seal resistance. GM1 gangliosides are enriched in the nodal and paranodal axolemma and maintain nodal sodium channel clustering and paranodal stabilization.[50] Additionally, the septate-like junctions at the paranode are formed by axonal contactin-associated protein (Caspr1) and contactin 1 that are tightly connected to neurofascin-155 at the paranodal myelin loops. Nodal sodium

channels are anchored to spectrin of the cytoskeleton via ankyrin-G, and to gliomedin of the Schwann cell microvilli via neurofascin-186. As such, changes in functioning of these proteins may potentially be reflected within the model by dysfunction of sodium channels and detachment of paranodal myelin loops.

Sensitivity of the model to parameter choices

Besides altering parameters to simulate pathology, it must be noted that small variations in any parameter within the model, e.g. dimensionality of the myelinated axon, ion channel conductances, gating kinetics, and longitudinal characteristics will cause fluctuations in excitability properties, levels of conduction slowing or block depending on the parameter's sensitivity within the model. Therefore, with the specific parameterization applied, the model structure, and simulation and stimulation settings, our findings should not be interpreted as rigid and absolute cut-off points regarding conduction slowing, block and varied response of the motor and sensory axon. More extensive and advanced probabilistic approaches are required to determine the contribution of these sources of variability.[79] Nevertheless, our simulation study provides a broad and quantitative insight into how single or interaction of multiple pathophysiological mechanisms may affect saltatory conduction, which otherwise cannot be systematically studied with experimental techniques.

Model limitations

The model includes the most prominent voltage-gated ion channels whose functioning has been experimentally studied in detail. As completely capturing the functioning of a human peripheral myelinated axon in a computational model is impossible, these models always come with certain simplifications. It has also been suggested that ion channel types are present in the myelin membrane.[80,81] The myelin sheath in our model involved a myelin conductance and capacitance, which has also previously been applied[11,14] generating physiological conduction velocities and excitability properties. Besides the gating kinetics, temperature also affects conductance, the electrogenic pump, and resting membrane potential.[13,60,63,82,83] For convenience, we kept these parameters constant, as their values are less unambiguous defined to set properly. In the simulated temperature range (30°C – 36°C), results matched experimental studies well, indicating the validity of our approach. The dynamics of extracellular and intracellular ion concentrations has not yet been incorporated into the model. The electrogenic pump represents a constant current, where more sophisticated models take into account its dependence on ion concentrations.[84] Repetitive nerve stimulation can result in potassium accumulation in the periaxonal space, which may also induce conduction block,[85] or affect resting membrane potential and excitability of the nerve.[86] As we restricted our study to simulations

of action potential propagation after applying single stimuli, the expectation is that the above factors will have only a limited effect on our findings. Simulations of pathology were implemented homogenously in the affected region. When myelinated axons are pathologically targeted, they are likely to be affected more heterogeneously. Disturbed sodium channel clustering may not only be reflected by blockage of channel conductance, but potentially also accompanies changes in gating kinetics. In pathological conditions, also implementing the expression of other sodium channel subtypes (e.g. Nav1.8) may become relevant to further refine the model as there is some evidence of their presence in some nodes of Ranvier.[87] As the membrane potential of the model is clamped changes to conductances do not affect the resting membrane potential. As such, the model allows studying changes to resting membrane potential as a separate mechanism. The above aspects can be further addressed in more detail in subsequent studies and provide interesting opportunities for improvements, depending on the research question posed.

CONCLUSION

With its current implementation, the presented model contains the most prominent biophysical aspects that appear necessary and sufficient to simulate saltatory conduction in motor and sensory axons. The link between these biophysical aspects and their varied impact on the emergence of block provides support that they may also partly contribute to the selective susceptibility in immune-mediated neuropathies. It further explains how action potential propagation becomes affected due to pathological mechanisms involved in immune-mediated neuropathies by focusing on perinodal changes. In various human neuropathies, such as anti-MAG neuropathy, these mechanisms may not remain restricted to the perinodal region, but may also involve morphological changes associated with demyelination.[74] It therefore also provides a valuable platform that enables the implementation of e.g. segmental, paranodal or juxtaparanodal demyelination[4,88,89] to further study their individual and composite impact on saltatory conduction. In CIDP and MMN, next to the morphological changes, also the interaction with increased or decreased currents through specific ion channels (e.g. juxtaparanodal fast potassium channels) is of clinical relevance to corporate into the model.[71] It may help to understand how these abnormalities can potentially be counteracted by specific pharmacological ion channel modifiers to prevent the occurrence of conduction block and restore action potential propagation. Computational models,[90] in conjunction with techniques to reliably assess the physiology and pathology in single human myelinated axons,[66,91] are valuable tools for providing insights into vital mechanisms that affect saltatory conduction, and into which component may potentially be targeted in immune-mediated neuropathies.

APPENDIX

In this section, we present the basic equations in the model underlying the ionic currents including their dynamics. For a more extensive description of the double cable structure with the corresponding differential equations, we would like to refer to the work of Danner et al.[35] The specific ionic currents including their gating properties were modeled according to the Hodgkin-Huxley formulation.[92] The transient and persistent sodium, slow and fast potassium, inward rectifying, and leak currents are described by

$$I_{Na_t} = g_{Na_t} m^3 h (V_{mem} - E_{Na}) \tag{1}$$

$$I_{Na_p} = g_{Na_p} p^3 (V_{mem} - E_{Na}) \tag{2}$$

$$I_{K_s} = g_{K_s} s (V_{mem} - E_K) \tag{3}$$

$$I_{K_f} = g_{K_f} n^4 (V_{mem} - E_K) \tag{4}$$

$$I_H = g_{HCN} q (V_{mem} - E_H). \tag{5}$$

$$I_{L_k} = g_{L_k} (V_{mem} - E_{L_k}). \tag{6}$$

The conductances g_{Nat}, g_{Nap}, g_{Ks}, g_{Kf}, g_{HCN}, and g_{Lk} are given in Table 2. The variables m, h, p, s, n, and q are the dimensionless gates involving the transient sodium activation and inactivation, persistent sodium activation, and slow and fast potassium activation, and HCN activation, respectively. V_{mem} represents the membrane potential. The ionic reversal potentials are given by [22,23]

$$E_{ion} = \frac{RT}{F} \log \left(\frac{[K]_{ex} + Sel_{ion}[Na]_{ex} - Sel_{ion}[K]_{ex}}{[K]_i + Sel_{ion}[Na]_i - Sel_{ion}[K]_i} \right) \tag{7}$$

with E_{ion} the reversal potentials for sodium E_{Na}, potassium E_K and inward rectifier E_H. E_{Lk} is set to V_{rest}. The applied channel selectivities, Sel_{ion} were for $Sel_{Na} = 0.9$, $Sel_K = 0$, and $Sel_H = 0.09$. [22] The applied intracellular and extracellular potassium and sodium concentrations were comparable to previous studies[13,24,32] with $[K]_{ex} = 5.6$ mM, $[K]_i = 155$ mM, $[Na]_i$

= 9 mM, $[Na]_{ex}$ = 144.2 mM, and F and R were Faraday's constant, 96485000 $^C/_{mol}$ and the gas constant, 8 315 569.8 $^J/_{K\,mol}$. The dynamics of the channel gates were described by:

$$\frac{dy}{dt} = [\alpha_y(1-y) - \beta_y y]Q_{10}^{\frac{T_{stim}-T_{ref}}{10}} \qquad (8)$$

with y the channel gates (i.e. *m, h, p, s, n, q*), where α_y and β_y were derived using the equations shown in Table 3 and corresponding parameters shown in Table 4.[11,22-24]

Table 3. Ion channel gating variables with their corresponding equations.

Ion channel gating variables	Equations
$\alpha_m, \alpha_p, \alpha_n, \alpha_s$	$\dfrac{A(V+B)}{1-e^{\frac{(-V-B)}{C}}}$
$\alpha_h, \beta_m, \beta_p, \beta_n, \beta_s$	$\dfrac{A(-V-B)}{1-e^{\frac{(V+B)}{C}}}$
β_h	$\dfrac{A}{1+e^{\frac{(-V-B)}{C}}}$
α_q	$Ae^{\frac{(-V-B)}{C}}$
β_q	$\dfrac{A}{e^{\frac{(-V-B)}{C}}}$

Table 4. Rate constants (A), half-activation potentials (B), and slope factors (C) for motor and sensory axon.

	A (ms^{-1}; T_{ref} = 20°C)		Half-activation potential, B (mV)		Slope factor, C (mV)	
	Motor	Sensory[a]	Motor	Sensory[a,b]	Motor	Sensory[a]
α_m	1.86	1.778	20.4	20.2	10.3	
β_m	0.0861	0.0824	25.7	25.5	9.16	
α_p	0.01	0.0096	27.0	26.8	10.2	
β_p	0.00025	0.00024	34.0	33.8	10.0	
α_h	0.0619	0.075	113.8	112.5	11.0	8.4
β_h	2.294	2.800	31.8	30.5	13.4	10.2
α_n	0.008		83.2		1.1	
β_n	0.0142		66		10.5	
α_s	0.00097		23.5		12.7	
β_s	0.00059		91.1		11.7	
α_q, β_q	0.0009		107.3	101.0	12.2	

[a] Changes of sensory to motor sodium channel activation gate (m, p) and inactivation gate (h) similar to that in Howells et al.[22]

[b] Depolarization of the half-activation of HCN-channels by 6.3 mV (see text).

The temperature dependencies are given by Q_{10} (Q_{10} = 2.2 for m-and p-gate, Q_{10} = 2.9 for h-gate, and Q_{10} = 3.0 for n-, s-, and q-gate). The default simulated temperature (T_{sim}) was 36°C and the reference temperature (T_{ref}) was 20°C. At t = 0, the initial conditions for the gating kinetics satisfied: [92]

$$y_{t=0} = \frac{\alpha_y}{\alpha_y + \beta_y} \tag{9}$$

where $y_{t=0}$ represents the initial state of the gates. To ensure a net zero current at resting membrane potential across the axonal membrane in the compartments with voltage-gated ion channels, a small auxiliary current is implemented to initialize the model.[93]

3

REFERENCES

1. Kieseier BC, Mathey EK, Sommer C, Hartung HP. Immune-mediated neuropathies. Nat Rev Dis Primers 4: 31, 2018.

2. Burke D, Kiernan MC, Bostock H. Excitability of human axons. Clin Neurophysiol 112: 1575-1585, 2001.

3. Franssen H. Relation between symptoms and pathophysiology in inflammatory neuropathies: Controversies and hypotheses. Neurosci Lett 596: 84-89, 2015.

4. Franssen H, Straver DC. Pathophysiology of immune-mediated demyelinating neuropathies--Part II: Neurology. Muscle Nerve 49: 4-20, 2014.

5. Yuki N, Yamada M, Koga M, et al. Animal model of axonal Guillain-Barre syndrome induced by sensitization with GM1 ganglioside. Ann Neurol 49: 712-720, 2001.

6. Blight AR. Computer simulation of action potentials and afterpotentials in mammalian myelinated axons: the case for a lower resistance myelin sheath. Neuroscience 15: 13-31, 1985.

7. Fitzhugh R. Computation of impulse initiation and saltatory conduction in a myelinated nerve fiber. Biophys J 2: 11-21, 1962.

8. Goldman L, Albus JS. Computation of impulse conduction in myelinated fibers; theoretical basis of the velocity-diameter relation. Biophys J 8: 596-607, 1968.

9. Halter JA, Clark JW Jr. A distributed-parameter model of the myelinated nerve fiber. J Theor Biol 148: 345-382, 1991.

10. Koles ZJ, Rasminsky M. A computer simulation of conduction in demyelinated nerve fibres. J Physiol 227: 351-364, 1972.

11. McIntyre CC, Richardson AG, Grill WM. Modeling the excitability of mammalian nerve fibers: influence of afterpotentials on the recovery cycle. J Neurophysiol 87: 995-1006, 2002.

12. Moore JW, Joyner RW, Brill MH, Waxman SD, and Najar-Joa M. Simulations of conduction in uniform myelinated fibers. Relative sensitivity to changes in nodal and internodal parameters. Biophys J 21: 147-160, 1978.

13. Smit JE, Hanekom T, Hanekom JJ. Modelled temperature-dependent excitability behaviour of a generalised human peripheral sensory nerve fibre. Biol Cybern 101: 115-130, 2009.

14. Stephanova DI, Bostock H. A distributed-parameter model of the myelinated human motor nerve fibre: temporal and spatial distributions of action potentials and ionic currents. Biol Cybern 73: 275-280, 1995.

15. Delmont E, Manso C, Querol L, et al. Autoantibodies to nodal isoforms of neurofascin in chronic inflammatory demyelinating polyneuropathy. Brain 140: 1851-1858, 2017.

Simulating perinodal changes observed in immune-mediated neuropathies – Impact on conduction in a model of myelinated motor and sensory axons | 59

3

16. Devaux JJ, Miura Y, Fukami Y, et al. Neurofascin-155 IgG4 in chronic inflammatory demyelinating polyneuropathy. Neurology 86: 800-807, 2016.

17. Susuki K. Node of Ranvier disruption as a cause of neurological diseases. ASN Neuro 5: 209-219, 2013.

18. Uncini A, and Kuwabara S. Nodopathies of the peripheral nerve: an emerging concept. J Neurol Neurosurg Psychiatry 86: 1186-1195, 2015.

19. Barrett EF, Barrett JN. Intracellular recording from vertebrate myelinated axons: mechanism of the depolarizing afterpotential. J Physiol 323: 117-144, 1982.

20. Burke D, Howells J, Kiernan MC. Sensory and motor axons are different: implications for neurological disease. Annals of Clinical Neurophysiology 19: 3-12, 2017.

21. Waxman SG, Kocsis JD, Stys PK. The axon New York: Oxford University Press, 1995.

22. Howells J, Trevillion L, Bostock H, Burke D. The voltage dependence of I(h) in human myelinated axons. J Physiol 590: 1625-1640, 2012.

23. Jankelowitz SK, Howells J, Burke D. Plasticity of inwardly rectifying conductances following a corticospinal lesion in human subjects. J Physiol 581: 927-940, 2007.

24. Kiernan MC, Isbister GK, Lin CS, Burke D, Bostock H. Acute tetrodotoxin-induced neurotoxicity after ingestion of puffer fish. Ann Neurol 57: 339-348, 2005.

25. Berthold CH, Rydmark M. Morphology of normal peripheral axons. In: The axon edited by Waxman SG, Kocsis JD, Stys PK: New York: Oxford University Press, p. 13 - 48, 1995.

26. Bostock H, Burke D, Hales JP. Differences in behaviour of sensory and motor axons following release of ischaemia. Brain 117 (Pt 2): 225-234, 1994.

27. Bostock H, Rothwell JC. Latent addition in motor and sensory fibres of human peripheral nerve. J Physiol 498 (Pt 1): 277-294, 1997.

28. Kiernan MC, Lin CS, Burke D. Differences in activity-dependent hyperpolarization in human sensory and motor axons. J Physiol 558: 341-349, 2004.

29. Mogyoros I, Kiernan MC, Burke D. Strength-duration properties of human peripheral nerve. Brain 119 (Pt 2): 439-447, 1996.

30. Mogyoros I, Kiernan MC, Burke D, Bostock H. Excitability changes in human sensory and motor axons during hyperventilation and ischaemia. Brain 120 (Pt 2): 317-325, 1997.

31. Ritchie JM. Physiology of axons. In: The axon, edited by Waxman SG, Kocsis JD, and Stys PK: New York: Oxford University Press, p. 68 - 96, 1995.

32. Schwarz JR, Eikhof G. Na Currents and Action-Potentials in Rat Myelinated Nerve-Fibers at 20-Degrees-C and 37-Degrees-C. Pflug Arch Eur J Phy 409: 569-577, 1987.

33. Schwarz JR, Reid G, Bostock H. Action-Potentials and Membrane Currents in the Human Node of Ranvier. Pflug Arch Eur J Phy 430: 283-292, 1995.

34. Danner SM, Hofstoetter US, Ladenbauer J, et al. Can the human lumbar posterior columns be stimulated by transcutaneous spinal cord stimulation? A modeling study. Artif Organs 35: 257-262, 2011.

35. Danner SM, Wenger C, Rattay F. Electrical stimulation of myelinated axons - An interactive tutorial supported by computer simulation. VDM Verlag Dr Müller, Saarbrücken 2011.

36. Krouchev NI, Danner SM, Vinet A, et al. Energy-optimal electrical-stimulation pulses shaped by the Least-Action Principle. PLoS One 9: e90480, 2014.

37. Waxman SG, Ritchie JM. Molecular dissection of the myelinated axon. Ann Neurol 33: 121-136, 1993.

38. Franssen H, Straver DC. Pathophysiology of immune-mediated demyelinating neuropathies-part I: neuroscience. Muscle Nerve 48: 851-864, 2013.

39. Kleinberg CS, Arroyo EJ, King C, Scherer SS. Na, K-ATPase isoforms in the PNS: Cell-type specific expression and internodal localization in myelinated axons. Journal of the Peripheral Nervous System 12: 45-45, 2007.

40. Baker M, Bostock H, Grafe P, Martius P. Function and distribution of three types of rectifying channel in rat spinal root myelinated axons. J Physiol 383: 45-67, 1987.

41. Kocsis JD, Eng DL, Gordon TR, Waxman SG. Functional differences between 4-aminopyridine and tetraethylammonium-sensitive potassium channels in myelinated axons. Neurosci Lett 75: 193-198, 1987.

42. Honmou O, Utzschneider DA, Rizzo MA, et al. Delayed depolarization and slow sodium currents in cutaneous afferents. J Neurophysiol 71: 1627-1637, 1994.

43. Mitrovic N, Quasthoff S, Grafe P. Sodium channel inactivation kinetics of rat sensory and motor nerve fibres and their modulation by glutathione. Pflugers Arch 425: 453-461, 1993.

44. Schwarz JR, Bromm B, Spielmann RP, Weytjens JL. Development of Na inactivation in motor and sensory myelinated nerve fibres of Rana esculenta. Pflugers Arch 398: 126-129, 1983.

45. Hindmarsh AC, Brown PN, Grant KE, et al. SUNDIALS: Suite of nonlinear and differential/algebraic equation solvers. Acm T Math Software 31: 363-396, 2005.

46. Hennings K, Arendt-Nielsen L, Andersen OK. Breakdown of accommodation in nerve: a possible role for persistent sodium current. Theor Biol Med Model 2: 16, 2005.

47. Hales JP, Lin CS, Bostock H. Variations in excitability of single human motor axons, related to stochastic properties of nodal sodium channels. J Physiol 559: 953-964, 2004.

48. Bostock H. The strength-duration relationship for excitation of myelinated nerve: computed dependence on membrane parameters. J Physiol 341: 59-74, 1983.

Simulating perinodal changes observed in immune-mediated neuropathies – Impact on conduction in a model of myelinated motor and sensory axons

61

3

49. Susuki K, Baba H, Tohyama K, et al. Gangliosides contribute to stability of paranodal junctions and ion channel clusters in myelinated nerve fibers. Glia 55: 746-757, 2007.

50. Susuki K, Rasband MN, Tohyama K, et al. Anti-GM1 antibodies cause complement-mediated disruption of sodium channel clusters in peripheral motor nerve fibers. J Neurosci 27: 3956-3967, 2007.

51. Susuki K, Yuki N, Schafer DP, et al. Dysfunction of nodes of Ranvier: a mechanism for anti-ganglioside antibody-mediated neuropathies. Exp Neurol 233: 534-542, 2012.

52. Kaji R. Physiology of conduction block in multifocal motor neuropathy and other demyelinating neuropathies. Muscle Nerve 27: 285-296, 2003.

53. Boyd IA, Kalu KU. Scaling factor relating conduction velocity and diameter for myelinated afferent nerve fibres in the cat hind limb. J Physiol 289: 277-297, 1979.

54. Davis FA, Schauf CL, Reed BJ, Kesler RL. Experimental studies of the effects of extrinsic factors on conduction in normal and demyelinated nerve. 1. Temperature. J Neurol Neurosurg Psychiatry 39: 442-448, 1976.

55. Lowitzsch K, Hopf HC, Galland J. Changes of sensory conduction velocity and refractory periods with decreasing tissue temperature in man. J Neurol 216: 181-188, 1977.

56. Paintal AS. Block of conduction in mammalian myelinated nerve fibres by low temperatures. J Physiol 180: 1-19, 1965.

57. Rasminsky M. The effects of temperature on conduction in demyelinated single nerve fibers. Arch Neurol 28: 287-292, 1973.

58. Kuhn A, Keller T, Lawrence M, Morari M. A model for transcutaneous current stimulation: simulations and experiments. Med Biol Eng Comput 47: 279-289, 2009.

59. Daskalova M, Stephanova DI. Strength-duration properties of human myelinated motor and sensory axons in normal case and in amyotrophic lateral sclerosis. Acta Physiol Pharmacol Bulg 26: 11-14, 2001.

60. Kovalchuk MO, Franssen H, Van Schelven LJ, Sleutjes B. Comparing excitability at 37 degrees C versus at 20 degrees C: Differences between motor and sensory axons. Muscle Nerve 57: 574-580, 2018.

61. De Jesus PV, Hausmanowa-Petrusewicz I, Barchi RL. The effect of cold on nerve conduction of human slow and fast nerve fibers. Neurology 23: 1182-1189, 1973.

62. Franssen H, Wieneke GH. Nerve conduction and temperature: necessary warming time. Muscle Nerve 17: 336-344, 1994.

63. Howells J, Czesnik D, Trevillion L, Burke D. Excitability and the safety margin in human axons during hyperthermia. J Physiol 591: 3063-3080, 2013.

64. Kiernan MC, Burke D, Andersen KV, Bostock H. Multiple measures of axonal excitability: a new approach in clinical testing. Muscle Nerve 23: 399-409, 2000.

65. Kiernan MC, Lin CS, Andersen KV, et al. Clinical evaluation of excitability measures in sensory nerve. Muscle Nerve 24: 883-892, 2001.

66. Sleutjes B, Drenthen J, Boskovic E, et al. Excitability tests using high-density surface-EMG: A novel approach to studying single motor units. Clin Neurophysiol 129: 1634-1641, 2018.

67. Burke D, Kiernan M, Mogyoros I, Bostock H. Susceptibility to conduction block - differences in the biophysical properties of cutaneous afferents and motor axons. In: Physiology of ALS and related diseases, edited by Kimura J, and Kaji R: Amsterdam: Elsevier, p. 43 - 53, 1997.

68. Nielsen VK. Sensory and motor nerve conduction in the median nerve in normal subjects. Acta Med Scand 194: 435-443, 1973.

69. Halar EM, DeLisa JA, Brozovich FV. Nerve conduction velocity: relationship of skin, subcutaneous and intramuscular temperatures. Arch Phys Med Rehabil 61: 199-203, 1980.

70. Tasaki I. Nervous transmission. Springfield, IL: C.C. Thomas, 1953.

71. Garg N, Park SB, Howells J, Vucic S, et al. Conduction block in immune-mediated neuropathy: paranodopathy versus axonopathy. Eur J Neurol 2019.

72. Cappelen-Smith C, Kuwabara S, Lin CS, Burke D. Abnormalities of axonal excitability are not generalized in early multifocal motor neuropathy. Muscle Nerve 26: 769-776, 2002.

73. Lafontaine S, Rasminsky M, Saida T, Sumner AJ. Conduction block in rat myelinated fibres following acute exposure to anti-galactocerebroside serum. J Physiol 323: 287-306, 1982.

74. Kawagashira Y, Koike H, Tomita M, et al. Morphological progression of myelin abnormalities in IgM-monoclonal gammopathy of undetermined significance anti-myelin-associated glycoprotein neuropathy. J Neuropathol Exp Neurol 69: 1143-1157, 2010.

75. Garg N, Park SB, Howells J, et al. Anti-MAG neuropathy: Role of IgM antibodies, the paranodal junction and juxtaparanodal potassium channels. Clin Neurophysiol 129: 2162-2169, 2018.

76. Misawa S, Kuwabara S, Kanai K, et al. Nodal persistent Na+ currents in human diabetic nerves estimated by the technique of latent addition. Clin Neurophysiol 117: 815-820, 2006.

77. Kwai NCG, Arnold R, Poynten AM, et al. In vivo evidence of reduced nodal and paranodal conductances in type 1 diabetes. Clin Neurophysiol 127: 1700-1706, 2016.

78. Yokota T, Saito Y, Miyatake T. Conduction slowing without conduction block of compound muscle and nerve action potentials due to sodium channel block. J Neurol Sci 124: 220-224, 1994.

79. Mirams GR, Pathmanathan P, Gray RA, et al. Uncertainty and variability in computational and mathematical models of cardiac physiology. J Physiol 594: 6833-6847, 2016.

80. Baker MD. Electrophysiology of mammalian Schwann cells. Prog Biophys Mol Biol 78: 83-103, 2002.

81. Chiu SY. Sodium currents in axon-associated Schwann cells from adult rabbits. J Physiol 386: 181-203, 1987.

82. Franssen H, Gebbink TA, Wokke JH, et al. Is cold paresis related to axonal depolarization? J Peripher Nerv Syst 15: 227-237, 2010.

83. Stephanova DI, Daskalova M. Effects of temperature on simulated electrotonic potentials and their current kinetics of human motor axons at 20 degrees C-42 degrees C. J Integr Neurosci 13: 447-464, 2014.

84. Dijkstra K, Hofmeijer J, van Gils SA, van Putten MJ. A Biophysical Model for Cytotoxic Cell Swelling. J Neurosci 36: 11881-11890, 2016.

85. Brazhe AR, Maksimov GV, Mosekilde E, Sosnovtseva OV. Excitation block in a nerve fibre model owing to potassium-dependent changes in myelin resistance. Interface Focus 1: 86-100, 2011.

86. Hageman S, Kovalchuk MO, Sleutjes B, et al. Sodium-potassium pump assessment by submaximal electrical nerve stimulation. Clin Neurophysiol 129: 809-814, 2018.

87. Han CY, Huang JY, and Waxman SG. Sodium channel Na(v)1.8 Emerging links to human disease. Neurology 86: 473-483, 2016.

88. Stephanova DI, Alexandrov AS, Kossev A, Christova L. Simulating focal demyelinating neuropathies: membrane property abnormalities. Biol Cybern 96: 195-208, 2007.

89. Stephanova DI, Daskalova MS, Alexandrov AS. Differences in membrane properties in simulated cases of demyelinating neuropathies: internodal focal demyelinations without conduction block. J Biol Phys 32: 61-71, 2006.

90. Stephanova DI, Daskalova MS. Differences between the channels, currents and mechanisms of conduction slowing/block and accommodative processes in simulated cases of focal demyelinating neuropathies. Eur Biophys J Biophy 37: 829-842, 2008.

91. Howells J, Matamala JM, Park SB, et al. In vivo evidence for reduced ion channel expression in motor axons of patients with amyotrophic lateral sclerosis. J Physiol 596: 5379-5396, 2018.

92. Hodgkin AL, Huxley AF. A Quantitative Description of Membrane Current and Its Application to Conduction and Excitation in Nerve. J Physiol-London 117: 500-544, 1952.

93. Carnevale NT, Hines ML. The NEURON Book. Cambridge University Press, 2009, p. 480.

4

Excitability of motor and sensory axons in Multifocal Motor Neuropathy

MARIA O. KOVALCHUK
HESSEL FRANSSEN
LEONARD H. VAN DEN BERG
LEONARD J. VAN SCHELVEN
BOUDEWIJN T.H.M. SLEUTJES

ABSTRACT

Objective. To assess excitability differences between motor and sensory axons of affected nerves in patients with multifocal motor neuropathy (MMN).

Methods. We performed motor and sensory excitability tests in affected median nerves of 20 MMN patients and in 20 age-matched normal subjects. CMAPs were recorded from the thenar and SNAPs from the 3rd digit. Clinical tests included assessment of muscle strength, two-point discrimination and joint position.

Results. All MMN patients had weakness of the thenar muscle and normal sensory tests. Motor excitability testing in MMN showed an increased threshold for a 50% CMAP, increased rheobase, decreased stimulus-response slope, fanning-out of threshold electrotonus, decreased resting I/V slope, shortened refractory period, and more pronounced superexcitability. Sensory excitability testing in MMN revealed decreased accommodation half-time and S2-accommodation and less pronounced subexcitability. Mathematical modeling indicated increased Barrett and Barrett conductance for motor fibers and increase in internodal fast potassium conductance for sensory fibers.

Conclusion. Excitability findings in MMN suggest myelin sheath or paranodal seal involvement in motor and paranodal detachment in sensory fibers.

Significance. Excitability properties of affected nerves in MMN differ between motor and sensory nerve fibers.

INTRODUCTION

Multifocal motor neuropathy (MMN) is a slowly progressive disorder in adults characterized by asymmetric weakness and muscle atrophy.[1-6] Sensory symptoms or signs are usually absent but have occasionally been reported in skin areas innervated by nerves with prominent motor axon loss.[7] Nerve conduction studies in MMN have shown segments in mixed nerves where impulse conduction is blocked or markedly slowed in motor axons but is normal in sensory axons. MMN is thought to be immune-mediated because approximately half of the patients have serum antibodies against ganglioside GM1 which is expressed on the nodal axolemma and perinodal myelin and because treatment with immunoglobulins improves signs and symptoms. [8-12]

The mechanism by which the immune-mediated process in MMN selectively affects motor axons is unresolved especially as, within one nerve, motor and sensory axons run close to each other and even within one fascicle.[13] Selective targeting of motor fiber GM1 may occur since the ceramide portion of GM1 in motor roots differs from that in sensory roots.[14] However, the ceramide portion is located in the bilipid membrane and is therefore unlikely to be antigenic; furthermore, the antigenic extracellular sugar portion of GM1 does not differ between motor and sensory GM1. Thus, unless the ceramide portion influences the three dimensional configuration of the sugar portion, the observed differences between motor and sensory GM1 cannot explain the selective motor vulnerability in MMN.[15] Motor and sensory axons also differ regarding expression or activity of axolemmal voltage-gated ion channels.[16-20] These differences, found at peripheral nerve level, may render motor fibers more vulnerable to develop conduction block when both motor and sensory fibers are targeted immunologically.[17,21,22]

The present study assessed if there are differences in ion channel activity between motor and sensory axons in MMN that exceed the differences between normal motor and sensory axons. In 20 MMN patients, all of whom had abnormal motor and normal sensory nerve conduction studies in the median nerve, we performed motor and sensory excitability tests of the median nerve at the wrist. The results of these tests were interpreted by mathematical modeling.

MATERIALS AND METHODS

Subjects

Patients and normal subjects gave informed consent. The investigation was performed in accordance with the Declaration of Helsinki and was approved by the local medical ethical committee. We investigated 20 patients with MMN (17 men, mean age 54.6 years, range 42-77) who fulfilled the EFNS/PNS criteria for MMN (Joint Task Force of the EFNS and the PNS, 2010)[23] and 20 age-matched normal subjects (11 men, mean age 51.2 years, range 31-71) without medical history and who did not use medication. The patients all received intravenous immunoglobulin therapy. The nerve conduction protocol to diagnose MMN consisted of bilateral investigation of arm nerves up to Erb's point (median to thenar and forearm, ulnar, radial, musculocutaneous), leg nerves up to the popliteal fossa (peroneal and tibial) and sensory conduction of the median, ulnar, radial and sural nerves. For excitability recordings, MMN patients had to have at least one of the following abnormalities on median nerve motor conduction studies: (a) conduction block in the forearm segment, defined according to criteria that take temporal dispersion into account[24], (b) demyelinative slowing, defined as distal motor latency (DML) $\geqslant$ 5.3ms, or forearm motor conduction velocity $\leqslant$ 38m/s, or CMAP duration prolongation in the forearm $\geqslant$ 30%[24], (c) motor axon loss, defined as CMAP amplitude < 3mV. Exclusion criteria for MMN patients were medication affecting peripheral nerve ion channel function (such as quinidine, lidocaine, amiodarone, sotalol, amlodipine, nilvadipine, amitriptyline), disorders potentially giving rise to peripheral neuropathy, and carpal tunnel syndrome (CTS). CTS was investigated by assessing the following antidromic sensory latency differences: (i) median versus ulnar nerve at the wrist to the 4th finger, (ii) median versus radial nerve to the 1st finger, and (iii) median nerve palm-finger segment versus median nerve wrist-palm segment with recording from the 3rd finger. If any of these latency differences exceeded 0.4ms, CTS was considered possible and the patient was excluded.

Temperature

Prior to excitability testing the median nerve was warmed by wrapping the forearm and hand for 30 minutes in a warm water blanket through which water of 37°C flowed constantly (Cincinnati Sub-zero Norm-O-Temp with Cincinnati Sub-zero maxi-therm lite infant hyper-hypothermia blanket for single patient use). During excitability testing the forearm and hand were kept in the blanket in order to keep nerve temperature constant. This warming time is based on previous studies.[25-27] Skin temperature was measured by means of a temperature sensor near the stimulating electrode. Since changes in DML were shown to more accurately reflect changes in nerve temperature than skin

temperature, DML was monitored every 1.6 seconds throughout each excitability test.[25] For excitability testing only, DML was defined as the point where the CMAP deviated 10% of its amplitude from baseline to peak. The change in distal motor and sensory latencies during testing was obtained by subtracting the mean of the first three values from the mean of the last three values.

Excitability testing

Excitability was measured in median motor and sensory axons at the wrist using Viking IV EMG apparatus (Nicolet Biomedical, Inc., Madison, Wisconsin), coupled to QTRAC-S software controlling the stimulation and acquisition using a data acquisition device (National Instruments Model PCI-6221) sampling at 10 kHz (TRONDNF, version 19-06-2015, institute of Neurology, Queen Square, London, UK) and an isolated bipolar constant current stimulator (DS5, Digitimer, UK). The Viking IV EMG amplified the signal with gain 40 (motor recordings) and 10000 (sensory recordings) and filters 20Hz to 10kHz for motor and 20Hz to 2kHz for sensory recordings. Non-polarizable surface electrodes (Red Dot, 3M Health Care, Germany) were used for stimulation with the cathode at the wrist and the anode 10cm proximal over the radial side of the forearm. For motor excitability tests, the CMAP of the abductor pollicis brevis muscle was recorded by surface electrodes in belly-tendon montage. For sensory excitability tests, the 3rd digit sensory nerve action potential (SNAP) was recorded by disposable ring electrodes (Natus, USA) around the proximal and distal interphalangeal joints. Conditioning stimuli were constant currents that either slightly depolarized resting membrane potential, slightly hyperpolarized resting membrane potential, or induced nerve action potentials. Except for assessment of charge-duration properties where 5 different test stimuli lengths were used, threshold changes induced by conditioning stimuli were assessed by test stimuli of 1.0 ms duration, both for motor and sensory excitability tests,[20] thereby allowing comparison between both axon types.[18,20] Threshold was defined as the test stimulus current needed for a target response (CMAP or SNAP) of 40% of its maximal amplitude.

Each excitability test comprised: stimulus response (SR) curve (relation between stimulus current and response amplitude), charge duration (Qt) relation (relation between stimulus charge (Q) and stimulus duration (t) with values for (t) being 0.2, 0.4, 0.6, 0.8, and 1.0 ms), threshold electrotonus (time course of threshold changes before, during and after a slight depolarizing conditioning current (not eliciting action potentials) or a slightly hyperpolarizing conditioning current; these conditioning currents were 40% or 20% of the current for an unconditioned target response), I/V relation (current-voltage relation: relation between the magnitude of a 200 ms duration conditioning current (varying from +50% [depolarizing] to -100% [hyperpolarizing]) and the threshold at the end of the conditioning current), recovery cycle (threshold changes estimated at

various intervals between 2 ms and 200 ms after a supramaximal conditioning stimulus eliciting action potentials).

We analyzed the following excitability indices: test stimulus current for a CMAP of 50% of its maximal amplitude, slope of the normalized SR curve (SR-slope), rheobase (slope of the Qt relation), strength-duration time constant (absolute value of the x-intercept of the Qt relation), TEd90-100 (threshold decrease at the end of the 40% depolarizing conditioning stimulus), TEdpeak (peak depolarizing threshold decrease during 40% depolarizing conditioning stimulus), S2-accommodation, second slow component of the accommodation to depolarization (difference between TEdpeak and TEd90-100), accommodation half-time (time between the onset of the conditioning stimulus and the time point where threshold decrease is halfway between TEdpeak andTEd90-100), TEh90-100 (threshold increase at the end of the 40% hyperpolarizing conditioning stimulus), resting and minimal I/V slope (slope between -10% and +10% conditioning stimuli and smallest slope in the hyperpolarizing part), refractory period (time between conditioning stimulus and return of threshold to baseline), 30% refractory period (time between conditioning stimulus and return of threshold to 30% above its unconditioned value), superexcitability (lowest threshold after refractory period), and subexcitability (highest threshold after superexcitability).

Excitability testing was performed 1 week prior to the next IVIg infusion in 16 patients; 3 patients were newly recruited and the excitability was assessed before their first treatment; 1 patient had his last IVIg infusion 10 years ago.

Clinical tests

Median nerve motor and sensory functions were tested clinically by (i) medical research council (MRC) grading of the abductor pollicis brevis muscle, (ii) joint position sense of the distal phalangeal joint of the middle finger for random 10 movements, (iii) static 2-point discrimination of the distal phalanx of the middle finger by an aesthesiometer (Downs, A-070-01-G) according to normative two point discrimination threshold values assessed by Van Nes et al (2008).[28]

Mathematical modeling

To investigate biophysical changes that may underlie altered excitability properties in MMN, the thresholds and their changes obtained during excitability recordings from MMN patients and normal subjects were fitted to an established mathematical model of the human myelinated axon using the MEMfit tool in QTRAC software.[18,29-31] First, a normal motor model was obtained from the motor excitability recordings of the normal

subjects. Second, the normal motor model was fitted to match the sensory excitability recordings in normal subjects, which was subsequently used to construct a normal sensory model. Third, the normal motor model was fitted to match the mean motor excitability recordings of the 20 MMN patients. Fourth, the normal sensory model was fitted to match the mean sensory nerve excitability recordings of the 20 MMN patients. Fifth, the normal motor model was fitted to match the motor excitability recordings of every individual MMN patient.

In all these procedures, 15 parameters were allowed to vary until fitting provided no further improvement. These parameters included 12 conductances , 2 permeabilities (nodal transient sodium permeability in cm^3 per second and persistent permeability as percentage of transient permeability) and pump currents. As resting membrane potential was not clamped, any change in the above described parameters was allowed to change resting membrane potential. Temperature effects on ion channels are taken into account by the Q_{10} values of gating kinetics.[19-29] To consider a small skin – nerve temperature gradient (Howells et al 2013), temperature was set at 34°C, which was kept unchanged throughout modeling. The discrepancy between excitability recordings and simulations was calculated by weighing the errors in the four excitability tests using the following factors: 0.5 (strength-duration), 2 (threshold electrotonus, as the changes to both ±40% and ±20% conditioning stimuli were modeled),1 (recovery cycle), and 1 (current-threshold).[33-34] The error between simulated threshold and mean of the recorded threshold was further weighed by the standard deviation at every recorded threshold.

Normal sensory model

To obtain the normal sensory model, we first adjusted the gating kinetics for sensory axons and varied the half-activation potential for hyperpolarization-activated cyclic nucleotide-gated (HCN) channels to account for the high variance in excitability recordings between subjects, as described by others.[18,33,35] Next, the above described 15 input parameters were varied in steps where not more than one parameter was changed at a time to avoid local optimization and over-fitting. By means of this procedure, we obtained the most likely prominent parameter underlying the biophysical difference between motor and sensory axons. Finally, to obtain an accurate reference model for comparison with sensory nerve excitability recordings in MMN, the sensory nerve excitability recordings of our normal subjects were fitted by allowing all 15 input parameters to vary yielding the normal sensory model.

4

Modeling motor excitability in MMN

In order to define a morphological component, the normal motor model was fitted to the mean motor excitability recordings of the 20 MMN patients by also varying the nodal and internodal membrane capacitance, myelin capacitance, and relative internodal length. Hence, next to the 15 parameters described above, this resulted in 19 input parameters being varied. Only one parameter was allowed to change at a time to determine the most prominent parameter that best explains the excitability differences between motor axons in MMN patients and normal subjects.

Modeling individual motor excitability in MMN

Excitability differences between MMN patients and normal subjects may result from physiological variability, pathophysiological variability, or both. We assumed that larger excitability differences are most likely related to pathophysiological changes whereas smaller differences can be the result of either physiological differences or small pathophysiological differences. Because the motor excitability recordings varied considerably between individual patients, they were ranked from most to least abnormal by assessing the weighted root mean square error (RMSE) for all four excitability tests. This was calculated by $\sqrt{(\Sigma \ [(X_{MMNi} - X_{HC\_\mu}) / X_{HC\_SD}]^2 / N)}$, where X_{MMNi} is the threshold for MMN patient i (i = 1 to 20), X_{HC_μ}, the mean threshold for normal subjects, X_{HC_SD} the standard deviation of the threshold for normal subjects, and N the number of thresholds. A weighed mean RMSE was then determined using the same weighting factors as described above.

Next, we applied the same fitting procedure as described above using the 19 input parameters to determine the single most prominent parameter which best explained the discrepancy within every individual MMN patient. This parameter has the highest rank (largest error reduction), which likely varies between individual patients. Within a patient, an individual fit may also yield a few single parameters that have approximately the same error reduction making them equally probable of explaining the excitability differences. Therefore, the parameter which is consistently highly ranked by showing a large error reduction within all MMN patients, will be the most interesting one. To preserve this highly relevant information for every parameter, their 20 error reductions, obtained from the 20 individual fits, were added together to yield a summed error reduction for every single parameter. Finally, we ranked the 19 parameters based on their summed error reduction from most to least reduction. This gives, complementary to modeling only the mean excitability differences between normal subjects and MMN patients, an additional indication on which single most prominent parameter is consistently high ranked in the analyses.

Modeling sensory excitability in MMN

The normal sensory model was fitted to match the mean sensory nerve excitability recordings in MMN by varying the above described 19 input parameters. Again, only one input parameter was varied per step.

Statistical analysis

Excitability indices in patients and normal subjects were compared by Mann-Whitney's U-test since the data was not normally distributed. Correlations between motor excitability indices versus anti-GM1antibodies, disease duration and CMAP amplitude were assessed by univariate analysis. Data is given as median unless specified otherwise. SPSS (version 22; IBM) was used for all analyses. P<0.05 was considered significant.

4

RESULTS

Clinical characteristics, laboratory results and nerve conduction study findings in MMN patients are presented in Table 1.Thenar muscle strength was decreased in all patients, whereas sensory tests were normal. No significant change in the median value of DML and DSL per excitability test was found both in MMN patients and normal subjects. It is therefore likely that nerve temperature changed very little during each individual excitability test.

Table 1. Characteristics of 20 MMN patients.

Age, mean (range)	54.6 years (42 – 77)
Gender	17 men, 3 women
Disease duration, mean (range)	117 months (13-378)
GM1 antibodies	8 patients (40%)
MRC score APB (number of patients)	0(1), 1(1), 2(4), 3(8), 4(6)
2-point discrimination in mm (number of patients)	1(1), 2(1), 3(5), 4(9), 5(4)
Joint position test	normal in 20 patients
DML demyelinating (>5.3ms)	8 (40%)
MCV demyelinating (<38m/s)	6 (30%)
Definite conduction block (CMAP area drop >50%)	9 (45%)
Possible conduction block (CMAP area drop >30%)	7 (35%)
Increased temporal dispersion (CMAP dur. prol. >30%)	10 (50%)
Distal CMAP amplitude <3mV (lower limit)	5 (25%)
Median CMAP amplitude (range), mV	13.7 (18.1)
Distal SNAP amplitude <7µV (lower limit)	0
Median SNAP amplitude (range), µV	30 (30)

MMN = multifocal motor neuropathy. MRC score = medical research council score. APB = abductor pollicis brevis muscle. DML = distal motor latency. MCV = motor conduction velocity. CMAP = compound muscle action potential. SNAP = sensory nerve action potential of 3rd digit. Dur. prol. = duration prolongation of the negative part of the CMAP on elbow versus wrist stimulation. Nerve conduction parameters obtained from the median nerve.

Excitability indices

Motor excitability in MMN (compared to normal subjects) showed an increased stimulus current for a CMAP of 50% of its maximal amplitude, decreased SR-slope, increased rheobase, fanning-out of threshold electrotonus (more positive TEd90-100ms, more negative TEh90-100ms, more positive TEdpeak), decreased resting I/V slope, shortened refractory period and more pronounced threshold changes during superexcitability (Table 2, Fig 1). Sensory excitability in MMN (compared to sensory excitability in normal subjects) showed

decreased S2-accommodation, decreased accommodation half-time and less pronounced threshold changes during subexcitability (Table 2, Fig 1). Thus, the number of significantly abnormal excitability indices was less in sensory than in motor axons (3 versus 9) and none of the indices that were significantly abnormal in sensory axons were so in motor axons.

Table 2. Excitability indices in MMN patients and normal subjects (n=20, median values).

	Motor			Sensory			P-value MMN motor vs MMN sensory	P-value healthy motor vs healthy sensory
	MMN	Normal	P-value	MMN	Normal	P-value		
I50% (mA)	6.15 (3.86)	3.90 (1.56)	0.01	3.10 (0.95)	2.69 (0.90)	ns	<0.001	<0.001
SR slope	3.07 (1.91)	4.35 (0.90)	0.01	1.67 (0.34)	1.78 (0.37)	ns	0.005	<0.001
SDTC (ms)	0.47 (0.07)	0.43 (0.06)	ns	0.51 (0.16)	0.54 (0.12)	ns	Ns	ns
Rheobase (mA)	3.68 (2.58)	2.59 (1.02)	0.03	1.93 (0.75)	1.46 (0.51)	ns	<0.001	<0.001
TEd90-100 (%)	50.42 (6.21)	44.25 (2.84)	<0.001	44.95 (4.65)	43.24 (3.35)	ns	<0.001	ns
TEh90-100 (%)	-135.20 (50.55)	-116.20 (14.04)	0.02	-89.14 (17.69)	-86.21 (11.74)	ns	<0.001	<0.001
TEdpeak (%)	70.77 (7.50)	65.60 (3.61)	0.001	58.50 (4.47)	58.73 (3.87)	ns	<0.001	<0.001
S2-acc. (%)	20.98 (3.92)	22.29 (3.13)	ns	13.42 (2.62)	16.29 (1.98)	0.02	<0.001	<0.001
Acc. half-time (ms)	36.56 (4.99)	36.34 (2.76)	ns	32.64 (2.82)	36.18 (3.69)	0.01	0.019	ns
Resting I/V slope	0.55 (0.10)	0.60 (0.06)	0.01	0.76 (0.13)	0.71 (0.11)	ns	<0.001	0.009
Minimal I/V slope	0.25 (0.06)	0.24 (0.04)	ns	0.28 (0.03)	0.26 (0.04)	ns	0.012	ns
RP (ms)	2.48 (0.28)	2.85 (0.24)	0.01	2.94 (0.83)	3.42 (0.53)	ns	0.002	<0.001
Superexcitability (%)	-27.86 (11.81)	-20.04 (4.45)	0.02	-11.14 (6.86)	-12.63 (6.12)	ns	<0.001	<0.001
Subexcitability (%)	16.66 (10.68)	16.69 (5.49)	ns	8.77 (3.24)	12.63 (4.11)	0.01	<0.001	0.009
30% RP (ms)	2.17 (0.14)	2.25 (0.14)	ns	2.40 (0.25)	2.50 (0.28)	ns	ns	0.009

MMN = multifocal motor neuropathy; $I_{50\%}$ = stimulus current needed to elicit a compound muscle or sensory action potential of 50% of its maximal amplitude; SR slope = maximal slope of stimulus response curve; SDTC = strength duration time constant; TEd = depolarizing threshold electrotonus; TEh = hyperpolarizing threshold electrotonus; TEdpeak = peak depolarizing threshold decrease during 40% depolarizing conditioning stimulus; S2-acc. = S2-accommodation; RP= refractory period; 30% RP = time between conditioning stimulus and return of threshold to 30% above its unconditioned value; ns = not significant (p> 0.05 for Mann-Whitney test).

Figure 1. Motor and sensory nerve excitability recordings in MMN and normal subjects.
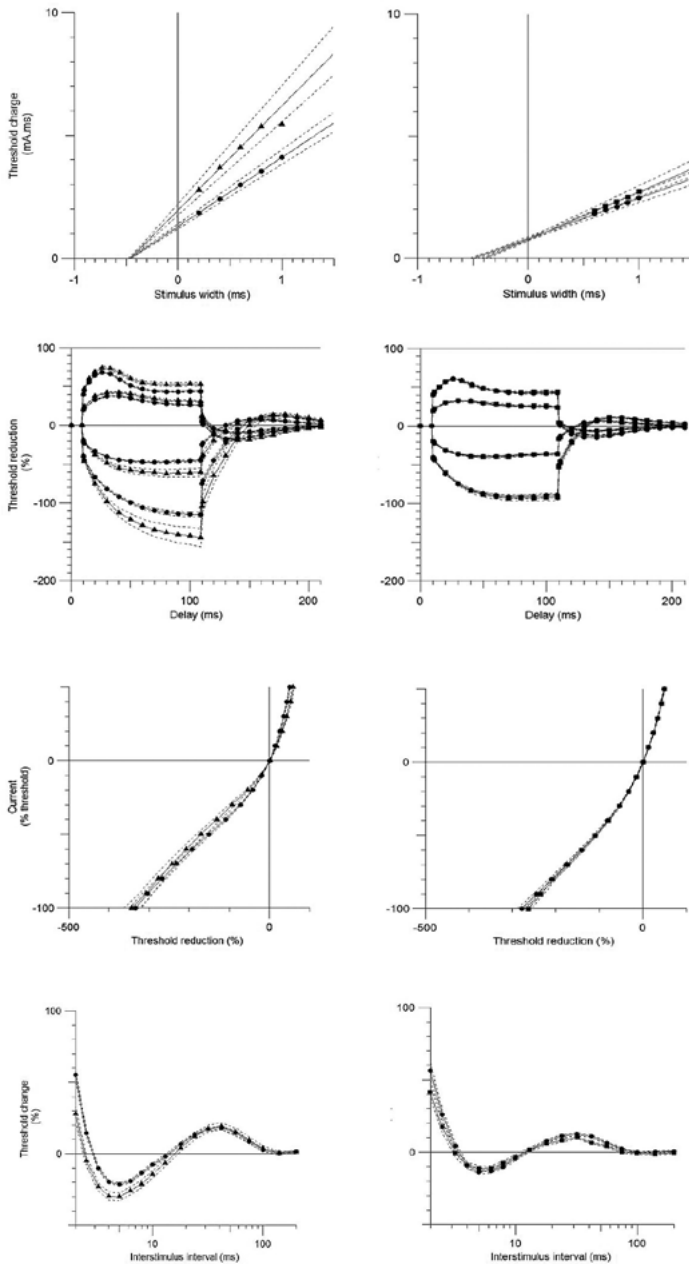

Figure 1 legend. Motor (left column), sensory (right column); normal subjects (●); MMN (▲). From top to bottom: the strength-duration relationship plotted as charge vs. stimulus duration, threshold electrotonus, current-voltage relationship, and the recovery cycle. Data presented as mean ± SE.

Sensory excitability compared to motor excitability in MMN patients showed significantly smaller test stimulus current for a 50% of an action potential maximal amplitude, smaller SR-slope, smaller rheobase, less positive TEd90-100, less negative TEh90-100, smaller S2-accommodation, smaller half-time accommodation, less positive TEdpeak, steeper resting I/V-slope, longer refractory period, and less pronounced threshold changes during superexcitability and subexcitability. Similar statistically significant differences were found between motor and sensory excitability indices of normal subjects where sensory excitability showed smaller SR-slope, smaller rheobase, less negative TEh90-100, smaller S2-accommodation, less positive TEdpeak, steeper resting I/V-slope, longer refractory period, and less pronounced threshold changes during superexcitability.

Correlation with laboratory, clinical and electrophysiological characteristics

No significant correlations were found between motor nerve excitability variables, anti-GM1 antibodies, disease duration and CMAP amplitude.

Modeling

Sensory excitability in normal subjects

Fitting the normal motor model to match the normal sensory nerve excitability recordings indicated that sensory axons were slightly more depolarized than motor axons (nodal resting membrane potential from -81.9 mV to -80.1 mV). Because we allowed resting membrane potential to vary with changes in other parameters (see methods), a more depolarized half-activation potential for HCN channels (Bq from -107.3 mV to -101.0 mV) and a decrease in relative nodal and internodal slow potassium conductance (Ks from 1.14 to 0.85) resulted in depolarization of resting membrane potential.

Modeling motor excitability in MMN

Fitting the mean motor excitability recordings in MMN to the normal motor model showed that the largest error reduction (52.2%) was achieved by a moderate increase in Barrett and Barrett conductance from 38.1 nS to 43.4 nS (Table 3). The second best fit was obtained with a membrane hyperpolarization of 1 mV which resulted in an error reduction of 51.6%.

Table 3. Modeling motor excitability in MMN.

Parameter*	Normal motor model	Best parameter fit	Error reduction (%)
Barrett andBarrett cond. (nS)	38.1	43.4	52.2
RMP, (mV)**	-81.9	-82.9	51.6
Internodal leak cond. (nS)	4.0	1.2	36.2
Relative nodal and internodal leak cond.	0.95	0.49	35.8
Relative K-cond.	0.84	0.80	31.4
Nodal leak cond. (nS)	1.70	0.03	30.2
Internodal fast K-cond. (nS)	92	46	29.1
Relative nodal and internodal fast K-cond.	1.0	0.83	25.5
Relative internodal length	1	0.9	17.0
Nodal fast K-cond. (nS)	19.1	15.9	16.1
% of persistent Na-perm. (%)	1.1	1.17	13.2
Nodal slow K-cond.(nS)	56.7	50.1	12.5
Relative nodal and internodal slow K-cond.	1.14	1.08	11.1
Ih cond. (nS)	6.9	4.3	8.2
Capacitance internode (pF)	0.327	0.308	6.1
Capacitance node (pF)	1.4	1.5	2.5
Capacitance myelin (pF)	1.55	1.65	1.4
Internodal slow K-cond. (nS)	0.685	0.685	0.0
Nodal Na-perm. (cm^{3}s^{-1} x 10^{-9})	4.35	4.35	0.0

* Ranking based on error reduction (from largest to least); ** Changes based on varying pump currents; Cond. = conductance; RMP = resting membrane potential; perm. =permeability; Ih = hyperpolarization-activated current.

Modeling individual motor excitability in the six most abnormal patients

Individual motor nerve excitability recordings from MMN patients had large RMSEs (median 2.0, range 0.6 – 6.4; Fig 2). The six MMN patients with RMSE exceeding 3.0 are described here. In a patient with RMSE 6.4, modeling suggested an increase in the Barrett and Barrett conductance (from 38.1 nS to 68.5 nS; error reduction 79%); the second best fit suggested a decrease in relative nodal and internodal leak conductance (from 0.95 to 0.01; error reduction 45%). In another patient with RMSE 5.0, the best fit was obtained by a hyperpolarizing resting membrane potential from -81.9 mV to -85.5 mV, resulting in a 36% error reduction, closely followed by an increased Barrett and Barrett conductance from 38.1 nS to 54.5 nS giving an error reduction of 33%. In the four other

patients modeling suggested a decreased internodal fast potassium conductance in one patient (from 92 nS to 22 nS; error reduction 25%), increased Barrett and Barrett conductance in two patients (from 38.1 nS to 58.7 nS and 54.2 nS; error reductions 63% and 59%), and a relative decrease in nodal and internodal leak conductance in one patient (from 0.95 nS to 0.29 nS; error reduction 17%). Arithmetic summation of the individual error reductions for every parameter in the six MMN patients with RMSE > 3.0, showed that the largest summed error reductions were obtained by increasing Barrett and Barrett conductance (summed error reduction 253%), followed by hyperpolarizing resting membrane potential (summed error reduction 189 %) and decreasing relative nodal and internodal leak conductance (summed error reduction 131%).

4

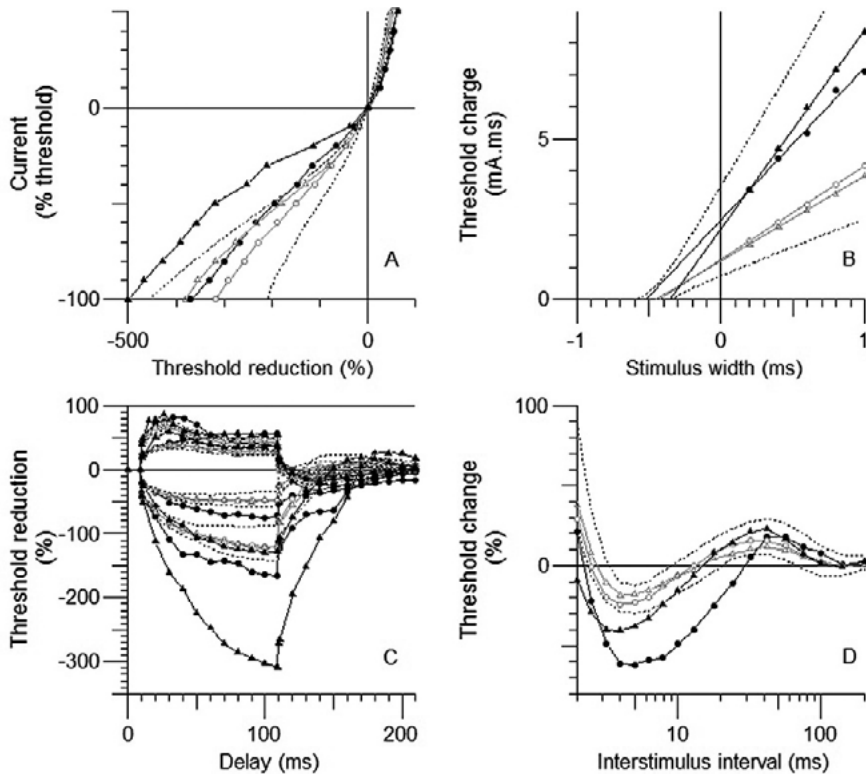**Figure 2.** Motor nerve excitability recordings of 4 MMN patients.

Figure 2 legend. (A) current-voltage relationship, (B) strength-duration relationship plotted as charge vs. stimulus duration, (C) threshold electrotonus, (D) recovery cycle. These four MMN patients compromised two MMN patients with the largest discrepancy (RMSE = 5.0 and 6.4; (▲), (●)), and two MMN patients with the least discrepancy (RMSE = 0.6 and 0.6; (Δ), (○)) compared to normal subjects. Dotted lines represent 95% confidence limits of normal subjects.

Modeling individual motor excitability in all MMN patients

When the above described procedure was applied to all 20 individual motor nerve excitability recordings in MMN, variations in the Barrettand Barrett conductance remained the highest ranked with a summed error reduction of 550%, the variations consisting of an increase in 16 patients and a decrease in 4 patients. This was followed by changes in resting membrane potential resulting in a summed error reduction of 446%, the changes being hyperpolarizing in 16 patients, depolarizing in 3 patients and none in 1 patient). Changes in relative nodal and internodal leak conductance accounted for a summed error reduction of 366 %, the changes consisting of an increase in 5 patients, a decrease in 14 patients and none in 1 patient (Table 4).

Modeling sensory excitability in MMN

Fitting the normal sensory model to match the sensory nerve excitability recordings in MMN showed that the largest error reduction (37%) was obtained by increasing the internodal fast potassium conductance (from 170 nS to 268 nS). In none of the sensory recordings of individual MMN patients, RMSE exceeded 3.0 (median 1.4, range 0.6 – 2.4).

Motor excitability indices from every individual MMN patient and normal subject were plotted against their corresponding sensory excitability indices (Fig. 3). The abnormal motor excitability indices (changes in horizontal direction) showed visually no clear overlap with the sensory excitability indices in MMN (changes in vertical direction, Fig 3).

Table 4. Modeling individual motor excitability in MMN.

Parameter*	Normal motor model	Best parameter fit	Error reduction (%)**	
		Median (range)	Median (range)	Summed
Barrett andBarrett cond., (nS)	38.1	42.8(34.0 – 68.5)	17.2 (6.0 – 79.4)	550
RMP, (mV)***	-81.9	-82.6 (-85.5 - -80.3)	16.1 (0 – 77.7)	446
Relative leak cond.	0.95	0.6 (<0.01 – 1.9)	14.4 (0 – 49.7)	366
Internodal leak cond. (nS)	4.0	1.5 (0.01 – 9.9)	13.1 (1.3 – 44.7)	345
Internodal fast K-cond. (nS)	92	47 (16 – 298)	12.3 (0 – 42.5)	317
Ih cond. (nS)	6.9	5.6 (0.1 – 45.5)	10.4 (0 – 48.0)	266
Capacitance node (pF)	1.4	1.5 (0.5 – 3.2)	8.4 (1.4 – 36.3)	256
Nodal leak cond.(nS)	1.70	0.41 (0.01 – 5.25)	10.5 (0 – 25.9)	229
Nodal and internodal fast Relative K-cond.	1.0	0.84 (0.83 – 1.34)	10.1 (0 – 22.6)	202
Nodal slow K-cond. (nS)	56.7	52.6 (50.3 – 70.8)	8.0 (0 – 35.8)	196
Nodal and internodal slow Relative K-cond.	1.14	1.06 (1.01 – 1.54)	8.2 (0 – 33.7)	194
Relative K-cond.	0.84	0.80 (0.79 – 0.96)	7.9 (0 – 27.0)	183
Nodal fast K-cond. (nS)	19.1	16.1 (15.1 – 27.5)	7.6 (2.5 – 20.8)	162
Relative internodal length	1	0.93 (0.79 – 1.39)	5.8 (0 – 22.9)	156
% of persistent Na-perm. (%)	1.1	1.17 (0.77 – 1.17)	5.6 (1.5 – 32.1)	156
Capacitance internode (pF)	0.327	0.308 (0.26 – 0.36)	4.9 (0 – 28.2)	152
Capacitance myelin (pF)	1.55	1.60 (1.50 – 2.85)	1.5 (0 – 36.7)	147
Internodal slow K-cond. (nS)	0.685	0.685 (0.33 – 36.5)	1.3 (0 – 16.2)	60
Nodal Na-perm. (cm^{3}s^{-1} x 10^{-9})	4.35	4.35 (3.3 – 4.35)	0 (0 – 35.5)	48

4

* Ranking based on the summed error reduction (from most to least); ** The median, range and summed error reductions obtained from the 20 individual fits for every parameter; *** Changes based on varying pump currents; Cond. = conductance; RMP = resting membrane potential; Ih = hyperpolarization-activated current; perm. = permeability.

Figure 3. Sensory nerve excitability indices plotted against motor nerve excitability indices within every normal subject and every MMN patient.
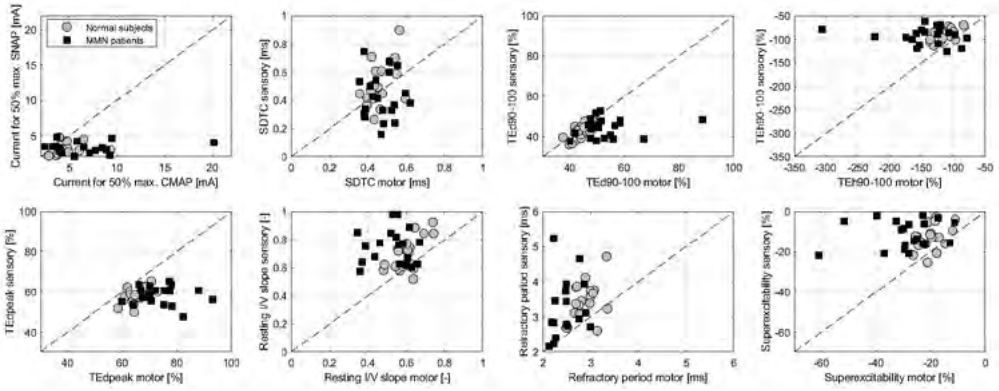

Figure 3 legend. Normal subjects (●, n = 20); MMN (■, n = 20). CMAP = compound muscle action potential; SNAP = sensory nerve action potential; SDTC = strength duration time constant; TEd = depolarizing threshold electrotonus; TEh = hyperpolarizing threshold electrotonus; I/V: current-voltage relation. Dotted lines represent unity line (y = x).

Correlation of motor excitability with modeling parameters

Considering, that the best fit of motor excitability in MMN to the normal motor model was achieved with increase in Barrett and Barrett conductance, we investigated the correlation between excitability parameters and Barrett and Barrett conductance. Using univariate linear regression, positive correlation with Barrett and Barret conductance was shown for both TEh90-100 (r = -0.90, p<0.001) and superexcitability (r = -0.56, p = 0.01) (Fig 4).

Figure 4. Correlation between TEh90-100 with Barrett and Barrett conductance (A) and superexcitability with Barrett and Barret conductance (B) in motor axons of MMN patients.
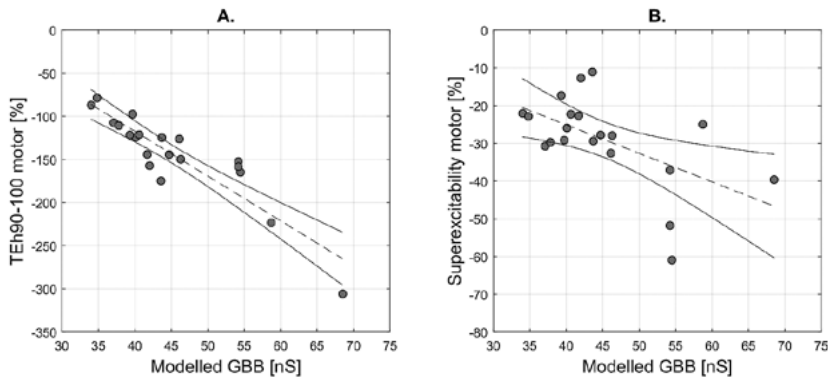

Figure 4 legend. Univariate linear regression showed r = -0.90, p<0.001 for (A); r = -0.56, p = 0.01 for (B).

Due to relatively small differences in RMSE between sensory healthy and sensory MMN compared to motor healthy and motor MMN, the risk was high to obtain false positive results, and the correlation analysis was not performed for this set of data.

DISCUSSION

Excitability studies of affected median nerves in MMN patients from the same site at the wrist showed different abnormalities in motor and sensory fibers. The excitability differences between motor and sensory axons in our normal subjects were qualitatively similar to those found in other studies.[20,22,36-39] Mathematical modeling showed that motor excitability changes in MMN were best explained by an increase in Barrett and Barrett conductance and the slight sensory excitability changes by an increase in fast potassium conductance. Importantly, the magnitude of the changes in Barrett and Barrett conductance varied in individual patients from minor to considerable.

The Barrett and Barrett conductance was proposed to explain the depolarizing and hyperpolarizing afterpotentials which occur as slow and small potential changes after an action potential.[40] It was hypothesized as a relatively low resistance pathway from the internodal peri-axonal space to the extracellular fluid via: (i) the myelin sheath, and (ii) the paranodal seals. The former might be represented anatomically by a radial pathway through non-compact myelin which was shown to pass low molecular weight fluorescent dyes and which would pass currents about a million times faster than helical paths.[41,42] Initially it was suggested that this radial path was formed by connexin-32 gap junctions. Subsequent studies made it likely that it is formed by gap junction complexes consisting of coupled connexin-29 and Kv1

ion channels that may form connections between axoplasm and Schwann cell cytoplasm of adjacent myelin layers lying over the juxtaparanode.[43]The second component of the Barrett and Barrett conductance, the paranodal seal, is represented anatomically by the septate-like junctions between peri-nodal Schwann cell loops and paranodal axolemma that were found on electron microscopy. These junctions are made of contactin, contactin associated protein, ceramide galactosyltransferase, neurofascin-155, and neurofascin-186 complexes.[44,45] The increased Barrett and Barrett conductance in our MMN patients may therefore be explained by demyelination, as found in some pathology studies,[46-47] as well as by paranodal detachment.

A previous excitability study in MMN patients, performed at sites distal to conduction block, showed changes closely resembling the changes induced by passing a hyperpolarizing DC-current through the nerve during excitability testing (except for late subexcitability which was normal in MMN but decreased during application of hyperpolarizing DC-currents).[48] It was hypothesized that sodium-potassium pumps failed at the lesion site (leading to increased inward persistent sodium current) and were hyperactive at adjacent healthy sites in order to remove the intra-axonal excess of sodium ions (leading to hyperpolarization of resting membrane potential since the pump expels more sodium ions than it puts back potassium ions into the axon. A subsequent motor excitability study in MMN revealed fanning out of threshold electrotonus and increased threshold changes during superexcitability.[49] Contrary to our results, modeling was consistent with loss of persistent sodium channel permeability and loss of potassium conductance which were explained by loss of protein expression distal to the site of conduction block, a difference that might be related to inclusion of nerves with demyelinative slowing only in our study. Remarkably, only one out of 11 sera of these MMN patients stained paranodal structures in teased rat nerve fibers.[49] Comparing motor to sensory excitability of MMN patients and normal controls in current study demonstrates a range of complicated changes in membrane properties of the motor nerves in MMN (Table 2, Fig 3).

The present study suggests that sensory axons in MMN could be mildly affected by a mechanism leading to an increase in fast potassium conductance. Such an increase would be consistent with the above described concept for motor axons of a leaky myelin sheath due to paranodal seal loss or demyelination, resulting in easier access to fast juxtaparanodal potassium channels, being an early stage of the nerve changes in MMN.

CONCLUSION

Excitability findings in MMN suggest demyelination or paranodal seal loss in motor axons and slight changes in sensory axons related to an increase in internodal fast potassium conductance, possibly due to paranodal seal involvement.

REFERENCES

1. Nobile-Orazio E. Multifocal motor neuropathy. J Neuroimmunol. 2001;115:4-18.

2. Nobile-Orazio E, Cappellari A, Priori A. Multifocal motor neuropathy: current concepts and controversies. Muscle Nerve 2005;31:663– 80.

3. Olney RK, Lewis RA, Putnam TD, Campellone JVJ. Consensus criteria for the diagnosis of multifocal motor neuropathy. Muscle Nerve 2003 27:117–121.

4. Slee M, Selvan A, Donaghy M. Multifocal motor neuropathy: the diagnsotic spectrum and response to treatment. Neurology 2007;69:1680-7.

5. Umapathi T, Hughes RA, Nobile-Orazio E, Léger JM. Immunosuppressant and immunomodulatory treatments for multifocal motor neuropathy. Cochrane Database Syst Rev. 2009;(1):CD003217.

6. Vlam L, van der Pol WL, Cats EA, Straver DC, Piepers S, et al. Multifocal motor neuropathy: diagnosis, pathogenesis and treatment strategies. Nat Rev Neurol. 201122;8:48-58.

7. Delmont E, Benaïm C, Launay M, Sacconi S, Soriani MH, Desnuelle C. Do patients having a decrease in SNAP amplitude during the course of MMN present with a different condition? J Neurol. 2009;256:1876-80.

8. Nobile-Orazio E, Meucci N, Barbieri S, Carpo M, Scarlato G. High-dose intravenous immunoglobulin therapy in multifocal motor neuropathy. Neurology. 1993;43:537-44.

9. Van den Berg LH, Franssen H, Wokke JH. Improvement of multifocal motor neuropathy during long-term weekly treatment with human immunoglobulin. Neurology. 1995 ;45:987-8.

10. Léger JM, Chassande B, Musset L, Meininger V, Bouche P, Baumann N. Intravenous immunoglobulin therapy in multifocal motor neuropathy: a double-blind, placebo-controlled study. Brain. 2001;124:145–153

11. Yuki N. Acute motor axonal neuropathy and multifocal motor neuropathy: more in common than not. Muscle Nerve. 2013;48:693-5.

12. Stangel M., Gold R., Pittrow D., Baumann U., Borte M., Fasshauer M., et al. Treatment of patients with multifocal motor neuropathy with immunoglobulins in clinical practice: the SIGNS registry. Ther Adv Neurol Disord. 2016; 9: 165–79.

13. Sunderland S. Nerves and Nerve Injuries. Second Edition. Edinburgh: Churchill Livingstone, 1978.

14. Ogawa-Goto K, Abe T. Gangliosides and glycosphingolipids of peripheral nervous system myelins--a minireview. Neurochem Res. 1998;23:305-10.

4

15. Susuki K, Yuki N, Schafer DP, Hirata K, Zhang G, Funakoshi K, et al. Dysfunction of nodes of Ranvier: a mechanism for anti-ganglioside antibody-mediated neuropathies. Exp Neurol 2012; 233:534-42.

16. Neumcke B. Differences in electrophysiological properties of motor and sensory nerve fibers. J Physiol, Paris, 1981; 77:1135-1138.

17. Kiernan MC, Mogyoros I, Burke D. Differences in the recovery of excitability in sensory and motor axons of human median nerve. Brain 1996;119:1099-105.

18. Howells J, Trevillion L, Bostock H, Burke D. The voltage dependence of I(h) in human myelinated axons. J Physiol 20121;590:1625-40.

19. Hofmeijer J, Franssen H, Van Schelven LJ, Van Putten MJAM. Why are sensory axons more vulnerable for ischemia than motor axons? PLOS-one. 2013;8:e67113.

20. Kovalchuk MO, Franssen H, Van Schelven LJ, Sleutjes BTHM. Comparing excitability at 37°C versus at 20°C: Differences between motor and sensory axons. Muscle Nerve. 2018;57:574-580.

21. Bostock H, Burke D, Hales JP. Differences in behavior of sensory and motor axons following release of ischaemia. Brain 1994;117:225-34.

22. Kiernan MC, Lin CS, Andersen KV, Murray NM, Bostock H. Clinical evaluation of excitability measures in sensory nerve. Muscle Nerve 2001;24:883-92.

23. European Federation of Neurological Societies/Peripheral Nerve Society guideline on management of multifocal motor neuropathy. Report of a joint task force of the European Federation of Neurological Societies and the Peripheral Nerve Society--first revision. Joint Task Force of the EFNS and the PNS. J Peripher Nerv Syst. 2010;15:295-301.

24. Van Asseldonk JT, Van den Berg LH, Wieneke GH, Wokke JH, Franssen H.Criteria for conduction block based on computer simulation studies of nerve conduction with human data obtained in the forearm segment of the median nerve. Brain. 2006;129:2447-60.

25. Geerlings AH, Mechelse K. Temperature and nerve conduction velocity, some practical problems. Electromyogr Clin Neurophysiol 1985;25:253-9.

26. Franssen H, Wieneke GH. Nerve conduction and temperature: necessary warming time. Muscle Nerve 1994;17:336-44.

27. Drenthen J, Blok JH, Dudok van Heel EB, Visser GH. Limb temperature and nerve conduction velocity during warming with hot water blankets. J Clin Neurophysiol 2008; 25: 104-10.

28. Van Nes SI, Faber CG, Hamers RMTP, Härschnitz O, Bakkers M, Hermans MCE, et al. on behalf of the perinoms study group. Revising two-point discrimination assessment in normal aging and in patients with polyneuropathies. J Neurol Neurosurg Psychiatry 2008;79:832-4.

29. Jankelowitz SK, Howells J, Burke D. Plasticity of inwardly rectifying conductances following a corticospinal lesion in human subjects. J Physiol. 2007;581:927-40.

30. Kiernan MC, Isbister GK, Lin CS, Burke D, Bostock H. Acute tetrodotoxin-induced neurotoxicity after ingestion of puffer fish. Ann Neurol. 2005;57:339–48.

31. Bostock H. MEMFIT: a computer program to aid interpretation of multiple excitability measurements on human motor axons. Clin Neurophysiol. 2006;117:S85.

32. Howells J, Czesnik D, Trevillion L, Burke D. Excitability and the safety margin in human axons during hyperthermia. J Physiol 2013;591:3063-80.

33. Tomlinson SE, Tan SV, Burke D, Labrum RW, Haworth A, Gibbons VS, et al. In vivo impact of presynaptic calcium channel dysfunction on motor axons in episodic ataxia type 2. Brain. 2016;139:380-91.

34. Boërio D, Bostock H, Spescha, Z'Graggen WJ. Potassium and the excitability properties of normal human motor axons in vivo. PLoS One. 2014;9:e98262.

35. Tomlinson SE, Tan SV, Kullmann DM, Griggs RC, Burke D, Hanna MG, et al. Nerve excitability studies characterize Kv1.1 fast potassium channel dysfunction in patients with episodic ataxia type 1. Brain. 2010;133:3530-40.

36. Bostock H, Rothwell JC. Latent addition in motor and sensory fibers of human peripheral nerve. J Physiol 1997;498:277-94.

37. Burke D, Kiernan M, Mogyoros I, Bostock H. Susceptibility to conduction block: differences in the biophysical properties of cutaneous afferents and motor axons. In: Kimura J, Kaji R, editors. Physiology of ALS and related disorders. Amsterdam: Elsevier Science BV; 1997. p 43-53.

38. Lin CS, Kuwabara S, Cappelen-Smith C. Responses of human sensory and motor axons to the release of ischaemia and to hyperpolarizing currents. J Physiol. 2002;541:1025-39.

39. Kiernan MC, Lin CS, Burke D. Differences in activity-dependent hyperpolarization in human sensory and motor axons. J Physiol. 2004;558:341-9.

40. Barrett EF, Barrett JN. Intracellular recording from vertebrate myelinated axons: mechanism of the depolarizing afterpotential. J Physiol. 1982;323:117-44.

41. Balice-Gordon RJ, Bone LJ, Scherer SS. Functional gap junctions in the schwann cell myelin sheath. J Cell Biol. 1998;142:1095-104.

42. Rosenbluth J, Mierzwa A, Shroff S. Molecular architecture of myelinated nerve fibers: leaky paranodal junctions and paranodal dysmyelination. Neuroscientist. 2013 ;19:629-41.

43. Rash JE, Vanderpool KG, Yasumura T, Hickman J, Beatty JT, Nagy JI. Kv1 channels identified in rodent myelinated axons, linked to Cx29 in innermost myelin: support for electrically active myelin in mammalian saltatory conduction. J Neurophysiol. 2016;115:1836-59.

4

44. Arroyo EJ, Scherer SS. On the molecular architecture of myelinated fibers. Histochem Cell Biol. 2000;113:1-18.

45. Pillai AM, Thaxton C, Pribisko AL, Cheng JG, Dupree JL, Bhat MA. Spatiotemporal ablation of myelinating glia-specific neurofascin (Nfasc(NF155)) in mice reveals gradual loss of paranodal axoglial junctions and concomitant disorganization of axonal domains. J Neurosci Res. 2009; 87:1773–1793.

46. Corbo M, Abouzahr MK, Latov N, Iannaccone S, Quattrini A, Nemni R, et al. Motor nerve biopsy studies in motor neuropathy and motor neuron disease. Muscle Nerve. 1997 ;20:15-21.

47. Kaji R, Oka N, Tsuji T, Mezaki T, Nishio T, Akiguchi I, et al. Pathological findings at the site of conduction block in multifocal motor neuropathy. Ann Neurol. 1993 ;33:152-8.

48. Kiernan MC, Guglielmi JM, Kaji R, Murray NM, Bostock H. Evidence for axonal membrane hyperpolarization in multifocal motor neuropathy with conduction block. Brain 2002;125:664-675.

49. Garg N, Park SB, Howells J, Vucic S, Yiannikas C, Mathey EK, et al. Conduction block in immune-mediated neuropathy: paranodopathy versus axonopathy. Eur J Neurol. 2019 (8):1121-1129. doi: 10.1111/ene.13953.

5

Nerve excitability at different target levels in Multifocal Motor Neuropathy

MARIA O. KOVALCHUK
HESSEL FRANSSEN
LEONARD H. VAN DEN BERG
LEONARD J. VAN SCHELVEN
BOUDEWIJN T.H.M. SLEUTJES

ABSTRACT

Introduction. Multifocal motor neuropathy (MMN) is a progressive immune-mediated disorder of peripheral nerves in adults, characterized by selective motor involvement, conduction block, and often presence of serum anti-GM1 antibodies. We investigated if MMN preferentially affects motor axons of specific diameter by assessing excitability of different target compound muscle action potentials (CMAPs).

Methods. In 38 patients with MMN we performed excitability tests of the median nerve at target CMAPs of 20%, 40%, and 60% of maximal CMAP amplitude. CMAPs were recorded from the thenar muscle. Nerve conduction findings included motor conduction block, demyelinative slowing, or normal values in the forearm region of the median nerve. The data was analyzed with Mauchly test of sphericity together and within-group repeated-measures ANOVA.

Results. The largest differences were observed between the 20% and 60% threshold levels (all p-value ≤0.01. At 20% compared to 60%, rheobase was lower, TEh90-100% less negative, fanning out of threshold electrotonus less prominent, resting and minimal current-voltage slopes steeper, TEd peak and S2 accommodation greater, refractory period (RP) lower; at 20% threshold RP was lower, supernormality more negative and subexcitability greater. Rheobase, TEh90-100%, S2-accommodation, fanning, minimal I/V slope differed significantly between 20% and 40%, and 40% and 60% thresholds. In 40% and 60% threshold levels also SDTC, TEdPeak and supernormality showed significant difference.

Conclusion. Excitability tests show differences at multiple target CMAP levels, which can be attributed to axonal fiber size or the extent of pathological process. Different subtypes of motor axons could be more vulnerable to develop axon damage along the course of MMN.

INTRODUCTION

Multifocal motor neuropathy is characterized by selective motor nerve involvement.[1] Despite the beneficial effect of immunoglobulin therapy axonal degeneration progresses.[2] Little is known on the mechanisms affecting specific motor fibers and the involvement of motor axons of different diameter along the disease course in MMN. We hypothesized that the selectivity of motor nerve damage in MMN is also present within motor axons of different diameter. To test this, we performed multiple nerve excitability measures at different target compound muscle action potential (CMAP) levels.

METHODS

5

We performed excitability tests of the median nerve at three target levels of the compound muscle action potential (CMAP): 20%, 40%, and 60% of the maximal CMAP. We investigated 38 patients (29 men, mean age 52 years, range 22-78) with MMN according to internationally accepted criteria (Joint Task Force of the EFNS and the PNS, 2010).[3] Compound muscle action potentials (CMAPs) were recorded from the thenar muscle. Nerve conduction findings included motor conduction block, demyelinative slowing, or normal values in the forearm region of the median nerve. Prior to the excitability testing the median nerve was warmed by wrapping the forearm and hand for 30 minutes in a warm water blanket through which water of 37°C flowed constantly (Cincinatti Sub-zero Norm-O-Temp with Cincinatti Sub-zero maxi-therm lite infant hyper-hypothermia blanket for single patient use). During excitability testing the forearm and hand were kept in the blanket in order to keep nerve temperature constant.[4]

All subjects gave signed informed consent and the investigation was done in accordance to the Declaration of Helsinki and was approved by the local medical ethical committee.

The data was analyzed with Mauchly test of sphericity together and within-group repeated-measures ANOVA.

RESULTS

The largest differences were observed between 20% and 60% threshold levels with p-value ⩽0.01: rheobase was lower at 20% target; TEh90-100% less pronounced at 20% threshold level; fanning out of threshold electrotonus was more prominent at 60% threshold level, resting and minimal current-voltage slopes were steeper at 20% threshold level,

TEd peak and S2 accommodation were greater at 20% threshold level; at 20% threshold RP was lower, supernormality more negative and subexcitability greater. Rheobase, TEh90-100%, S2-accommodation, fanning, minimal I/V slope differed significantly between 20% and 40%, and 40% and 60% thresholds. SDTC, TEdPeak and supernormality showed p-value of ≤ 0.01 between 40% and 60% threshold levels.

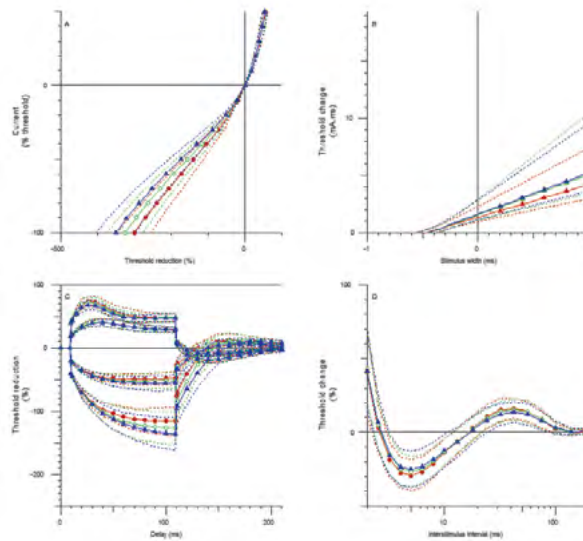**Figure 1.** Mean excitability recordings of MMN patients.

Figure 1 legend. 20% target = red; 40% target = green; 60% target = blue. Data presented as mean (SD), n=38.

DISCUSSION

In the axonal excitability measurement, threshold estimation is done by proportional threshold tracking. Threshold is usually defined as the test stimulus current needed to produce a target compound muscle action potential (CMAP) of 40% of its maximal amplitude.[5,6] Multiple nerve excitability measurement at different target levels has been earlier investigated in animal models, healthy subjects and patients with diabetic neuropathy and amyotrophic lateral sclerosis.[7-9]

Excitability recordings applied at different target CMAP levels may be useful in revealing selective nerve excitability abnormalities in MMN suggesting that different types of motor axons are affected differently along the course of MMN. The present investigation showed that excitability measures in MMN are not similar in motor axons with different thresholds. Comparison with healthy subjects is necessary to conclude our findings are abnormal.

The recruitment of motor units is a complicated process and may follow different orders during voluntary and electrical recruitment.[10,11] Controversy exists regarding to the recruitment order with electrical stimulation: (i) preferential activation of fast-contracting motor units;[12] (ii) motor units are excited in no strict order;[13,14] (iii) weaker units are excited before stronger units.[11] During voluntary contractions, motor units are recruited in order small-before-large.[15]

The recruitment order may become disorganized in pathological conditions.[16] This complexity imposes some limitations when analyzing multiple excitability data from different target thresholds: (i) different degree of axon loss prevents to conclude a simple relation between specific myelinated fibre type and excitability variables at a certain target level; (ii) recruitment order may be lost due to methodological and/or pathological conditions; (iii) subgroups of axons whith their specific recruitment order make it highly likely that each component of multiple nerve excitability tests track different types of axons.

Our findings require further studies to elucidate if multiple excitability measurements assessed at different threshold levels improve our knowledge of motor unit recruitment and are helpful in explaining pathogenesis of peripheral nerves and motor neuron disorders.

5

REFERENCES

1. Vlam L, van der Pol WL, Cats EA, Straver DC, Piepers S, Franssen H, van den Berg LH. Multifocal motor neuropathy: diagnosis, pathogenesis and treatment strategies. Nat Rev Neurol. 2011 Nov 22;8(1):48-58.

2. Terenghi F, Cappellari A, Bersano A, Carpo M, Barbieri S, Nobile-Orazio E. Neurology. 2004 Feb 24;62(4):666-8. How long is IVIg effective in multifocal motor neuropathy?

3. European Federation of Neurological Societies/Peripheral Nerve Society guideline on management of multifocal motor neuropathy. Report of a joint task force of the European Federation of Neurological Societies and the Peripheral Nerve Society--first revision. Joint Task Force of the EFNS and the PNS. J Peripher Nerv Syst. 2010 Dec;15(4):295-301.

4. Drenthen J, Blok JH, Dudok van Heel EB, Visser GH. Limb temperature and nerve conduction velocity during warming with hot water blankets. Journal of Clinical Neurophysiology 2008; 25: 104-10.

5. Bostock H, Cikurel K, Burke D. Threshold tracking techniques in the study of human peripheral nerve. Muscle Nerve. 1998;21:137–158.

6. Kiernan MC, Bostock H, Park SB, et al. Measurement of axonal excitability: Consensus guidelines. Clin Neurophysiol. 2019 Aug 2. pii: S1388-2457(19)31170-8.

7. Accornero N, Bini G, Lenzi GL, Manfredi M. Selective activation of peripheral nerve fibre groups of different diameter by triangular shaped stimulus pulses. J Physiol. 1977;273:539 –560.

8. Shibuta Y, Nodera H, Mori A, et al. Peripheral nerve excitability measures at different target levels: the effects of aging and diabetic neuropathy. J Clin Neurophysiol. 2010 Oct;27(5):350-7.

9. Shibuta Y, Shimatani Y, Nodera H, et al. Increased variability of axonal excitability in amyotrophic lateral sclerosis. Clin Neurophysiol. 2013 Oct;124(10):2046-53.

10. Thomas CK, Johansson RS, Bigland-Ritchie B. Attempts to physiologically classify human thenar motor units. J Neurophysiol 1991;65:1501–1508.

11. Thomas CK, Nelson G, Than L, Zijdewind I. Motor unit activation order during electrically evoked contractions of paralyzed or partially paralyzed muscles. Muscle Nerve. 2002 Jun;25(6):797-804.

12. Trimble MH, Enoka RM. Mechanisms underlying the training effects associated with neuromuscular electrical stimulation. Phys Ther 1991;71:273–281.

13. Dengler R, Stein RB, Thomas CK. Axonal conduction velocity and force of single human motor units. Muscle Nerve 1988; 11:136–145.

14. McComas AJ, Fawcett PR, Campbell MJ, Sica RE. Electrophysiological estimation of the number of motor units within a human muscle. J Neurol Neurosurg Psychiatry 1971;34:121–131.

15. Calancie B, Bawa P. Motor unit recruitment in humans. In: Binder MD, Mendell LM, editors. The segmental motor system. New York: Oxford University Press; 1990. p 75–95.

16. Kayagil TA, Grimes JP, Grill WM. Mechanisms underlying reversal of motor unit activation order in electrically evoked contractions after spinal cord injury. Muscle Nerve. 2008;37:210 –218.

5

Acute Effects of Riluzole and Retigabine on Axonal Excitability in Patients With Amyotrophic Lateral Sclerosis: A Randomized, Double-Blind, Placebo-Controlled, Crossover Trial

MARIA O. KOVALCHUK
JULES A.A.C. HEUBERGER
BOUDEWIJN T.H.M. SLEUTJES
DIMITRIOS ZIAGKOS
LEONARD H. VAN DEN BERG
TOBY A. FERGUSON
HESSEL FRANSSEN
GEERT JAN GROENEVELD

ABSTRACT

Increased excitability of motor neurons in patients with amyotrophic lateral sclerosis may be a relevant factor leading to motor neuron damage. This randomized, double-blind, 3-way cross-over, placebo-controlled study evaluated peripheral motor nerve excitability-testing as biomarker of hyperexcitability and assessed effects of riluzole and retigabine in 18 patients with amyotrophic lateral sclerosis. We performed excitability-testing at baseline, and twice after participants had received a single dose of either 100mg riluzole, 300mg retigabine or placebo. Between- and within-day repeatability was at least acceptable for 14 out of 18 recorded excitability variables. No effects of riluzole on excitability-testing were observed, but retigabine significantly decreased strength-duration time-constant (9.2%) and refractoriness at 2ms (10.2 percentage points) compared to placebo. Excitability-testing was shown to be a reliable biomarker in patients with amyotrophic lateral sclerosis, and the acute reversal of previously abnormal variables by retigabine justifies long-term studies evaluating impact on disease progression and survival.

INTRODUCTION

Amyotrophic lateral sclerosis (ALS) is a progressive and fatal neurodegenerative disease characterized by ongoing loss of motor neurons. In ALS the unique phenomenon of increased membrane excitability in both peripheral and central motor neurons can be observed, presenting clinically as fasciculations, muscle cramps, hyper-reflexia, and spasticity.[1] Excitability-testing is a neurophysiological tool which allows non-invasive assessment of axolemmal voltage-gated ion channel activity in motor axons of a peripheral nerve. In ALS, it showed evidence of increased persistent sodium-conductance and reduced potassium-conductance, both of which may contribute to axonal hyperexcitability and fasciculation.[2-6] Furthermore, presence of increased persistent sodium-conductance was shown to be correlated with more rapid functional decline and shorter survival,[7, 8] and presence of fasciculation with shorter survival.[9] Because increased membrane excitability in ALS may be a relevant step in the cascade leading to structural damage of motor neurons,[10] early identification of hyperexcitable motor neurons may provide an argument for initiating neuroprotective intervention.[7, 11] Retigabine, a potassium-channel activator, was shown to reduce increased cellular membrane excitability and improve cell survival in an in vitro model of ALS.[12] Riluzole, the only registered drug for treatment of ALS, partially normalized some excitability variables in peripheral and cortical motor neurons of patients with ALS.[13] Modulation of hyperexcitability could therefore serve as a proof-of-pharmacology biomarker to assess effects of therapeutic interventions in ALS. The present study aimed to validate motor nerve excitability-testing of the median nerve as a biomarker of hyperexcitability and assessed pharmacodynamic effects of retigabine and riluzole in patients with ALS.

METHODS

Subjects

Eighteen patients with ALS, aged between 18 and 80 years were enrolled in the study, which was performed at the University Medical Center Utrecht in Utrecht, The Netherlands in collaboration with the Centre for Human Drug Research, Leiden, The Netherlands. Patients were recruited via the department's patient database, through advertisements, and the newsletters of the "Vereniging Spierziekten Nederland" (VSN), the organization for patients with neuromuscular disorders in the Netherlands. All patients gave written informed consent prior to any study-related activity, after which a screening visit evaluated eligibility. Main inclusion criteria were: mastery of the Dutch language, diagnosis of definite, probable, or probable laboratory-supported ALS according to the revised

El Escorial criteria of 1998,[14] fasciculations in the lower arm to be used for excitability measurements observed by the treating neurologist, CMAP of the abductor pollicis brevis muscle in the arm with fasciculations exceeding 1 mV, as well as no history of diabetes, neuropathy, or neuromuscular disorders other than ALS, carpal tunnel syndrome, trauma to the upper extremities or other orthopedic conditions that might affect the electrophysiological measurements, and no medication that might affect electrophysiological measurements, other than that used in the study. During the trial, the inclusion criterion for fasciculations was modified to include subjects with fasciculations anywhere in the arm, not only in the lower arm, and an exclusion for history of alcohol or drug dependence was removed. These changes were made in order to facilitate patient recruitment and were not considered to impact the study validity.

Experimental design

We performed a randomized, double blind, 3-way cross-over, placebo controlled study of the test-retest reliability of peripheral motor nerve excitability and the effects of oral retigabine and riluzole on these measurements in patients with ALS. Visits were scheduled a week apart in order to allow a sufficiently long washout of riluzole and retigabine. Eligible subjects arrived at the research unit on the morning of a treatment visit, and after passing a brief re-eligibility and health check, they underwent baseline excitability-testing. Capsules with medication were then swallowed with water on an empty stomach, after which regular blood samples were collected for pharmacokinetic analysis. Subjects were required to remain fasted until 2.5 hours after dosing, although water was allowed. At 1.5 and 6 hours after dosing excitability-testing was repeated. Blood samples for pharmacokinetic analysis were taken pre-dose and 0.5, 1, 1.5, 2, 2.5, 3, 4, 6 and 7 hours after dosing. After the last blood sample the subject was discharged.

Since riluzole is the standard treatment for ALS patients (50 mg b.i.d.), we instituted a one-day washout of riluzole before each dosing occasion to minimize the effect of the drug on excitability variables. Although the half-life of riluzole is approximately 9-15 hours[15] and not all of the drug was expected to have washed out of the system after 24 hours, it was deemed unethical to have a longer washout period as this might have impacted the efficacy of the treatment, and the willingness of the patients to participate in the study.

The study was approved by the Independent Ethics Committee of the Foundation 'Evaluation of Ethics in Biomedical Research' (Stichting Beoordeling Ethiek Biomedisch Onderzoek), Assen, The Netherlands. The study was registered in the Dutch Trial Registry (Nederlands Trial Register, NTR) under study number NTR6278 and was carried out between November 2015 and April 2017.

Treatment, randomization and masking

Subjects received a single dose of 100 mg (2x50 mg) riluzole (Rilutek, Sanofi, Paris, France), 300 mg (100 and 200 mg) retigabine (Trobalt, Glaxo Smith Kline, Brentford, UK) as encapsulated tablets or matching placebo capsules. Subjects were randomly assigned to a treatment order, with a balanced design using a code generated by an un-blinded statistician who was otherwise not involved in the execution of the study. A masked physician enrolled patients into the study. Until study closure the treatment codes were only available to this statistician and the Leiden University Medical Center (LUMC) pharmacy, which distributed the study agents.

Motor nerve excitability testing

Motor excitability was measured in the median nerve at the wrist. The setup consisted of Viking IV EMG apparatus (Nicolet Biomedical, Inc., Madison, Wisconsin), coupled to a computer (PCI-6221, National instruments) running QTRAC-S software (TROND-NF, version 19-06-2015, Institute of Neurology, Queen Square, London, UK) and an isolated bipolar constant current stimulator (DS5, Digitimer, UK model D185-HB4). The median nerve was stimulated at the wrist via non-polarizable surface electrodes (cathode at the wrist; anode 10cm proximal over the radial side of the forearm). The thenar CMAP was recorded by surface electrodes in a belly-tendon montage. The distance between active recording electrode and stimulating cathode was 7cm. The median nerve was warmed to 37°C by wrapping the forearm and hand for 30 minutes in a warm water blanket through which water at 37°C flowed constantly (Cincinnati Sub-zero Norm-O-Temp with Cincinnati Sub-zero maxi-therm lite infant hyper-hypothermia blanket for single patient use).[16] During excitability-testing the forearm and hand were kept in the blanket with flowing water at 37°C in order to maintain a constant nerve temperature. Skin temperature was continuously monitored by means of a sensor near the stimulating cathode. Distal motor latency (DML) was measured every 1.6 seconds during each excitability-testing in order to check if changes in nerve temperature resulted in conduction changes. DML was defined as the point where the CMAP deviated by 10% of its amplitude from baseline to peak. These procedures were based on previous studies.[16-18]

To examine axonal excitability parameters a specific sequence of conditioning and test stimuli were applied to the nerve. Conditioning stimuli were constant currents that either slightly depolarized resting membrane potential, slightly hyperpolarized resting membrane potential, or induced nerve action potentials. Threshold was defined as the test stimulus current needed for a target CMAP of 40% of its maximum amplitude.

Each excitability test consisted of: stimulus response (SR) curve (relation between stimulus current and response amplitude), charge-duration (Qt) relation (relation between stimulus charge and stimulus duration), threshold electrotonus (time course of threshold changes during a depolarizing or hyperpolarizing conditioning current of 100 ms of 20% or 40% of the current for an unconditioned target response), I/V relation (relation between the magnitude of a 200 ms duration conditioning current, varying from 50% depolarizing to 100% hyperpolarizing, and the threshold at its end), recovery cycle (time-course of the threshold changes after a supramaximal conditioning stimulus eliciting action potentials).

The following parameters were determined: threshold for an unconditioned target response of 50% (stimulus current required to evoke a CMAP of 50% of maximal), rheobase (slope of the Qt relation), strength-duration time constant (SDTC; absolute value of the x-intercept of the Qt relation), TEd90-100 (threshold decrease at the end of the 40% depolarizing conditioning stimulus), TEd40-60 (threshold decrease at 40-60 ms of the 40% depolarizing conditioning stimulus), TEdpeak (maximal threshold decrease during 40% depolarizing conditioning stimulus), S2-accommodation (difference between TEdpeak and TEd90-100), accommodation half-time (time between the onset of the conditioning stimulus and the time point where threshold decrease is halfway between TEdpeak and TEd90-100), TEh90-100 (threshold increase at the end of the 40% hyperpolarizing conditioning stimulus), fanning (sum of the absolute values of TEd90-100 and TEh90-100), resting I/V slope (slope between -10% and +10% conditioning stimuli), minimal I/V slope (smallest slope in the hyperpolarizing part of the I/V curve), hyperpolarizing I/V-slope (slope between 100% and 80% hyperpolarizing conditioning stimuli), refractoriness at 2 ms (threshold change at the conditioning-test interval of 2 ms), refractory period (time between conditioning stimulus and return of threshold to baseline), superexcitability (lowest threshold after refractory period) and subexcitability (highest threshold after superexcitability).

Primary endpoints were repeatability of these variables as assessed by Cronbach's alpha, and effects of riluzole and retigabine on the variables compared to placebo.

Controls

In a separate study, we also investigated excitability by the same methods in eighteen age-matched healthy controls (9 men, median age 53 years, range 35 – 71) who had no neurological symptoms and did not use medication.

ALSFRS-R

The ALSFRS-R[19] evaluating disability in patients with ALS was performed at baseline and approximately 3 months after the first dose. This revised version of the ALSFRS, which incorporates additional assessments of dyspnea, orthopnea, and the need for ventilatory support, retains the properties of the original scale and shows strong internal consistency and construct validity. The rating scale is a validated, reliable, rating instrument for monitoring the progression of disability in patients with ALS.[20,21]

Data management

All data were stored in a clinical trial database (Promasys, Omnicomm Inc., Fort Lauderdale, USA) and checked for accuracy and completeness. We performed a blinded data review before code-breaking and analysis according to a standard procedure at CHDR.

Statistical analysis

Pharmacokinetic parameters, including maximum plasma concentration (Cmax) and time to Cmax (Tmax), were determined by standard non-compartmental methods using R software version 3.4.0. Test-retest reliability of the primary endpoints was assessed by Cronbach's alpha, where a sample of 18 subjects was considered to be sufficient. An interim analysis evaluating between-day repeatability by Cronbach's alpha was performed after 12 patients had completed the study. A value of at least 0.7 (acceptable repeatability) was needed for at least one of the variables that were deemed most relevant – refractoriness at 2 ms, SDTC, superexcitability, TEd40-60 or TEd90-100 – to proceed with the final 6 patients. To establish whether significant treatment effects could be detected on the excitability parameters, a mixed model analysis of covariance was used with treatment, time and treatment by time as fixed factors and subject, subject by treatment and subject by time as random factors, and the average baseline measurement as covariate. The Kenward-Rogers approximation was used to estimate denominator degrees of freedom and model parameters were estimated using the restricted maximum likelihood method. To determine treatment effects on excitability parameters the estimated averages of both post-dose time points for each treatment were compared with placebo. Missing data were not imputed, but were estimated within the statistical model. Residual Q-Q plots were used to check the assumption of normality of the error term in the mixed effects model together with the Shapiro-Wilk test for normality. Parameters violating the assumption of normality were log-transformed and after the analysis were back-transformed so that the results can be interpreted as a percentage change.

The excitability variables of ALS patients at the first, pre-dose, visit were compared with those obtained in the healthy controls by unpaired Student's t-test.

The correlation between the difference in ALSFRS-R scores (at baseline and at 3 months) and the first visit pre-dose excitability parameters was calculated using Spearman correlation. Significance level was set at $p < 0.05$ and 95% confidence intervals of the estimated difference between the treatment and placebo groups are presented. All calculations were performed using SAS for windows V9.4 (SAS Institute, Inc., Cary, NC, USA).

RESULTS

The interim analysis showed at least acceptable repeatability (alpha >0.7) for all five pre-determined variables (data not shown). Therefore, in total, eighteen patients with ALS were included and all subjects completed the study (Figure 1), with recruitment running from October 2015 to December 2016, and the last follow-up phone call taking place in April 2017. Baseline characteristics are displayed in Table 1. Participants tolerated the study and treatments well. One subject did not complete the 6 h measurement of the first visit (riluzole occasion) because of adverse events consisting of nausea and vomiting due to a migraine attack. It was considered unlikely that this was related to the study treatment. There were 15 adverse events in the retigabine-arm, 14 in the riluzole-arm, and 6 in the placebo-arm. All events were grade 1-2 and none was reported more than twice per arm, except for dizziness (reported 3 times in the retigabine-arm) and somnolence (reported 7 times in the retigabine and 3 times in the placebo-arm).

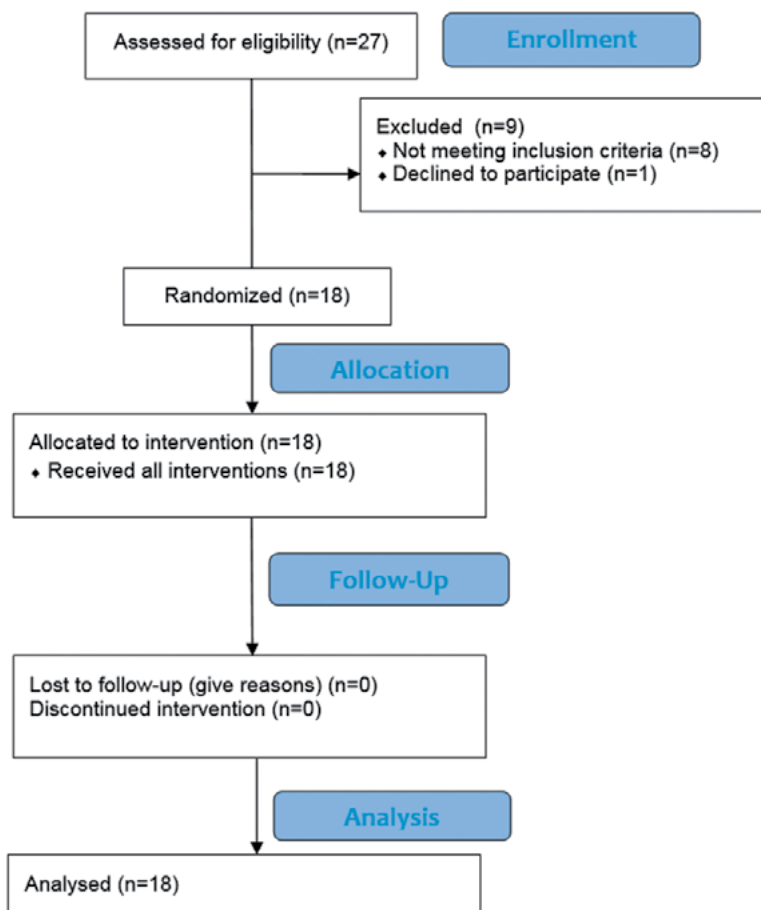Acute Effects of Riluzole and Retigabine on Axonal Excitability in Patients With Amyotrophic
Lateral Sclerosis: A Randomized, Double-Blind, Placebo-Controlled, Crossover Trial

105

Figure 1. Study flow diagram.

Table 1. Demographics.

N	18
Age (years)	58.6 (37 – 76)
Weight (kg)	85.0 (8.2)
Height (cm)	182.1 (6.7)
Sex (Female/Male)	1 (6%) / 17 (94%)
Time since symptom onset (months)	28.9 (6.9–106.7)
Time since diagnosis (months)	13.7 (3.0–62.5)
Taking standard riluzole treatment	17 (94%)
Riluzole treatment duration (months)	12.8 (2-61)
ALSFRS-R at baseline	38 (29 - 45)
Familial history of ALS (Yes/No)	4 (22%) / 14 (78%)

Values are presented as mean (SD or range where appropriate).

Pharmacokinetics

Pharmacokinetic analysis showed mean Cmax for riluzole of 343 ng/mL (range: 102-646 ng/mL) and for retigabine of 604 ng/mL (271-997 ng/mL), both on average at 1 hour post-dose (riluzole range: 0.5-3 hours; retigabine range: 0.5-4 hours), see Figure 2. Variability in Cmax was moderate with a coefficient of variation (CoV) of 48% for riluzole and 36% for retigabine. Tmax was more variable for retigabine (CoV 90%) than for riluzole (CoV 66%). Mean riluzole concentration before dosing for all treatment periods combined was 12 ng/mL (range: <1-75.7 ng/mL), and 10 ng/mL (1.9-22.3 ng/mL) for the placebo treatment period.

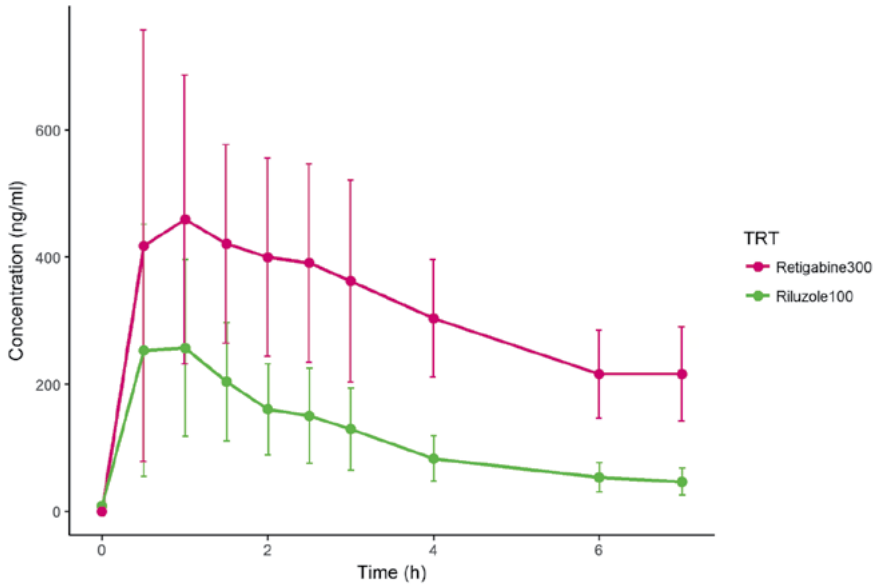**Figure 2.** Pharmacokinetics of riluzole and retigabine.

Figure 2 legend. Mean with standard deviation concentration-time profiles in plasma per treatment (TRT).

Baseline electrophysiological characteristics and test-retest reliability

Baseline electrophysiological characteristics, as well as repeatability for excitability-testing are presented in Table 2. Repeatability between each baseline measurement (inter-occasion), as determined by Cronbach's alpha, showed that the majority of variables had an acceptable (Cronbach's alpha > 0.7) to excellent repeatability. Only accommodation half-time showed Cronbach's alpha much lower than 0.7; rheobase, SDTC and threshold for a target CMAP of 50% were just below the threshold of Cronbach's alpha >0.7. Within the placebo visit (intra-occasion), repeatability was just below acceptable for SDTC, and well below 0.7 for accommodation half-time, but good to excellent for all other parameters. When compared to controls, the excitability variables obtained in ALS patients at the pre-dose visit showed greater changes in TEd40-60 (53.0 ± (SEM) 1.2% versus 47.3 ± 0.9%, $p < 0.001$) and TEd90-100 (48.8 ± 1.6% versus 44.1 ± 0.7%, $p = 0.008$), longer accommodation half-time (38.7± 1.0 ms, versus 35.8 ± 0.7 ms, $p = 0.02$), increased super-excitability (-27.4 ± 2.1%, versus 20.5 ± 1.0%, $p = 0.004$), and decreased subexcitability (11.9 ± 1.0% versus 16.7 ± 1.3%, $p = 0.006$). Other variables, including SDTC (0.46 ± 0.02 ms versus 0.45 ± 0.01 ms, $p = 0.86$), were not significantly different.

Table 2. Baseline excitability characteristics, variability and repeatability.

Parameter	Mean	Inter-subject CV (%)	Intra-subject CV (%)	Model-based Intra-subject CV (%)	Inter-occasion Cronbach's alpha	Intra-occasion Cronbach's alpha
CMAP (mV)	7.2	54.2	25.8	13.9 *	0.96	0.97
Threshold for 50% CMAP (mA)	5.95	52.7	39.2	21.8 *	0.68	0.90
Strength-duration						
Rheobase (mA)	3.98	57.6	43.7	23.3 *	0.68	0.89
SDTC (ms)	0.459	14.8	11.0	8.3 *	0.69	0.67
Threshold electrotonus						
TEdpeak (%)	68.8	8.8	4.7	3.8	0.90	0.94
S2 accommodation (%)	20.8	20.4	14.1	12.4	0.80	0.84
Accommodation half-time (ms)	38.4	12.9	11.8	10.5	0.36	0.43
TEd40-60 (%)	52.5	9.6	6.0	4.6	0.84	0.90
TEd90-100 (%)	47.9	11.6	6.0	6.1	0.91	0.95
TEh90-100 (%)	-127.9	21.3	8.7	7.5	0.94	0.95
Fanning (%)	171.6	16.3	7.8	5.7	0.93	0.95
Current-threshold relation						
Resting I/V-slope	0.55	20.3	11.5	7.3 *	0.81	0.92
Minimum I/V-slope	0.24	27.3	12.3	10.3 *	0.92	0.93
Hyperpolarizing I/V-slope	0.33	27.2	19.0	20.0 *	0.79	0.89
Recovery cycle						
Refractoriness at 2ms (%)	41.9	62.5	45.5	20.9	0.73	0.83
Superexcitability (%)	-26.4	29.7	11.9	9.5	0.95	0.94
Subexcitability (%)	11.7	36.9	22.3	18.5	0.84	0.84
Refractory period (ms)	2.6	11.9	7.7	4.7	0.81	0.91

Excitability variables mean and inter- and intra-subject CV based on baseline measurements at each visit, and intra-subject variability based on the statistical model. Cronbach's alpha for each excitability parameter calculated for each of the three baseline measurements (inter-occasion) and for the three measurements within the placebo visit (intra-occasion). Repeatability based on Cronbach's alpha: <0.5, unacceptable; 0.5-0.6, poor; 0.6-0.7, questionable; 0.7-0.8, acceptable; 0.8-0.9, good; 0.9-1.0 excellent. *Intra-subject variability of the LOG-transformed data.

Effects of riluzole and retigabine on motor nerve excitability

Figure 3i shows the mean excitability recordings at pre-dose and after a single dose of 100 mg riluzole at 1.5 and 6 hours. No statistically significant effects were observed for riluzole on any of the excitability measures compared to placebo. Figure 3ii shows the mean excitability recordings at pre-dose and after a single dose of 300 mg retigabine at 1.5 and 6 hours. Significant treatment effects were observed for retigabine, showing the following effects compared to placebo: increase in hyperpolarizing I/V-slope (21.7%), resting I/V-slope (6.1%), minimum I/V-slope (8.5%), rheobase (28.0%), threshold for

a target CMAP of 50% (25.0%), accommodation half-time (3.15ms), decrease in SDTC (9.2%), refractoriness at 2ms (10.2 percent point, or arithmetic difference) and refractory period (0.17ms) (Table 3, Figure 4).

Figure 3. Mean excitability recordings pre-dose (black), and 1.5 hours (red) and 6 hours (green) after a single dose of 100 mg riluzole (i) and 300 mg retigabine (ii).
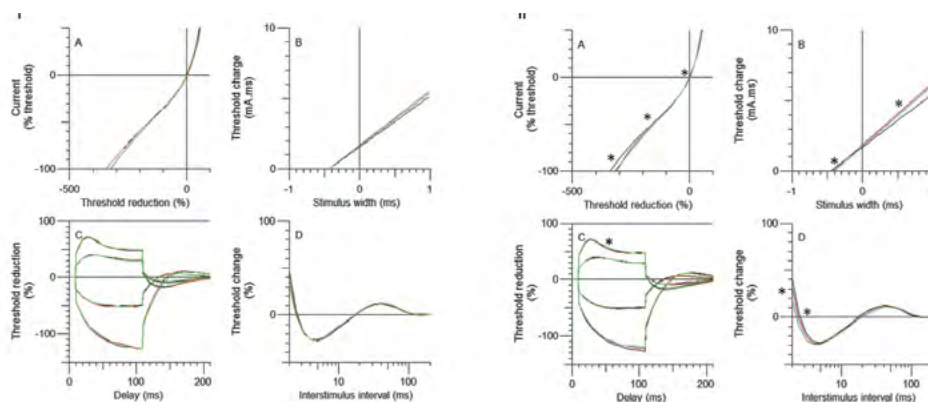

Figure 3 legend. (A) current/voltage relationship, (B) strength-duration properties plotted as stimulus charge versus stimulus duration, (C) threshold electrotonus, (D) recovery cycle. Asterixes indicate significant treatment effects on thresholds (see Table 3).

Table 3. Treatment effects on parameters of motor nerve excitability.

Parameter	Contrast retigabine vs placebo	Contrast riluzole vs placebo
CMAP (mV)	5.64 vs. 5.82 -3.1% (-14.0%, 9.1%) p=0.584	5.24 vs. 5.82 -9.9% (-20.5%, 2.1%) p=0.097
Threshold for 50% CMAP (mA)	5.97 vs. 4.78 25.0% (7.6%, 45.2%) p=0.005	5.54 vs. 4.78 16.1% (-0.3%, 35.2%) p=0.055
Strength-duration		
Rheobase (mA)	4.02 vs. 3.14 28.0% (9.1%, 50.1%) p=0.004	3.63 vs. 3.14 15.4% (-2.0%, 35.7%) p=0.083
SDTC (ms)	0.416 vs. 0.458 -9.2% (-14.1%, -3.9%) p=0.001	0.455 vs. 0.458 -0.6% (-6.1%, 5.1%) p=0.821

Threshold electrotonus		
TEdpeak (%)	68.31 vs. 69.42 -1.12 (-3.03, 0.80) p=0.241	69.09 vs. 69.42 -0.33 (-2.27, 1.61) p=0.730
S2 accommodation (%)	21.29 vs. 20.52 0.77 (-1.14, 2.68) p=0.415	19.44vs. 20.52 -1.08 (-3.02, 0.85) p=0.260
Accommodation half-time (ms)	39.88 vs. 36.74 3.15 (0.91, 5.38) p=0.007	36.50 vs. 36.74 -0.24 (-2.51, 2.03) p=0.831
TEd40-60 (%)	53.29 vs. 53.36 -0.070 (-1.849, 1.709) p=0.936	52.96vs. 53.36 -0.399 (-2.200, 1.401) p=0.652
TEd90-100 (%)	47.09 vs. 48.84 -1.748 (-3.867, 0.372) p=0.102	49.73vs. 48.84 0.896 (-1.259, 3.051) p=0.401
TEh90-100 (%)	-121.60 vs. -122.70 1.093 (-5.722, 7.907) p=0.746	-127.71 vs. -122.70 -5.016 (-11.872, 1.840) p=0.146
Fanning (%)	164.16 vs. 168.45 -4.28 (-11.85, 3.28) p=0.255	174.25 vs. 168.45 5.80 (-1.91, 13.51) p=0.134
Current-threshold relation		
Resting I/V-slope	0.593 vs. 0.559 6.1% (0.6%, 11.8%) p=0.030	0.570 vs. 0.559 1.9% (-3.4%, 7.5%) p=0.471
Minimum I/V-slope	0.258 vs. 0.238 8.5% (0.0%, 17.7%) p=0.0498	0.232 vs. 0.238 -2.6% (-10.2%, 5.7%) p=0.494
Hyperpolarizing I/V-slope	0.345 vs. 0.283 21.7% (3.5%, 43.0%) p=0.019	0.309 vs. 0.283 9.2% (-7.0%, 28.3%) p=0.271
Recovery cycle		
Refractoriness at 2ms (%)	24.76 vs. 34.95 -10.192 (-17.160, -3.224) p=0.006	34.00 vs. 34.95 -0.950 (-8.027, 6.127) p=0.784
Superexcitability (%)	-27.78 vs. -26.41 -1.361 (-3.165, 0.442) p=0.134	-25.52 vs. -26.41 0.889 (-0.914, 2.693) p=0.322
Subexcitability (%)	10.78 vs. 11.97 -1.196 (-2.715, 0.323) p=0.117	12.03 vs. 11.97 0.059 (-1.472, 1.591) p=0.937
Refractory period (ms)	2.41 vs. 2.58 -0.17 (-0.27, -0.06) p=0.003	2.57 vs. 2.58 -0.01 (-0.12, 0.09) p=0.788

Estimated mean of both post-dose time points for each treatment versus placebo. Treatment effects depicted as the estimated mean difference with placebo (95% CI of the difference).

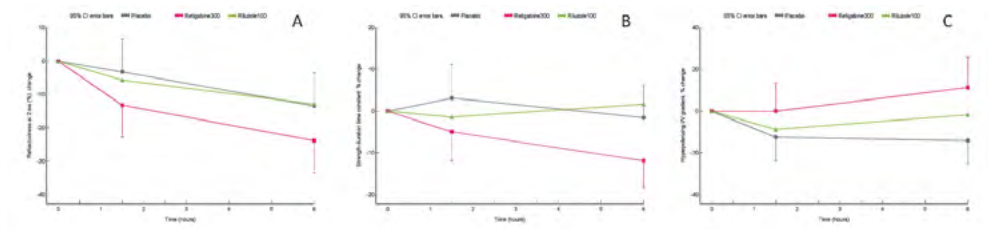**Figure 4.** Change from baseline plot of the treatment effect on excitability variables.

Figure 4 legend. (A) refractoriness at 2 ms, (B) strength duration time constant and (C) hyperpolarizing I/V-slope. CI, Confidence interval; Retigabine300, retigabine 300 mg treatment; Riluzole100, riluzole 100 mg treatment.

Predictive value of excitability measures

None of the excitability-variables at baseline showed a significant correlation with clinical deterioration by a functional decline in ALSFRS-R score between baseline and 3 months.

6

DISCUSSION

Excitability-testing was shown to produce repeatable results in patients with ALS, both within and between visits, for all 18 variables except accommodation half-time. Although riluzole did not show effects, retigabine had significant effects on several excitability-variables when compared to placebo. No correlation between ALSFRS-R and excitability-variables was found.

Electrophysiological characteristics and variability

Inter-subject variability for parameters such as CMAP, refractoriness at 2ms, rheobase, I/V-slopes, super- and subexcitability was relatively high (CV of 27-63%), which may likely be related to differences in the disease state of the patients. Intra-subject variability is, therefore, more informative on variability, and CVs were indeed much smaller. The statistical model-based estimate of the intra-subject CV for all parameters ranged from 4-23%, and was for most CVs very similar to statisti cal model based estimate found in healthy volunteers.[14] Only the CVs of accommodation half-life, TEd90-100, TEh90-100 and hyperpolarizing I/V slope were more than 1.5 times greater than found by Tomlinson et al.[22]

Pharmacokinetics

The Cmax of riluzole for all but three subjects (mean 343 ng/mL, range 102-646 ng/mL) and of retigabine for all subjects (mean 604 ng/mL, range 271-997 ng/mL) was above the approximate therapeutic levels of 173 ng/mL for riluzole[23] and 250 ng/mL for retigabine[24] as expected with the selected supra-therapeutic doses. Mean plasma concentration of riluzole before dosing for all treatment periods was 12 ng/mL (range <1–75.7 ng/mL) as could be expected after approximately 24 h-washout of riluzole; thereby levels were approximately 30 times lower than at Cmax during the riluzole period. As the riluzole concentration exerting 50% of the maximal effect (IC50) on voltage gated sodium channels is approximately 0.3 μM (or 70 ng/mL),[25] the mean post-washout level of 12 ng/mL is unlikely to have affected sodium channel function. Two subjects had significantly higher riluzole baseline levels at one visit (with 63.2 and 75.7 ng/mL), possibly due to not having followed the instruction to omit their regular evening dose of riluzole. Both instances occurred during retigabine treatment periods. It is, however, unlikely that this influenced the observed effects in the retigabine treatment arm, especially as no effect of riluzole was observed in the riluzole treatment arm. Sensitivity analysis, with exclusion of these occasions did not produce a different outcome, with one exception: that retigabine effects on minimum I/V-slope and resting I/V-slope did not reach significance (borderline) (data not shown).

Effects of retigabine on peripheral nerve excitability

In human peripheral motor nerve, five types of voltage-gated potassium channels have been described depending on their gating modes, activation-deactivation time and conductance, with a large overlap between their kinetic properties.[26,27] These five types give rise to three types of potassium-currents on single axon recordings: fast, intermediate and slow. Slowly activating potassium channels of the axonal membrane belong to Kv7.2-Kv7.5 subtypes, coded by the KCNQ genes.[28,29] In vitro studies and animal models of epilepsy and pain showed that retigabine hyperpolarizes resting axonal membrane potential by inducing these potassium channel subtypes to open which, in turn, enhances outward slow potassium currents and produces a hyperpolarizing shift of the half-activation potential of these channels.[30,31] Excitability-variables assessed after potassium channel activators such as retigabine and flupirtine administration are, therefore, expected to reflect either potassium channel activation or the resulting hyperpolarization of resting membrane potential.[28,29]

In our study, a single dose of retigabine resulted in significant changes in various axonal excitability-parameters. Strength duration properties showed a decrease in SDTC and increase in rheobase. Both can be explained by either hyperpolarization of resting membrane potential (since hyperpolarization decreases nodal persistent sodium current),[32,33] or a de-

crease in nodal electrical capacitance. As it is unlikely that retigabine induces histological changes resulting in decreased nodal capacitance, hyperpolarization of resting membrane potential is the most likely mechanism. Membrane hyperpolarization also results in increased threshold current needed to evoke a target CMAP of 50% of its maximum amplitude, similar to the findings in previous studies.[34] In the current-threshold relationship, a steeper hyperpolarizing I/V slope was found, producing a larger inward rectification, which is also expected to be enhanced when the axonal membrane potential becomes more hyperpolarized. Furthermore, in the present study, retigabine reduced refractoriness at 2 ms and refractory period, which is consistent with a decrease in sodium-channel inactivation due to membrane hyperpolarization.[35,36] Shortening of the refractory period may also be due to early repolarization of the action potential. Early repolarization by retigabine has been observed previously as a result of membrane hyperpolarization induced by a hyperpolarizing shift of the voltage dependence of slow potassium channels.[37] This effect is most likely due to the greater number of potassium channels open at hyperpolarized membrane potentials. As riluzole has been previously shown to reduce refractoriness at 2 ms,[13] this observed effect of retigabine might be beneficial in ALS.

In the recovery cycle, retigabine did not induce significant changes in superexcitability and late subexcitability; this could be due to a plasma concentration being too low to induce detectable effects, as shown in a study with flupirtine.[38] In our study, we determined subexcitability after only a single supramaximal pre-conditioning pulse, where previous studies applied multiple pre-conditioning supramaximal pulses,[34, 39] known to enhance late after-hyperpolarization, increasing subexcitability[40] and the sensitivity to detect treatment-induced changes.

Retigabine did not normalize any of the parameters that were found to be significantly different from healthy controls in our study. It did however, change SDTC in the direction of normalization, a variable that has previously been shown to be abnormally increased in patients with ALS.[2, 4-6] There was no significant correlation between retigabine concentration and effects on excitability variables (not shown), however, the appropriate approach would be to develop a population pharmacokinetic-pharmacodynamic model, which will be explored in the future. In any case, the chosen study design and statistical analysis ensure that the observed effects are induced by retigabine and cannot for example be explained by disease progression.

Effects of riluzole on peripheral nerve excitability

In our study, a single dose of riluzole had no significant effects on excitability-variables. It is possible that the period of riluzole administration in our study was too short, since riluzole administration of, on average, 7 weeks in patients with ALS decreased refracto-

6

riness at 2 ms and superexcitability.[13] Nevertheless, we expected an effect on excitability-variables after a single-dose of riluzole, as it inhibits persistent sodium currents and shifts the voltage dependence of sodium channel inactivation in a negative direction.[41] Another possible explanation of the lack of effect in our study may be related to the low riluzole concentrations that were still present during the baseline measurement, despite the preceding washout of standard riluzole treatment. This seems, however, unlikely because concentrations were approximately 5 times below the IC50 for voltage-gated sodium channels and because no effect of riluzole on excitability-variables was found in the riluzole-naïve patient of our study. Also, riluzole might have been less effective due to persistent sodium channels remaining in an open state.[13] Finally, there are indications that riluzole might lose its efficacy in later stages of the disease,[42,43] and our patients had been diagnosed, on average, more than a year prior to starting the study. A hypothesis for this loss of efficacy is that upregulation of efflux transporters in disease-affected regions,[44] such as P-glycoprotein (PGP) and breast cancer resistance protein (BCRP), would lead to very low concentrations at the target site.

Relation with disease progression

A relation between SDTC and ALSFRS-R[8] decline and SDTC and survival[7] have been reported, but in the current study no correlation was observed between any of the excitability parameters and disease progression as measured by a change in ALSFRS-R. This could be due to the shorter follow-up (3 months compared to 6 months) and/or lower number of subjects in our study (18 versus 60). When the follow-up was extended in our study in an ad-hoc analysis to, on average, 14.5 months (range 5.8 to 20.2 months) after baseline ALSFRS-R, again no significant correlation was found between excitability parameters and change in ALSFRS-R normalized for interval (time between baseline and second questionnaire) (data not shown).

Limitations

The most important limitation of our study was a lack of complete washout of standard riluzole treatment as described in the previous sections. As all but one participant were men, one should be cautious in extrapolating the results to female patients. Four (22%) of the enrolled patients had a familial history of ALS and therefore probably a hereditary form in which the pathophysiological mechanism might differ from that in patients with sporadic ALS.

Clinical implications

This study shows that a single dose of retigabine has a greater effect on peripheral nerve excitability than a single dose of riluzole, the current registered treatment for ALS. Pre-

vious studies showed that a prolonged SDTC is related to more rapid disease progression and shorter survival.[7, 8] Although SDTC in our ALS patients was not statistically different from that in healthy controls, retigabine induced shortening of this variable. Long-term retigabine administration may, therefore, reverse the increased persistent sodium current underlying SDTC prolongation which was suggested to induce hyper-excitability and motor neuron death.[8, 12]

If, in the future, peripheral nerve excitability proves to be predictive of clinical outcome, it might be a very useful, non-invasive biomarker to test for potential treatments for ALS, and measure treatment efficacy on a much shorter basis compared to the sensitivity of the ALSFRS-R or survival measures.

Study Highlights

• *What is the current knowledge on the topic?*

Patients with amyotrophic lateral sclerosis show increased membrane excitability in peripheral and central motor neurons, which may be a relevant factor leading to motor neuron damage. Current approved treatment with riluzole decreases hyperexcitability, indicating this could be a therapeutic target.

• *What question did this study address?*

The aim of this study was to validate peripheral motor nerve excitability-testing as biomarker of hyperexcitability and assess effects of riluzole and retigabine in patients with amyotrophic lateral sclerosis.

• *What does this study add to our knowledge?*

Between- and within-day repeatability was good for most excitability testing parameters and a single dose of retigabine, but not riluzole normalized several relevant markers indicating hyper-excitability in these patients.

• *How might this change clinical pharmacology or translational science?*

Peripheral nerve excitability could be a very useful and quick, non-invasive biomarker to test for potential treatments for ALS, and measure treatment efficacy. Retigabine may be such a treatment reversing hyper-excitability, justifying long-term studies looking at impact on disease progression and survival.

REFERENCES

1. Bae JS, Simon NG, Menon P, Vucic S, Kiernan MC. The puzzling case of hyperexcitability in amyotrophic lateral sclerosis. J Clin Neurol 2013;9:65-74.

2. Kanai K, Kuwabara S, Misawa S, Tamura N, Ogawara K, Nakata M, Sawai S, Hattori T, Bostock H. Altered axonal excitability properties in amyotrophic lateral sclerosis: impaired potassium channel function related to disease stage. Brain 2006;129:953-62.

3. Park SB, Kiernan MC, Vucic S. Axonal Excitability in Amyotrophic Lateral Sclerosis : Axonal Excitability in ALS. Neurotherapeutics 2017;14:78-90.

4. Vucic S, Kiernan MC. Axonal excitability properties in amyotrophic lateral sclerosis. Clin Neurophysiol 2006;117:1458-66.

5. Geevasinga N, Menon P, Howells J, Nicholson GA, Kiernan MC, Vucic S. Axonal ion channel dysfunction in c9orf72 familial amyotrophic lateral sclerosis. JAMA Neurol 2015; 72:49-57.

6. Menon P, Kiernan MC, Vucic S. ALS pathophysiology: insights from the split-hand phenomenon. Clin Neurophysiol 2014;125:186-93.

7. Kanai K, Shibuya K, Sato Y, Misawa S, Nasu S, Sekiguchi Y, Mitsuma S, Isose S, Fujimaki Y, Ohmori S, Koga S, Kuwabara S. Motor axonal excitability properties are strong predictors for survival in amyotrophic lateral sclerosis. J Neurol Neurosurg Psychiatry 2012;83:734-8.

8. Shibuya K, Misawa S, Kimura H, Noto Y, Sekiguchi Y, Iwai Y, Shimizu T, Mizuno T, Nakagawa M, Kuwabara S. Increased motor axonal persistent sodium currents predict rapid functional declines in amyotrophic lateral sclerosis. Neurol Clin Neurosci 2016;4:108-11.

9. Krarup C. Lower motor neuron involvement examined by quantitative electromyography in amyotrophic lateral sclerosis. Clin Neurophysiol 2011;122:414-22.

10. Kuwabara S, Misawa S. Axonal ionic pathophysiology in human peripheral neuropathy and motor neuron disease. Curr Neurovasc Res 2004;1:373-9.

11. de Carvalho M. Why is ALS so excited? Clin Neurophysiol 2011;122:1689-90.

12. Wainger BJ, Kiskinis E, Mellin C, Wiskow O, Han SS, Sandoe J, Perez NP, Williams LA, Lee S, Boulting G, Berry JD, Brown RH Jr Cudkowicz ME, Bean BP, Eggan K, Woolf CJ. Intrinsic membrane hyperexcitability of amyotrophic lateral sclerosis patient-derived motor neurons. Cell Rep 2014;7:1-11.

13. Vucic S, Lin CS, Cheah BC, Murray J, Menon P, Krishnan AV, Kiernan MC. Riluzole exerts central and peripheral modulating effects in amyotrophic lateral sclerosis. Brain 2013;136:1361-70.

14. Brooks BR, Miller RG, Swash M, Munsat, TL, World Federation of Neurology Research Group on Motor Neuron, D. El Escorial revisited: revised criteria for the diagnosis of amyotrophic lateral sclerosis. Amyotroph Lateral Scler Other Motor Neuron Disord 2000;1: 293-9.

15. Le Liboux A, Lefebvre P, Le Roux Y, Truffinet P, Aubeneau M, Kirkesseli S, Montay G. Single- and multiple-dose pharmacokinetics of riluzole in white subjects. J Clin Pharmacol 1997;37:820-7.

16. Drenthen J, Blok JH, van Heel EB, Visser GH. Limb temperature and nerve conduction velocity during warming with hot water blankets. J Clin Neurophysiol 2008;25: 104-10.

17. Franssen H, Wieneke GH. Nerve conduction and temperature: necessary warming time. Muscle Nerve 1994;17:336-44.

18. Geerlings AH, Mechelse K. Temperature and nerve conduction velocity, some practical problems. Electromyogr Clin Neurophysiol 1985;25:253-9.

19. Cedarbaum JM, Stambler N, Malta E, Fuller C, Hilt D, Thurmond B, Nakanishi A. The ALSFRS-R: a revised ALS functional rating scale that incorporates assessments of respiratory function. BDNF ALS Study Group (Phase III). J Neurol Sci 1999;169:13-21.

20. Kaufmann P, Levy G, Montes J, Buchsbaum R, Barsdorf AI, Battista V, Arbing R, Gordon PH, Mitsumoto H, Levin B, Thompson JL; QALS study group. Excellent inter-rater, intra-rater, and telephone-administered reliability of the ALSFRS-R in a multicenter clinical trial. Amyotroph Lateral Scler 2007;8:42-6.

21. Kollewe K, Mauss U, Krampfl K, Petri S, Dengler R, Mohammadi B. ALSFRS-R score and its ratio: a useful predictor for ALS-progression. J Neurol Sci 2008;275:69-73 .

22. Tomlinson SE, Tan SV, Kullmann DM, Burke D, Hanna MG, Bostock H. Axonal Excitability Changes in Genetic Neuronal Ion Channel Disorders. Journal of the Peripheral Nervous System 2009;14:144-5.

23. Agency, E.M. SmPC Rilutek. <http://www.ema.europa.eu/docs/en_GB/document_library/EPAR_-_Product_Information/human/000109/WC500056586.pdf> 2018.

24. Gunthorpe MJ, Large CH, Sankar R. The mechanism of action of retigabine (ezogabine), a first-in-class K+ channel opener for the treatment of epilepsy. Epilepsia 2012;53: 412-24.

25. Huang CJ, Harootunian A, Maher MP, Quan C, Raj CD, McCormack K, Numann R, Negulescu PA, González JE. Characterization of voltage-gated sodium-channel blockers by electrical stimulation and fluorescence detection of membrane potential. Nat Biotechnol 2006;24:439-46.

26. Bostock H, Baker M. Evidence for two types of potassium channel in human motor axons in vivo. Brain Res 1988;462:354-8.

27. Reid G, Scholz A, Bostock H, Vogel W. Human axons contain at least five types of voltage-dependent potassium channel. J Physiol 1999;518(Pt 3):681-96.

28. Schwarz JR, Glassmeier G, Cooper EC, Kao TC, Nodera H, Tabuena D, Kaji R, Bostock H KCNQ channels mediate IKs, a slow K+ current regulating excitability in the rat node of Ranvier. J Physiol 2006;573:17-34.

29. Devaux JJ, Kleopa KA, Cooper EC, Scherer SS. KCNQ2 is a nodal K+ channel. J Neurosci 2004;24:1236-44.

30. Tatulian L, Delmas P, Abogadie FC, Brown DA. Activation of expressed KCNQ potassium currents and native neuronal M-type potassium currents by the anti-convulsant drug retigabine. J Neurosci 2001;21:5535-45.

31. Wua YJ,Dworetzky SI. Recent developments on KCNQ potassium channel openers. Curr Med Chem 2005;12:453-60.

32. Kiernan MC, Bostock H. Effects of membrane polarization and ischaemia on the excitability properties of human motor axons. Brain 2000;123(Pt 12):2542-51.

33. Bostock H., Rothwell JC. Latent addition in motor and sensory fibres of human peripheral nerve. J Physiol 1997;498(Pt 1):277-94.

34. Lang PM, Fleckenstein J, Passmore GM, Brown DA, Grafe P. Retigabine reduces the excitability of unmyelinated peripheral human axons. Neuropharmacology 2008;54:1271-8.

35. Kiernan MC, Guglielmi JM, Kaji R, Murray NM, Bostock H. Evidence for axonal membrane hyperpolarization in multifocal motor neuropathy with conduction block. Brain 2002;125:664-75.

36. Kiernan MC, Mogyoros I, Burke D. Differences in the recovery of excitability in sensory and motor axons of human median nerve. Brain 1996;119(Pt 4):1099-105.

37. Corbin-Leftwich A, Mossadeq SM, Ha J, Ruchala I, Le AH,Villalba-Galea CA. Retigabine holds KV7 channels open and stabilizes the resting potential. J Gen Physiol 2016;147:229-41.

38. Fleckenstein J, Sittl R, Averbeck B, Lang PM, Irnich D, Carr RW. Activation of axonal Kv7 channels in human peripheral nerve by flupirtine but not placebo - therapeutic potential for peripheral neuropathies: results of a randomised controlled trial. J Transl Med 2013;11:34.

39. Sittl R, Carr RW, Schwarz JR, Grafe P. The Kv7 potassium channel activator flupirtine affects clinical excitability parameters of myelinated axons in isolated rat sural nerve. J PeripherNerv Syst 2010;15:63-72.

40. Baker M, Bostock H, Grafe P, Martius P. Function and distribution of three types of rectifying channel in rat spinal root myelinated axons. J Physiol 1987;383:45-67.

41. Bellingham MC. A review of the neural mechanisms of action and clinical efficiency of riluzole in treating amyotrophic lateral sclerosis: what have we learned in the last decade? CNS Neurosci Ther 2011;17:4-31.

42. Zoccolella S, Beghi E, Palagano G, Fraddosio A, Guerra V, Samarelli V, Lepore V, Simone IL, Lamberti P, Serlenga L, Logroscino G; SLAP registry. Riluzole and amyotrophic lateral sclerosis survival: a population-based study in southern Italy. Eur J Neurol 2007;14:262-8.

43. Schuster JE, Fu R, Siddique T, Heckman CJ. Effect of prolonged riluzole exposure on cultured motoneurons in a mouse model of ALS. J Neurophysiol 2012;107:484-92.

44. Jablonski MR, Jacob DA, Campos C, Miller DS, Maragakis NJ, Pasinelli P, Trotti D. Selective increase of two ABC drug efflux transporters at the blood-spinal cord barrier suggests induced pharmacoresistance in ALS. Neurobiol Dis 2012;47:194-200.

7

Influence of intravenous immunoglobulin on nerve excitability in Multifocal Motor Neuropathy

MARIA O. KOVALCHUK
HESSEL FRANSSEN
LEONARD H. VAN DEN BERG
LEONARD J. VAN SCHELVEN
RUBEN P.A. VAN EIJK
BOUDEWIJN T.H.M. SLEUTJES

ABSTRACT

Introduction. The use of intravenous immunoglobulin (IVIg) in patients with multifocal motor neuropathy (MMN) is associated with the improvement in muscle strength. The exact mechanism of action of IVIg stays unclear, probably related to the decrease in complement deposition on GM1 epitopes, influence on axolemmal ion channel properties, or both. The present study was undertaken to assess the change in excitability parameters induced by IVIg infusion.

Methods. We performed excitability tests in 42 MMN patients (33 men, mean age 52.7 years) on IVIg treatment. Compound muscle action potentials (CMAPs) were recorded from the thenar prior to the IVIg infusion (pre-infusion) and at the time of maximal clinical improvement following IVIg infusion (post-infusion). Clinical tests included assessment of muscle strength, two-point discrimination test and joint position test. Wilcoxon signed-rank test was used for comparing pre-infusion and post-infusion excitability parameters.

Results. On the group level no difference between pre-infusion and post-infusion IVIg excitability parameters was found. Within subject analysis showed statistically significant decrease in TEdpeak following IVIg infusion (p=0.04).

Conclusion. Immunoglobulin produces changes in membrane properties of the peripheral motor nerve in MMN.

INTRODUCTION

Multifocal motor neuropathy (MMN) presents with asymmetric, slowly progressive muscle weakness and muscle atrophy, in the absence of sensory deficit. Routine nerve conduction studies show signs of demyelination or conduction block in motor fibers only.[1-3] The pathogenesis of MMN is considered to be immune-mediated, because around half of the patients (25% to 85%) have serum antibodies against ganglioside GM1, and up to 90% of patients respond to immunoglobulin therapy.[4-8] Ganglioside GM1, sialic acid-containing glycosphingolipid, is expressed in peripheral nerves and was shown to be targeted by autoantibodies, bringing to complement activation, deposition of membrane attack complex and damaging nodal and paranodal regions.[9-15]

Intravenous immunoglobulin (IVIg) is approved for several autoimmune disorders, including chronic inflammatory demyelinating polyneuropathy (CIDP) and MMN.[16] Immune-modulating effect of IVIg is mediated through numerous subunits of the immune system.[6,17-20] Although the long-term effect of immunoglobulin in inflammatory neuropathies was reported, its influence on ongoing axonal degeneration remains controversial.[21-24] The exact mechanism of improving muscle strength by immunoglobulin is unclear. It was suggested that immunoglobulins could promote functional recovery of the damaged motor nerves in patients with CIDP and MMN.[24,25] To examine this hypothesis, excitability testing was performed in MMN and CIDP patients, and showed the reduction of persistent sodium current in MMN together with axonal hyperpolarization in CIDP patients following IVIg administration.

To investigate the effect of IVIg on nerve excitability in MMN and its relation to the muscle strength, we compared motor excitability parameters of the median nerve prior to IVIg and at the time of maximal clinical improvement following IVIg administration. Axonal excitability was assessed in 42 patients diagnosed with MMN. Based on motor nerve conduction studies, patients were divided in groups with (i) demyelinating features and/or conduction block; (ii) axonal loss; and (iii) normal nerve conduction.

MATERIALS AND METHODS

Subjects

We performed motor excitability tests at the median nerve at the wrist in 42 MMN patients (33 men, mean age 52.7 years) on IVIg treatment with no medication affecting peripheral nerve and no history of peripheral nerve disorder. The diagnosis of MMN was

in accordance with the EFNS/PNS criteria for MMN.[26] Patients were divided into three groups according to the nerve conduction findings in the median nerve in the forearm: (i) conduction block: segmental reduction of compound muscle action potential (CMAP) area ⩾ 30%, or demyelination (conduction velocity ⩽ 38 m/s and/or DML ⩾ 5.3 ms and/or increased CMAP duration prolongation in the forearm ⩾30% (n=20); (ii) axonal loss: CMAP amplitude ⩽ 3 mV (n=2); (iii) normal motor nerve conduction (n=20).

In case if a medication affecting peripheral nerve ion channel function was taken (such as quinidine, lidocaine, amiodarone, sotalol, amlodipine, nilvadipine, amitriptyline), disorders potentially giving rise to peripheral neuropathy, and carpal tunnel syndrome (CTS), the patient was not included in the study.

Maintenance IVIg treatment consisted of a 0.4-1.0 g/kg every 2 to 6 weeks (Table 1). Two patients were newly diagnosed with MMN and received their first IVIg course of cumulative dose of 2.0 g/kg in 5 days. Six patients were tested prior to their second treatment, so that the frequency of IVIg administration has not yet been established.

Two patients discontinued the participation after the first visit: in one patient the CMAP was too low to result in a proper excitability testing; another subject could not attend the second visit due to personal reasons.

All patients gave written informed consent. The investigation was performed in accordance with the Declaration of Helsinki and was approved by the local medical ethical committee.

Excitability testing

Excitability was measured in median motor nerve at the wrist using Viking IV EMG apparatus (Nicolet Biomedical, Inc., Madison, Wisconsin), coupled to QTRAC-S software (TRONDNF, version 19-06-2015, institute of Neurology, Queen Square, London, UK) and an isolated bipolar constant current stimulator (DS5, Digitimer, UK). Non-polarizable surface electrodes (Red Dot, 3M Health Care, Germany) were used for median nerve stimulation with the cathode at the wrist and the anode 10cm proximal over the radial side of the forearm. The CMAP of the abductor pollicis brevis (APB) muscle was recorded by surface electrodes in belly-tendon montage. Prior to excitability testing the median nerve was warmed by wrapping the forearm and hand for 30 minutes in a warm water blanket through which water of 37°C flowed constantly (Cincinnati Sub-zero Norm-O-Temp with Cincinnati Sub-zero maxi-therm lite infant hyper-hypothermia blanket for single patient use). During excitability testing the forearm and hand were kept in the blanket in order to keep nerve temperature constant.[27,28]

For excitability testing similar characteristics and protocol was used as described earlier.[29]

We analyzed the following excitability indices: test stimulus current for a CMAP of 50% of its maximal amplitude, slope of the normalized SR curve (SR-slope), rheobase (slope of the charge (Q)-duration (t) relation), strength-duration time constant (absolute value of the x-intercept of the Qt relation), TEd90-100 (threshold decrease at the end of the 40% depolarizing conditioning stimulus), TEdpeak (maximal threshold decrease during 40% depolarizing conditioning stimulus), fanning (sum of the absolute values of TEd90-100 and TEh90-100); S2-accommodation, second slow component of the accommodation to depolarization (difference between TEdpeak and TEd90-100), accommodation half-time (time between the onset of the conditioning stimulus and the time point where threshold decrease is halfway between TEdpeak andTEd90-100), TEh90-100 (threshold increase at the end of the 40% hyperpolarizing conditioning stimulus), resting I/V slope (slope between -10% and +10% conditioning stimuli), minimal I/V slope (smallest slope in the hyperpolarizing part of the current-voltage relation), refractory period (time between conditioning stimulus and return of threshold to baseline), 30% refractory period (time between conditioning stimulus and return of threshold to 30% above its unconditioned value), superexcitability (lowest threshold level following refractory period), and sub-excitability (highest threshold level following superexcitability).

7

Design of the study

Excitability testing was performed twice in every MMN patient – close to the mainte-nance IVIg infusion (on the same day or few days before) and at the peak of clinical im-provement following IVIg, based on patient's personal impression. If the patient had no clinical change after the medication, the post-infusion excitability testing was done in the middle between two infusions. On each visit MRC score of the APB muscle was as-sessed, two-point discrimination test and joint position test were performed (Downs, A-070-01-G).[30]

Statistical analysis

Excitability indices between pre-infusion and post-infusion groups and within individ-ual patients were compared by Wilcoxon signed-rank test. Data is given as median un-less specified otherwise. SPSS (version 25; IBM) was used for all analyses. P<0.05 was considered significant.

RESULTS

Patient's clinical and laboratory data is summarized in Table 1. Thenar muscle strength was decreased in 37 patients, whereas sensory tests were normal. Seventeen patients did not report any obvious clinical improvement. The DML value was stable along each excitability test; it is therefore likely that nerve temperature changed very little during each individual excitability test.

Table 1. Characteristics of 42 MMN patients.

Age, years	62.5 (22–78)
Gender	33 men, 9 women
Treatment duration, months	30.5 (1–97)
Frequency of IVIg infusions, weeks (nr of patients)	2(11), 3(4), 4(17), 5(2), 6(1)
MRC score change, APB muscle (nr of patients)	Increase (11), no change (28), decrease (2)
Post-infusion visit*, days	16 (3–36)
GM1 antibodies	14 patients (33%)

MMN = multifocal motor neuropathy; IVIg = intravenous immunoglobulin; nr = number; MRC = medical research council; APB = abductor pollicis brevis; GM1 = ganglioside GM1; second visit was usually associated with the time of maximal clinical improvement. Data presented as median (range) or number (%).

Excitability indices

On the group level no difference between pre-infusion and post-infusion IVIg excitability parameters was found. Within subject analysis showed statistically significant decrease in TEdpeak following IVIg infusion (p=0.04) (Table 2).

Table 2. Excitability indices in MMN patients.

Variable	Pre-infusion	Post-infusion	P-value
Strength-duration time constant, ms	0.46	0.44	0.12
Rheobase, mA	3.63	3.12	0.47
TEd90-100, %	48.54	47.37	0.07
TEh90-100, %	-126.54	-124.72	0.15
TEdpeak, %	70.03	68.34	0.04
S2-accommodation, %	21.64	21.06	0.22
Half-time Accommodation, ms	36.80	37.50	0.15
Fanning, %	175.08	170.79	0.11
Resting I/V slope	0.56	0.58	0.16
Minimal I/V slope	0.25	0.25	0.97
RP, ms	2.71	2.67	0.7
Superexcitability, %	-26.08	-25.42	0.13
Subexcitability, %	15.02	14.79	0.46
RP30%, ms	2.28	2.24	0.53

Mean values of motor excitability parameters paired for each MMN patient before (Pre-infusion), n=42, and after (Post-infusion) IVIg administration, n=40. TEd = depolarizing threshold electrotonus; TEh = hyperpolarizing threshold electrotonus; RP = refractory period. P-Value<0.05 Wilcoxon signed rank test.

7

DISCUSSION

Immunoglobulin is the only approved treatment in MMN.[31-33] Although the majority of patients demonstrate increase in muscle strength and reduce of fatigue, the favorable response is short-lasting, requiring maintenance treatment every 2 to 6 weeks. In some patients the effectiveness of the treatment often declines with time.[34]

The effect of immunoglobulin in dysimmune neuropathies is primary considered to be exerted via anti-inflammatory pathways.[6,35-37] The presence of antibodies against gangliosides permits to consider MMN as the complement mediated pathology.[6,38] GM1 gangliosides are specifically essential in the attachment of paranodal myelin to the axon and holding clusters of ion channels in the node of Ranvier.[39] In animal model of acute motor axonal neuropathy (AMAN), a form of Guillain-Barré syndrome clinically similar to MMN, anti-GM1 antibodies were shown to be associated with the activation of complement, formation and deposition of membrane attack complex, resulting in struc-

tural damage of the nodal-paranodal region, demyelination, disruption of ion channel integrity and finally to axonal degeneration. [12,40]

The relatively rapid response to IVIg cannot be attributed to remyelination, but the functional recovery via axolemmal ion channels could be a candidate of the potential mechanism of IVIg action. Previous report suggests a decrease in persistent Na+ current in MMN patients following IVIg treatment.[25] This could be associated with the reduction of intraaxonal sodium ions accumulation, favourable for the demyelinated nerves.[41-43] In our study we did not obtain any result consistent with this previous finding. Because different excitability technique and excitability protocol were used, and the exact timing of post-infusion testing in the previous testing is unknown, the actual comparison of our data is limited. The correlation between MRC score and change in excitability has not been earlier confirmed, and authors argue towards a early and transitory effect of immunoglibulint treatment.[25]

Although we did not record change in excitability following IVIg except one parameter, the influence of immunoglobulin on membrane properties is still not excluded – assessing the activity of sodium-potassium pump would probably add to our knowledge on the energy disturbances at the damaged nerves in MMN.[41-43] Performing extensive excitability recording immediately after the drug administration together with long follow-up excitability testing would probably reveal functional modulation of the membrane properties, as shown in CIDP.[24] The report on the decrease of conduction block and reinnervation in long-term IVIg treatment supports this idea.[44,45]

REFERENCES

1. Bouche P, Moulonguet A, Younes-Chennoufi AB, et al. Multifocal motor neuropathy with conduction block: a study of 24 patients. J Neurol Neurosurg Psychiatry. 1995 Jul;59(1):38-44.

2. Leger JM, Behin A: Multifocal motor neuropathy. Curr Opin Neurol 2005; 18: 567–573.

3. Meuth SG, Kleinschnitz C. Multifocal motor neuropathy: update on clinical characteristics, pathophysiological concepts and therapeutic options. Eur Neurol. 2010;63(4):193-204.

4. Nobile-Orazio E, Meucci N, Barbieri S, et al. High-dose intravenous immunoglobulin therapy in multifocal motor neuropathy. Neurology. 1993 Mar;43(3 Pt 1):537-44.

5. Pestronk A, Choksi R. Multifocal motor neuropathy. Serum IgM anti-GM1 ganglioside antibodies in most patients detected using covalent linkage of GM1 to ELISA plates. Neurology. 1997 Nov;49(5):1289-92.

6. Piepers S, Jansen MD, Cats EA, et al. IVIg inhibits classical pathway activity and anti-GM1 IgM-mediated complement deposition in MMN. J Neuroimmunol. 2010 Dec 15;229(1-2):256-62.

7. van Schaik IN, van den Berg LH, de Haan R, Vermeulen M. Intravenous immunoglobulin for multifocal motor neuropathy. Cochrane Database Syst Rev. 2005;(2):CD004429.

8. Leger JM, Viala K, Cancalon F, et al. Intravenous immunoglobulin as short- and long-term therapy of multifocal motor neuropathy: a retrospective study of response to IVIg and of its predictive criteria in 40 patients. J. Neurol. Neurosurg. Psychiatry 79, 93–96 (2008).

9. Uncini A, Santoro M, Corbo M, Lugaresi A, Latov N. Conduction abnormalities induced by sera of patients with multifocal motor neuropathy and anti-GM1 antibodies. Muscle Nerve. 1993 Jun;16(6):610-5.

10. van Schaik IN, Bossuyt PM, Brand A, Vermeulen M. Diagnostic value of GM1 antibodies in motor neuron disorders and neuropathies: a meta-analysis. Neurology 45, 1570–1577 (1995).

11. Willison HJ, Yuki N. Peripheral neuropathies and anti-glycolipid antibodies. Brain. 2002 Dec;125(Pt 12):2591-625.

12. Susuki K, Rasband MN, Tohyama K, et al. Anti-GM1 antibodies cause complement-mediated disruption of sodium channel clusters in peripheral motor nerve fibers. J Neurosci. 2007 Apr 11;27(15):3956-67.

13. Yuki N. Human gangliosides and bacterial lipo-oligosaccharides in the development of autoimmune neuropathies. Methods Mol Biol. 2010;600:51-65

7

14. Cats EA, van der Pol WL, Piepers S, et al. Correlates of outcome and response to IVIg in 88 patients with multifocal motor neuropathy. Neurology 2010;75:818–25

15. Harschnitz O, Jongbloed BA, Franssen H, et al. MMN: from immunological cross-talk to conduction block. J Clin Immunol. 2014 Jul;34 Suppl 1:S112-9.

16. Galeotti C, Kaveri SV, Bayry J. IVIG-mediated effector functions in autoimmune and inflammatory diseases. Int Immunol. 2017 Dec 30;29(11):491-498.

17. Yuki N, Miyagi F. Possible mechanism of intravenous immunoglobulin treatment on anti-GM1 antibody-mediated neuropathies. J Neurol Sci. 1996 Jul;139(1):160-2.

18. Dalakas M. Mechanisms of action of IVIg and therapeutic considerations in the treatment of acute and chronic demyelinating neuropathies. Neurology 2002;59:13–21.

19. Créange A, Gregson NA, Hughes RA. Intravenous immunoglobulin modulates lymphocyte CD54 and monocyte FcgammaRII expression in patients with chronic inflammatory neuropathies. J Neuroimmunol 2003;135:91–5.

20. Baerenwaldt A, Biburger M, Nimmerjahn F. Mechanisms of action of intravenous immunoglobulins. Expert Rev Clin Immunol. 2010;6(3):425-434

21. Van den Berg-Vos RM, Franssen H, Wokke JH, et al. Multifocal motor neuropathy: long-term clinical and electrophysiological assessment of intravenous immunoglobulin maintenance treatment. Brain 125, 1875–1886 (2002).

22. Terenghi, F. et al. How long is IVIg effective in multifocal motor neuropathy? Neurology 62, 666–668 (2004).

23. Vucic S, Black KR, Chong PS, Cros D. Multifocal motor neuropathy: decrease in conduction blocks and reinnervation with long-term IVIg. Neurology 63, 1264–1269 (2004).

24. Lin CS, Krishnan AV, Park SB, Kiernan MC. Modulatory effects on axonal function after intravenous immunoglobulin therapy in chronic inflammatory demyelinating polyneuropathy. Arch Neurol. 2011 Jul;68(7):862-9.

25. Boërio D, Créange A, Hogrel JY, et al. Nerve excitability changes after intravenous immunoglobulin infusions in multifocal motor neuropathy and chronic inflammatory demyelinating neuropathy. J Neurol Sci. 2010;292(1-2):63-71.

26. European Federation of Neurological Societies/Peripheral Nerve Society guideline on management of multifocal motor neuropathy. Report of a joint task force of the European Federation of Neurological Societies and the Peripheral Nerve Society--first revision. Joint Task Force of the EFNS and the PNS. J Peripher Nerv Syst. 2010 Dec;15(4):295-301.

27. Franssen H, Wieneke GH. Nerve conduction and temperature: necessary warming time. Muscle Nerve 1994 Mar;17(3):336-44.

28. Drenthen J, Blok JH, Dudok van Heel EB, Visser GH. Limb temperature and nerve conduction velocity during warming with hot water blankets. Journal of Clinical Neurophysiology 2008; 25: 104-10.

29. Kovalchuk MO, Franssen H, Van Schelven LJ, Sleutjes BTHM. Comparing excitability at 37°C versus at 20°C: Differences between motor and sensory axons. Muscle Nerve. 2018 Apr;57(4):574-580.

30. Van Nes S, Faber CG, Hamers RMTP, et al. on behalf of the perinoms study group. Revising two-point discrimination assessment in normal aging and in patients with polyneuropathies. J Neurol Neurosurg Psychiatry 2008;79:832-4.

31. Van den Berg LH, Kerkhoff H, Oey PL, et al. Treatment of multifocal motor neuropathy with high dose intravenous immunoglobulins: a double blind, placebo controlled study. J Neurol Neurosurg Psychiatry 1995;59:248–252.

32. Federico P, Zochodne DW, Hahn AF, Brown WF, Feasby TE. Multifocal motor neuropathy improved by IVIg. Randomized, double-blind, placebo-controlled, cross-over study. Neurology 2000;55:1256–1261.

33. Terenghi F, Cappellari A, Bersano A, Carpo M, Barbieri S, Nobile-Orazio E. Neurology. 2004 Feb 24;62(4):666-8. How long is IVIg effective in multifocal motor neuropathy?

34. Lutz HU, Stammler P, Bianchi V, et al. Intravenously applied IgG stimulates complement attenuation in a complement-dependent autoimmune disease at the amplifying C3 convertase level. Blood. 2004 Jan 15;103(2):465-72.

35. van Sorge NM, Yuki N, Jansen MD, et al. Leukocyte and complement activation by GM1-specific antibodies is associated with acute motor axonal neuropathy in rabbits. J Neuroimmunol. 2007;182(1–2):116–23.

36. Hughes R. The role of IVIg in autoimmune neuropathies: the latest evidence. J Neurol. 2008 Jul;255 Suppl 3:7-11.

37. Yuki N, Watanabe H, Nakajima T, Späth PJ. IVIG blocks complement deposition mediated by anti-GM1 antibodies in multifocal motor neuropathy. J Neurol Neurosurg Psychiatry. 2011 Jan;82(1):87-91.

38. Susuki K, Baba H, Tohyama K, Kanai K, Kuwabara S, Hirata K, et al. Gangliosides contribute to stability of paranodal junctions and ion channel clusters in myelinated nerve fibers. Glia. 2007;55(7):746–57.

39. Susuki K, Yuki N, Schafer DP, Hirata K, Zhang G, Funakoshi K, et al. Dysfunction of nodes of Ranvier: a mechanism for anti-ganglioside antibody-mediated neuropathies. Exp Neurol 2012; 233:534-42.

7

40. Craner MJ, Newcombe J, Black JA, Hartle C, Cuzner ML, Waxman SG. Molecular changes in neurons in multiple sclerosis: altered axonal expression of Nav1.2 and Nav1.6 sodium channels and Na+/Ca2+ exchanger. Proc Natl Acad Sci U S A 2004;101:8168–73.

41. Bechtold DA, Smith KJ. Sodium-mediated axonal degeneration in inflammatory demyelinating disease. J Neurol Sci 2005;233:27–35.

42. Stys PK, Waxman SG. Activity-dependent modulation of excitability: implication for axonal physiology and pathophysiology. Muscle Nerve 1994;17:969–74.

43. Hageman S, Kovalchuk MO, Sleutjes BTHM, van Schelven LJ, van den Berg LH, Franssen H. Sodium-potassium pump assessment by submaximal electrical nerve stimulation. Clin Neurophysiol 2018;129:809-814

44. Vucic S, Black KR, Chong PS, Cros D. Multifocal motor neuropathy: decrease in conduction blocks and reinnervation with long-term IVIg. Neurology 2004;63:1264–9.

45. Vucic S, Black K, Baldassari LE, et al. Long-term effects of intravenous immunoglobulin in CIDP. Clin Neurophysiol 2007;118:1980–4.

8

Sodium-potassium pump assessment by submaximal electrical nerve stimulation

STEVEN HAGEMAN
MARIA O. KOVALCHUK
BOUDEWIJN T.H.M. SLEUTJES
LEONARD J. VAN SCHELVEN
LEONARD H. VAN DEN BERG
HESSEL FRANSSEN

ABSTRACT

Objective. Sodium-potassium pump dysfunction in peripheral nerve is usually assessed by determining axonal hyperpolarization following maximal voluntary contraction (MVC) or maximal electrical nerve stimulation. As MVC may be unreliable and maximal electrical stimulation too painful, we assessed if hyperpolarization can also be induced by submaximal electrical nerve stimulation.

Methods. In 8 healthy volunteers different submaximal electrical stimulus trains were given to the median nerve at the wrist, followed by 5 minute assessment of thresholds for compound muscle action potentials of 20%, 40% or 60% of maximal.

Results. Threshold increase after submaximal electrical nerve stimulation was most prominent after an 8Hz train of at least 5 minutes duration evoking submaximal CMAPs of 60%. It induced minimal discomfort and was not painful. Threshold increase after MVC was not significantly higher than this stimulus train.

Conclusion. Submaximal electrical stimulation evokes activity dependent hyperpolarization in healthy test subjects without causing significant discomfort.

Significance. Sodium-potassium pump function may be assessed using submaximal electrical stimulation.

INTRODUCTION

Excitability studies suggested that sodium-potassium pump dysfunction in peripheral nerve motor axons may contribute to the pathogenesis of diabetic neuropathy and amyotrophic lateral sclerosis.[1,2] In these studies pump function was assessed by determining threshold increase for motor axon excitation following maximal voluntary contraction (MVC) of a muscle innervated by those axons. This threshold increase arises because the intra-axonal sodium accumulation and potassium loss resulting from sustained nerve impulse firing is restored by temporarily increased pump activity. Because, per cycle, the pump removes 3 positive sodium-ions from the axon and puts only 2 positive potassium-ions back into the axon, its action results in a net loss of positive charge at the inside of the axolemma, giving rise to axonal hyperpolarization and threshold increase.[3]

The use of MVC to assess pump-function in patients has, however, potential drawbacks since subjects may not fully activate their muscle, the precise firing rate in axons is unknown in a given patient, and unstable or blocked impulse propagation proximal to the testing site may preclude MVC.[4] Repetitive electrical nerve stimulation to activate the pump instead of MVC avoids these drawbacks, but using maximal electrical nerve stimuli can cause significant patient discomfort.

The present study assessed if trains of submaximal electrical nerve stimuli are tolerable and cause sufficient axonal hyperpolarization to assess pump function.

8

METHODS

Subjects

We investigated 8 subjects (7 men, mean age 35 years). All subjects were healthy, except for one who had carpal tunnel syndrome. Informed consent was obtained from all subjects. The investigation was done in accordance to the Declaration of Helsinki and was approved by the local medical ethics committee.

Protocol

The right median nerve was stimulated at the wrist via non-polarizable surface electrodes (Red Dot, 3M Health Care, Germany; cathode at the wrist; anode 10cm proximal over the radial aspect of the forearm) and the thenar compound muscle action potential (CMAP) was recorded by surface disk electrodes of 10mm diameter in a belly-tendon

montage. The set-up consisted of: (i) a Viking IV EMG-apparatus (Nicolet Biomedical, Inc., Madison, Wisconsin) for recording thenar CMAPs and delivering stimulus trains to the median nerve at the wrist, (ii) an isolated bipolar constant current stimulator (DS5, Digitimer, UK model D185-HB4) for delivering test and conditioning stimuli at the wrist, and (iii) a computer (PCI-6221, National instruments) running QtracS software (TRONDNF, version 19-06-2015, Institute of Neurology, Queen Square, London, UK) for controlling test and conditioning stimuli. Test stimuli were 1.0ms duration current pulses which estimated the threshold current for a CMAP of a given percentage of its maximal amplitude by means of proportional threshold tracking. Target CMAP is defined as this percentage of the maximal CMAP amplitude used for threshold tracking. To control for fatigability and other changes in the maximal CMAP amplitude, a supra-maximal electrical stimulus was provided every stimulus cycle to assess the maximal CMAP amplitude at that moment.

Tests consisted of the following parts: (i) tracking baseline threshold for 1 minute, (ii) delivering a stimulus train to induce a threshold change, and (iii) tracking thresholds after the stimulus train for 5 minutes. Train CMAP is defined as the amplitude of the CMAPs during the stimulus train as a percentage of the maximal CMAP amplitude. The train CMAPs in a stimulus train varied from 40% to 100% of the maximal CMAP. Stimuli in a train were rectangular pulses of 0.2ms duration. Thresholds were assessed by test stimuli delivered at 2Hz for target CMAPs of 20%, 40% or 60%. Mean threshold was calculated every 30 seconds. Threshold increase was normalized by defining it with respect to the mean baseline threshold. Per recording we measured normalized peak-threshold increase and normalized end-threshold increase. Per subject, each of the test paradigms was conducted on a different day. We also assessed threshold recovery after MVC or submaximal electrical nerve stimulation by calculating the recovery rate. This was defined as the mean absolute threshold change per minute over the first 3 minutes after MVC or submaximal electrical stimulus train.

To exclude threshold changes induced by temperature change during testing, we monitored skin temperature continuously by a temperature sensor at the wrist. For the same purpose, we also assessed distal motor latency (DML) every 1.6 seconds throughout each test, since changes in DML reflect changes in nerve temperature.[5]

Immediately after the test, subjects were asked to score discomfort based on a 9-point comfort scale[6], containing: painful (0), hurting (1), concerning pressure (2), irritant (3), constantly annoying (4), occasionally annoying (5), constantly noticeable (6), occasionally noticeable (7) and not noticeable (8).

The study consisted of 4 parts. First, a preliminary investigation was conducted in 7 subjects to assess if a threshold increase was induced by stimulus train rates of 7, 8, 10, 15, or 20 Hz and stimulus train durations of 1, 2, 5, 7, or 10 minutes. Next, the 4 electrical stimulation paradigms protocols yielding the most prominent threshold increases were selected from the results of the first part and systematically tested in all subjects. Then, the paradigm resulting in the largest threshold increase and the smallest discomfort was tested 3 times in every subject to assess reproducibility by means of the coefficient of variation (CoV) within each subject. CoV was defined as the standard deviation of the peak thresholds, divided by the mean of the peak thresholds. Finally, threshold increase after MVC for 1 minute was compared with threshold increase after a submaximal electrical stimulus train.

We also assessed how accurately the setting for a train CMAP of 60% actually induced a CMAP of 60% of its maximal amplitude. In 3 subjects an 8Hz stimulus train with a train CMAP of 60% was given, but instead of recording the threshold changes, the amplitude of every CMAP was recorded using the CMAP-scan application[7] on another Viking EMG apparatus (Version 20.1, Natus Neurology Incorporated, Inc, Middleton, WI, USA).

To confirm that the observed threshold increase following submaximal electrical nerve stimulation indeed reflected hyperpolarization of resting membrane potential[8], an extra excitability test was performed in 3 subjects, assessing those excitability parameters that are most sensitive to changes in membrane potential. [8-10] Thus, the following parameters were tested before and after a stimulus train with a train CMAP 60% for 7 minutes: strength-duration time constant (SDTC) which is the absolute value of the x-intercept of the Qt relation (relation between stimulus charge and stimulus duration, calculated using pulses of 0.2, and 1.0ms); hyperpolarizing threshold electrotonus 90-100ms (TEh90-100) which is the threshold increase at the end of a 40% hyperpolarizing conditioning stimulus of 100ms; depolarizing threshold electrotonus 90-100ms (TEd90-100) which is the threshold decrease at the end of a 40% depolarizing conditioning stimulus of 100ms; fanning which is the sum of the absolute values of TEd90-100 and TEh90-100; supernormality which is the decrease of the threshold 6.3ms after a preceding supramaximal pulse.

8

Analysis

Statistical analysis was performed with SPSS (version 21; IBM). To assess normality we applied the Shapiro-Wilk test. Since data were not normally distributed, statistical analysis of thresholds and discomfort scores was performed by the Wilcoxon signed test. $P < 0.05$ was considered statistically significant. All data is presented as median and interquartile range (IQR) unless specified otherwise.

RESULTS

Basic investigations

The preliminary investigation showed that at least 5 minutes of electrical nerve stimulation at a rate of 8Hz was required to obtain reproducible threshold increases. Based on these results, 4 electrical stimulus train paradigms were systematically tested in all subjects (Table 1, Figure 1). This showed that the highest peak threshold increases were induced by the paradigm using a train CMAP of 60% for 7 minutes and a target CMAP of 20% as well as by the paradigm using a train CMAP of 100% for 5 minutes and a target CMAP of 40%. Findings in the subject with carpal tunnel syndrome were not different from those in the other subjects, except that more current was needed to evoke a maximal CMAP. However, no conclusions should be drawn from this, since we did not systematically study the differences between healthy subjects and those with carpal tunnel syndrome.

Table 1. Thresholds after 8Hz electrical stimulus trains or maximal voluntary contraction.

Paradigm	Target CMAP	Median peak-threshold (IQR)	Median end-threshold (IQR)
Train CMAP 40% - 5min	20%	1.06 (1.04-1.09)	1.00 (0.99-1.02)
Train CMAP 60% - 5min	40%	1.10 (1.06-1.12)	1.04 (1.03-1.06)
Train CMAP 60% - 7min	20%	1.14 (1.10-1.15)	1.07 (1.05-1.09)
	40%	1.11 (1.08-1.12)	1.06 (1.03-1.07)
Train CMAP 100% - 5min	40%	1.15 (1.06-1.21)	1.05 (1.01-1.09)
MVC – 1 min	20%	1.22 (1.15-1.24)	1.09 (1.07-1.11)
	40%	1.23 (1.16-1.24)	1.08 (1.07-1.10)
	60%	1.24 (1.16-1.25)	1.07 (1.06-1.11)

CMAP = compound muscle action potential. Min = duration of stimulus train in minutes. MVC = maximal voluntary contraction. Thresholds are given relative to the baseline threshold and are displayed as the median in 8 subjects. End thresholds were determined 5 minutes after the stop of stimulation or MVC.
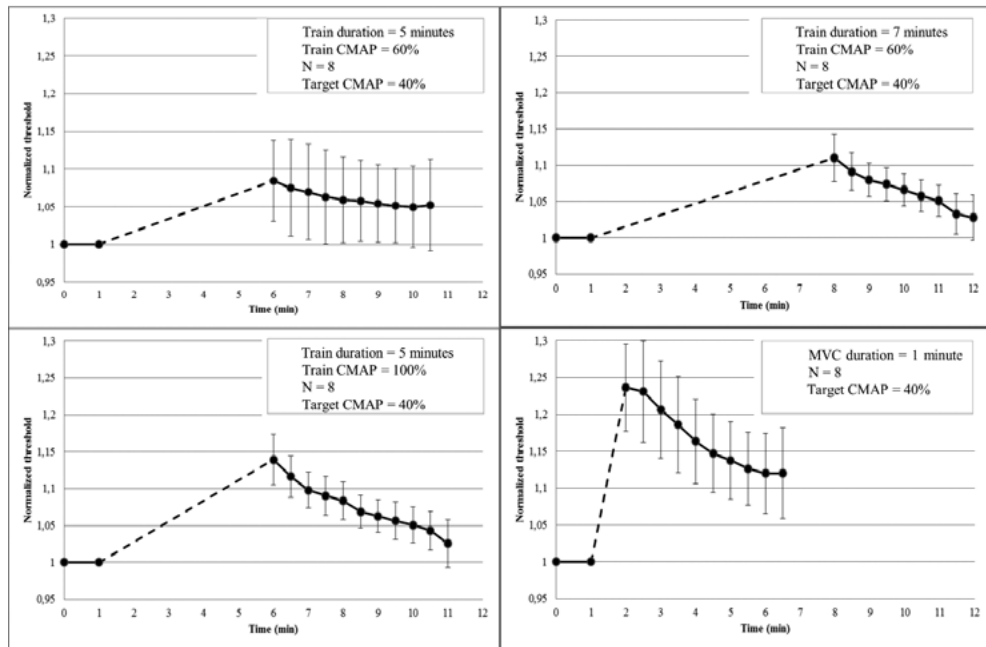
Figure 1. Comparison of stimulus trains and maximal voluntary contraction.

Figure 1 legend. Threshold increase induced by 3 different electrical stimulus trains (left upper and lower, right upper) or maximal voluntary contraction (right lower). Dots represent normalized mean thresholds of 30 seconds and bars the standard error of the mean. The interrupted line represents the period of electrical stimulation or maximal voluntary contraction. CMAP = compound muscle action potential. MVC = maximal voluntary contraction.

8

Discomfort

None of the subjects scored the electrical stimulation paradigms as 0 (painful) or 1 (hurting). The median discomfort score for train CMAPs of 40% was 5.5 (IQR 5.0-6.0) and that for train CMAPs of 100% was 5.0 (IQR 4.0-5.0). Train CMAPs of 60% caused the least discomfort: using a train duration of 5 minutes the median score was 7.0 (IQR 5.5-7.0) and for 7 minutes the median score was 7.0 (IQR 6.0-7.0), indicating that the tests using a train CMAP of 60% were the best tolerable. One subject even found electrical stimulation rather pleasant. Remarkably, the median discomfort score for MVC was worse (5.5, IQR 4.0-6.0) than that for train CMAPs of 60%, probably because of the pain induced by having to maintain full contraction.

Reproducibility

Reproducibility was assessed per subject for 7 minutes duration stimulus trains of 8Hz evoking a train CMAP of 60%, since this paradigm induced the highest threshold increase and caused the least discomfort. Median intra-subject CoV was 4.1% (IQR 0.8-8.2) when threshold increase was assessed for a target CMAP of 20% and 5.5% (IQR 2.7-9.0) when it was assessed for a target CMAP of 40%. This difference was not significant (p = 0.26, n = 8).

Maximal voluntary contraction

Generally, MVC for 1 minute induced higher threshold increases than electrical stimulus trains when similar train CMAPs were evoked. This was shown for train CMAPs of 100% for 5 min evoking target CMAPs of 40% (p = 0.05, n = 8), train CMAPs of 60% for 5 min evoking target CMAPs of 40% (p = 0.03, n = 8), and train CMAPs of 40% for 5 min evoking target CMAPs of 20% (p = 0.03, n = 8). No difference was found between the threshold increases induced by MVC and train CMAPs of 60% for 7 minutes evoking target CMAPs of 20% (p = 0.32, n = 8). No correlation was found between peak threshold change after train CMAPs of 60% for 7 minutes evoking target CMAPs of 40%, and the peak threshold change after MVC (r = 0.10, p = 0.82, n = 8).

Recovery

Normalized thresholds slowly decreased after MVC or submaximal electrical nerve stimulation. Recovery rates were -2.91% per minute (IQR -4.04% to -1.42%) using a train CMAP of 100% for 5 minutes, -0.92% per minute (IQR -2.71% to 0.72%) using a train CMAP of 60% for 5 minutes, -1.62% per minute (IQR -2.47% to -0.82%) using a train CMAP of 60% for 7 minutes and -4.95% per minute (IQR -5.73% to -2.29%) after MVC. The difference between MVC and train CMAP 60% for 5 minutes was significant (p = 0.04, n = 8), but other recovery rates did not differ significantly.

Temperature

Median skin temperature at the start of every experiment was 31.8°C (IQR 31.0-32.6°C) and the median skin temperature shift within each test 0.6°C (IQR 0.4-1.0°C). Median DML at the start of each experiment was 5.4ms (IQR 5.1-5.8) and the median DML shift within each test 0.1ms. There was no correlation between skin temperature and threshold change for any of the tests (r = -0.12 , p = 0.51) or recovery rate (r =-0.12 , p= 0.51).

Test accuracy

The tests assessing the accuracy of train CMAPs of 60% showed that the median train CMAP amplitude was 58% (IQR 52%-63%) of the maximal CMAP amplitude (figure 2). Excitability tests performed immediately after 8Hz electrical nerve stimulation evoking train CMAPs of 60% for 7 minutes showed more prominent supernormality, fanning-out of threshold electrotonus and decreased SDTC (figure 3); these changes are consistent with axonal hyperpolarization.

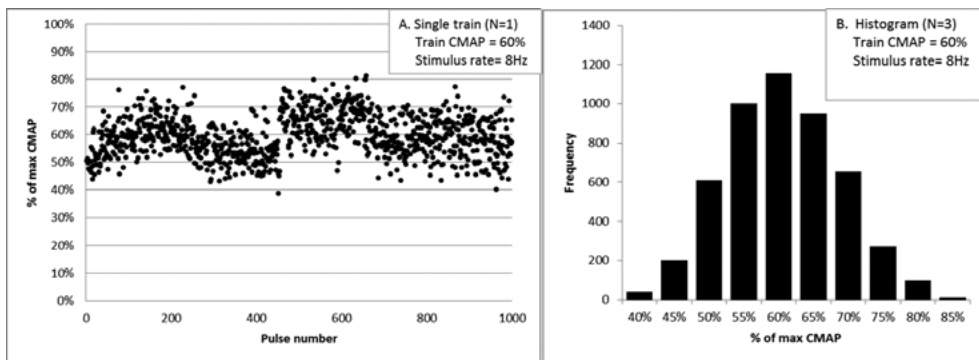**Figure 2.** Accuracy of train CMAP.

Figure 2 legend. Accuracy of train CMAPs aimed at 60% of maximal and evoked by 1000 stimuli with a rate of 8Hz. (A) recording in a single subject. (B) histogram of 3000 stimuli in 3 subjects. CMAP = compound muscle action potential.

8

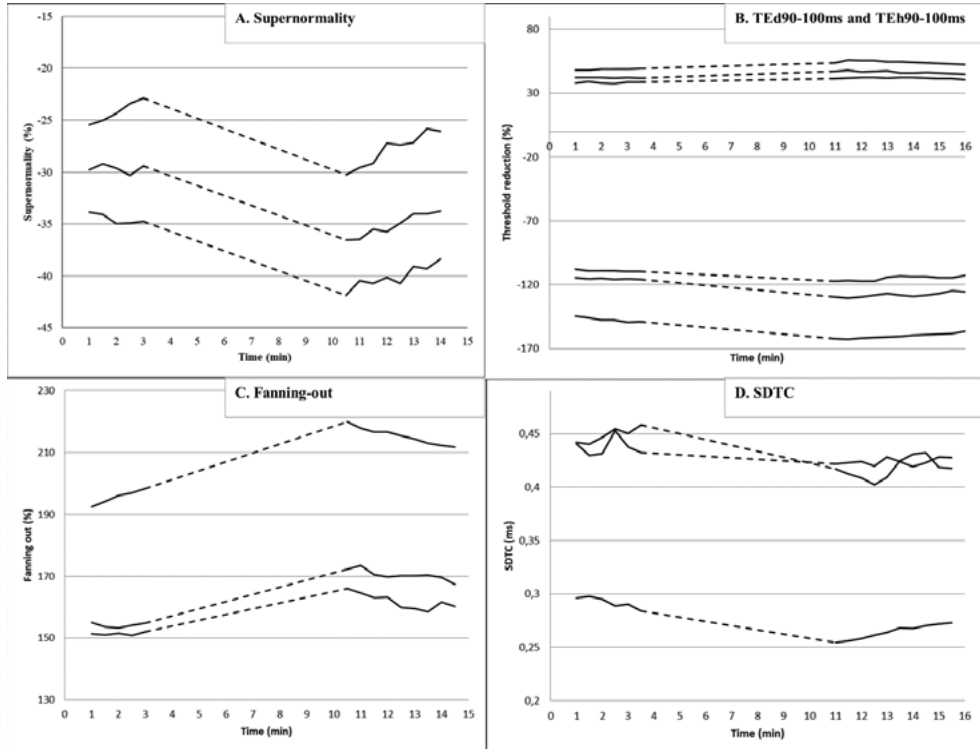**Figure 3.** Change in excitability parameters induced by a submaximal electrical stimulus train.

Figure 3 legend. Stimulus train duration 7 minutes, stimulus rate 8Hz, train CMAP 60%, and target CMAP 40%. Every line represent a single test on a single subject. A: supernormality at 6.3ms. B: TEd90-100($\bullet$) and TEh90-100($\circ$). C: fanning, defined as the sum of the absolute value of TEd90-100 and TEh90-100. D: SDTC calculated by linear interpolation of thresholds for 40% target CMAPs evoked by electrical stimuli of 0.2ms and 1ms duration. CMAP = compound muscle action potential. SDTC = strength-duration time constant. TEd90-100 = depolarizing threshold electrotonus at 90-100ms. TEh90-100 = hyperpolarizing threshold electrotonus 90-100ms.

DISCUSSION

Of several electrical stimulation paradigms tested, one paradigm was shown to induce the largest and most reproducible threshold increases without being painful. This paradigm consisted of delivering a 7 minutes duration electrical stimulus train of 8Hz evoking train CMAPs of 60% ofmaximal, followed by threshold assessment for a target CMAP of 20% for 5 minutes. The resulting threshold increase was 14% and the paradigm was considered noticeable but not painful. We also showed that the threshold increase induced by submaximal nerve stimulation resulted in excitability changes compatible with hyperpolarization of axonal resting membrane potential. MVC for 1 minute induced a larger threshold increase (22-24%) than the above described best electrical stimulation paradigm, but the difference was statistically not significant. Other studies found a threshold increase after MVC of 17-20% [2,9-11]. Intra-subject reproducibility of the best electrical stimulation paradigm was similar to that reported for MVC by others.[12] We also showed that submaximal nerve stimulation can be used to assess the threshold recovery rate. As the rate of recovery reflects sodium-potassium pump activity[13,14], changes in recovery rate may be a very sensitive parameter in detecting sodium-potassium pump dysfunction. This can give important insights into the capacity of motor axons to handle an activity-dependent increase in intra axonal sodium load.[15]

The electrical stimulus rate of 8Hz that yielded the most prominent threshold increase in the present study is physiologically appropriate for testing sodium-potassium pump function. This is because 125ms (the interval between 2 stimuli of 8Hz) is longer than the duration of the recovery cycle (approximately 100ms) so that the axon can fully recover between stimuli.[16-18] With shorter stimulus intervals the next action potential is evoked in the subexcitable period of the previous one so that threshold change will reflect the sum of subexcitability and increased pump activation which both increase threshold. When stimulus interval is further decreased, the threshold change reflects the sum of supernormality (which decreases threshold) and increased pump activity (which increases threshold). These shorter stimulus intervals are, therefore, unsuitable to assess pump function since they are also affected by other processes than pump activity. It must also be emphasized that conditions with abnormally long recovery cycles, such as arising from long standing axonal depolarization (for instance due to low temperature),[19] probably require train stimulus rates slower than 8Hz.

The above described considerations also apply for MVC since this is sustained by nerve action potentials starting at a rate of 50Hz (corresponding to an action potential interval of 20ms) and finishing at 20Hz which corresponds to an action potential interval of

8

50ms.[20-22] Furthermore, in patients with muscle weakness, MVC may be unreliable due to inability of the relevant nerve to generate nerve action potentials, for instance due to conduction block proximal to the site of testing. In those situations, trains of submaximal electrical nerve stimuli can be a beneficial approach to assess pump function.

CONCLUSION

Submaximal electrical stimulation is a reliable method for inducing activity dependent hyperpolarization in healthy subjects. The increased standardization and low discomfort make this suitable and reliable alternative to MCV in the assessment of sodium-potassium pump function in motor axons. Future research validating this method in patients with muscle weakness should enable its use in clinical practice.

REFERENCES

1. Vucic S, Krishnan AV, Kiernan MC. Fatigue and activity dependent changes in axonal excitability in amyotrophic lateral sclerosis. J Neurol Neurosurg Psychiatry 2007;78:1202-8

2. Krishnan AV, Lin CSY, Kiernan MC. Activity-dependent excitability changes suggest Na+/K+ pump dysfunction in diabetic neuropathy. Brain 2008;131:1209-16

3. Skou JC. The influence of some cations on an adenosine triphosphatase from peripheral nerves. Biochim Biophys Acta. 1957;2:394-401.

4. Cappelen-Smith C, Kuwabara S, Lin CSY, Mogyoros I, Burke D. Activity-Dependent Hyperpolarization and Conduction Block in Chronic Inflammatory Demyelinating Polyneuropathy. Ann Neurol 2000;48:826-32.

5. Franssen H, Wieneke GH. Nerve conduction and temperature: necessary warming time. Muscle Nerve 1994;17:516-22.

6. O'Brian S, Packman A, Onslow M, Cream A, O'Brian N, Bastock K. Is listener comfort a viable construct in stuttering research? J Speech Lang Hear Res. 2003;46:503-9.

7. Sleutjes BTHM, Montfoort I, Maathuis EM, Drenthen J, Doorn PA, Visser GH, Blok JH. CMAP scan discontinuities: Automated detection and relation to motor unit loss. Clin Neurophysiol. 2014;125:388–395

8. Vagg R, Mogyoros I, Kiernan MC, Burke D. Activity-dependent hyperpolarization of human motor axons produced by natural activity. J Physiol 1998;507:919-25.

9. Bostock H, Bergmans J. Post-tetanic excitability changes and ectopic discharges in a human motor axon. Brain 1994;117:913-28.

10. Kiernan MC, Lin CS, Burke D. Differences in activity-dependent hyperpolarization in human sensory and motor axons. J Physiol 2004;558:341-9

11. Kuwabara S, Lin CS, Mogyoros I, Cappelen-Smith C, Burke D. Voluntary contraction impairs the refractory period of transmission in healthy human axons. J Physiol 2001;531:265-75.

12. Milder DA, Sutherland EJ, Gandevia SC, McNulty PA. Sustained Maximal Voluntary Contraction Produces Independent Changes in Human Motor Axons and the Muscle They Innervate. PLoS One 2014;9:e91754.

13. Moldovan M, Krarup C. Persistent abnormalities of membrane excitability in regenerated mature motor axons in cat. J Physiol 2004a; 560: 795 - 806

14. Moldovan M, Krarup C. Mechanisms of hyperpolarization in regenerated mature motor axons in cat. J Physiol 2004b;560: 807-19

15. Moldovan M, Krarup C. Evaluation of Na+/K+ pump function following repetitive activity in mouse peripheral nerve. J Neurosci Methods 2006;155: 161 - 71

8

16. Bergmans, J. 1970. Physiology of single human fibres. Vander, Univ. Louvain, Belgium.

17. Kiernan, MC, Mogyoros I, Burke D. Changes in excitability and impulse transmission following prolonged repetitive activity in normal subjects and patients with a focal nerve lesion. Brain 1996;119:2029-37.

18. Lin CSY, Mogyoros I, Burke D. Recovery of excitability of cutaneous afferents in the median and sural nerves following activity. Muscle Nerve 2000;23:763-70.

19. Franssen H, Gebbink TA, Wokke JH, van den Berg LH, van Schelven LJ. Is cold paresis related to axonal depolarization? J Peripher Nerv Syst. 2010;15:227-37

20. Bellemare F, Woods JJ, Johansson R, Bigland-Ritchie B. Motor-unit discharge rates in maximal voluntary contractions of three human muscles. J Neurophysiol 1983;50:1380-92.

21. Bigland-Ritchie B, Johansson R, Lippold OC, Smith S, Woods JJ. Changes in motor neurone firing rates during sustained maximal voluntary contractions. J Physiol 1983;340:335-46.

22. Marsden CD, Meadows JC, Merton PA. Isolated single motor units in human muscle and their rate of discharge during maximal voluntary effort. J Physiol 1971;217 Suppl:12P-13P.

9

**Excitability tests
using high-density surface-EMG:
A novel approach
to studying single motor units**

BOUDEWIJN T.H.M. SLEUTJES
JUDITH DRENTHEN
ERNEST BOSKOVIC
LEONARD J. VAN SCHELVEN
MARIA O. KOVALCHUK
PAUL G.E. LUMENS
LEONARD H. VAN DEN BERG
HESSEL FRANSSEN

ABSTRACT

Objective. To study excitability of single motor units (MUs) using high-density surface-EMG.

Methods. Motor unit action potentials (MUAPs) were evoked by submaximal stimulation of the median nerve at the wrist and recorded with a 9 x 14 electrode grid on the skin overlying the thenar muscles. For excitability tests of single MUs, the most optimal specific single-channel surface-EMG signal was selected based on the spatiotemporal profile of single MUs. Results: Axonal excitability measures were successfully obtained from 14 single MUs derived from ten healthy subjects. Selecting the optimal single-channel surface-EMG signals minimized interference from other single MUs and improved signal-to-noise ratio. The muscle fiber conduction velocity (MFCV) could also be derived from the unique spatiotemporal profile of single MUs.

Conclusion. High-density surface-EMG helps to isolate single MUAP responses, making it a suitable technique for assessing excitability in multiple single motor axons per nerve. Significance: Our method enables the reliable study of ion channel dysfunction in single motor axons of nerves without any requirement for specific conditions, such as prominent MU loss or enlarged MUAPs due to collateral sprouting.

INTRODUCTION

Excitability in single human motor axons was studied extensively by Joseph Bergmans in the 1970s.[1] In his early pioneering work, single motor unit action potential (MUAP) responses were recorded using surface electromyography (EMG). His approach involved major challenges: isolating electrically recruited single MUAP responses and monitoring the threshold manually by careful investigation of the motor units' all-or-none activity. The introduction of automated threshold tracking techniques[2-4] facilitated studies on excitability in single human motor axons, including their activity after applying polarizing currents[5,6], after ischemia[7,8], and after tetanic stimulation[9], their strength-duration properties[10], their threshold behavior[11-13], and low-threshold properties[14]. These studies in single motor axons provided insight into the biophysical basis underlying their excitability properties. In parallel, excitability tests with single-channel surface-EMG were further refined and standardized by Bostock et al.[15,16] for application in a clinical setting.

The majority of the excitability studies using a standard protocol[16] assess properties of a group of motor axons by tracking a fixed compound muscle action potential (CMAP) amplitude. Although this may be sufficient in many cases, excitability tests in single MUAPs have the potential to assess, more directly, pathophysiological events that are masked in excitability tests using CMAP recordings[17,18]. Despite this advantage, the fact that the number of studies on single MUAPs is relatively limited may partly be due to the difficulty in identifying isolated single MUAP responses reliably, especially in the presence of other MUAPs whose thresholds often overlap. Furthermore, prior to the recordings, the unique location and size of single MUs within the muscle is not known. Hence, excitability tests with single-channel surface-EMG also become susceptible to suboptimal electrode positioning and they are time-consuming due to the repositioning required.

With a view to overcoming the challenges associated with identifying single MUAPs, high-density surface-EMG has been introduced[19-22]. In high-density surface-EMG, multiple electrodes are positioned over the entire muscle, adding spatial information to single MUAPs. Their spatiotemporal profile helps their identification significantly compared to single-channel surface-EMG[23-25]. This has led to various potentially clinically relevant applications at single MU level[22,26-29].

To date, excitability studies in single MUs have relied solely on information from single-channel surface-EMG[10-12,14]. In this study, we assess the excitability in single MUs where the novelty lies in the integration of high-density surface-EMG with excitability testing. We hypothesize that improved identification of single MUs by using high-density surface-EMG will facilitate excitability testing. To evaluate this hypothesis, we applied our novel approach in healthy subjects.

9

MATERIALS AND METHODS

Subjects

Ten healthy subjects (mean age, 30.1 years; range 18 – 43 years; 6 men) participated in this study. None of them had a history of any condition that could affect motor axon function. All subjects gave informed consent for the experiments. The investigation was in accordance with the principles of the Declaration of Helsinki and approved by the local ethical committee.

Single MUAP registration using high-density surface-EMG

Single MUAPs were recorded by applying a 9 x 14 array of densely spaced electrodes attached to the skin over the thenar muscle group[18,26] of the left (n = 4), or right (n = 6) hand. The electrodes had an inter-electrode distance of 4 mm overlaying a skin area of 32 x 52 mm. The long axis was positioned transversally over the thenar muscles (Fig. 1). This enables identification of single MUAPs by their spatiotemporal profile (Fig. 2, 3A and 3B). The reference electrode was positioned on the dorsal side of the metacarpophalangeal joint of the second finger. The ground electrode was attached to the dorsum of the hand. The high-density surface-EMG signals were recorded using an ActiveTwo amplifier system (BioSemi, Amsterdam, The Netherlands), band pass filtered (2.5Hz – 500 Hz) and sampled at 4096 Hz.

Figure 1. A schematic drawing of the right hand.
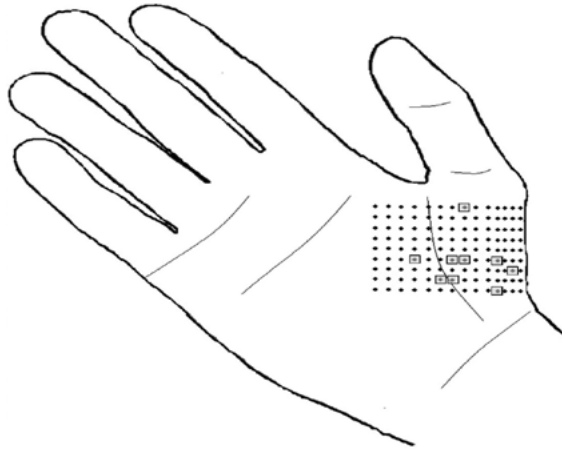

Figure 1 legend. Dots indicate the 9 x 14 electrode array overlaying the thenar muscle group. In six of the ten subjects, 9 single MUAPs were recorded from the right hand. The 9 gray boxes represent the 9 selected positions in the 9 x 14 electrode array, which provided the single-channel surface-EMG signals for excitability testing.

Figure 2. The spatiotemporal profile of a single MUAP.
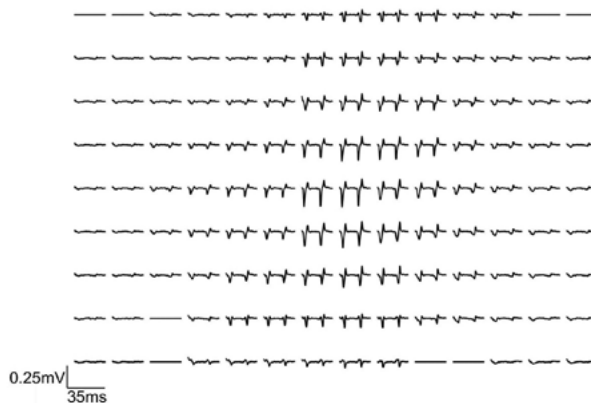

0.25mV
35ms

Figure 2 legend. Single MUAP together with its F-wave, which was recorded during excitability testing in one of the subjects. The characteristic spatiotemporal profile of the single MUAP and its F-wave further confirmed that the threshold of a 'true' single MUAP was tracked.

9

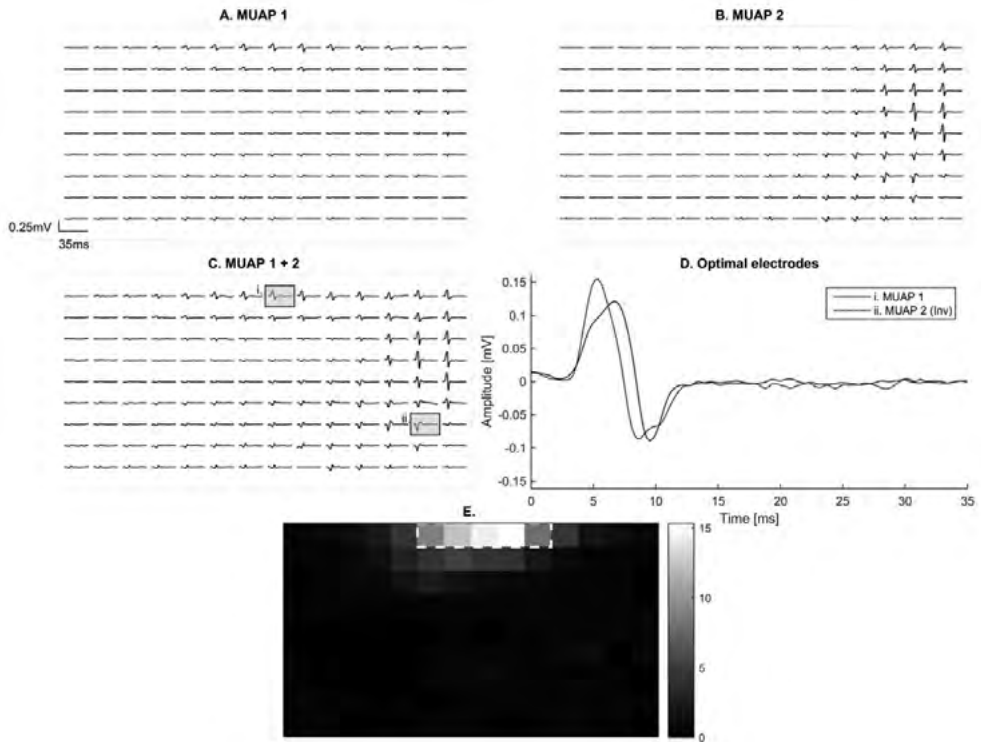**Figure 3.** Spatiotemporal muscle response of a single MUAP.

Figure 3 legend. (A) Spatiotemporal muscle response of a single MUAP, recorded with a 9x14 high-density surface-EMG electrode array. (B) Spatiotemporal muscle response of another single MUAP which was simultaneously active with the single MUAP depicted in (A). (C) Spatiotemporal muscle response of the 2 overlapping MUAPs from (A) and (B). The two small gray boxes illustrate the two optimal electrodes (i., MUAP 1; ii. MUAP 2) from which the single-channel surface-EMG signals were used for excitability testing. (D) Enlarged view of the responses of MUAP 1 (black) and MUAP 2 (dashed dotted; inverted) obtained from the optimal electrodes (i. and ii.) from (C). Signals were inverted for excitability testing. Electrodes which had poor contact with the skin are visible as flat lines. (E) The root-mean-square (RMS) map from (A) in µVms. Five channels exceeded the threshold of 50% of the maximum RMS amplitude (see methods), represented by the white dashed square, resulting in a coverage of 4%.

To visualize the monopolar 126-channel surface-EMG signals and properly integrate the ActiveTwo system with the excitability software, the freely online available LabView based acquisition software for this system (ActiView, BioSemi, Amsterdam, The Netherlands) was modified. The modified acquisition program allowed each single-channel surface-EMG signal from the 126-channel surface-EMG signals to be selected by the operator for excitability testing, since the excitability testing setup is based on a single-chan-

nel surface-EMG technique. This single-channel surface-EMG signal was DA-converted (PCI-6251, National instruments) giving a 1000x amplification of the electrode signal. This analog output signal was connected to the AD-converter (PCI-6221, National instruments) of the excitability setup, and subsequently fed into the excitability software (Qtrac-S, TRONDNF, version 19/06/2015, Institute of Neurology, Queen Square, London, UK). As such, online visual feedback could be obtained both from the high-density surface-EMG signal in the acquisition software and from the selected single-channel surface-EMG signal in the excitability software. Transcutaneous electrical stimuli (pulse width, 1 ms) were delivered every two seconds by an isolated bipolar constant current apparatus (DS5, Digitimer, UK model D185). A trigger device was developed which connected the current apparatus with the high-density surface-EMG acquisition software to visualize the triggered single MUAP responses. The median nerve was stimulated at several sites on the wrist, up to approximately 10 cm from the wrist crease (cathode) via non-polarizable surface electrodes (Red dot, 3M electrodes Health care). The anode was positioned approximately 10 cm proximally, on the radial side of the forearm. The skin temperature was measured at the stimulation site using an infrared thermometer (KM814, Comark Limited, Stevenage, UK)

Selection of single MUAPs

The following approach was applied to determine the optimal single-channel surface-EMG signal for excitability testing. At every stimulus site, the stimulus intensity was slightly increased until a first low-threshold MU was activated showing typical all-or-none responses. This was assessed using the visual feedback provided by both the modified acquisition and the excitability software. Subsequently, the stimulus intensity was again slightly increased to determine whether this first single MUAP had a threshold and profile distinct from other single MUAPs. Throughout this searching procedure, the selection of the optimal single-channel surface-EMG signal was qualitatively judged by taking into account (1) the spatiotemporal profile of the investigated single MUAP (e.g. by selecting a channel on the high-density grid with largest surface-EMG signal to improve signal-to-noise ratio), and (2) other single MUAP profiles with a very similar threshold (e.g. by selecting a channel on the high-density grid with the least surface-EMG signal interference of the other single MUAPs). Since every single MU is characterized by its own anatomical position in the muscle, this approach makes optimal use of the topographical information provided by the high-density surface-EMG signal. Applying this procedure means that the single MUAP is not restricted to the first activated low-threshold MU. After assessing these factors, the optimal single MUAP and corresponding optimal single-channel surface-EMG signal were determined for excitability testing.

9

Single-channel surface-EMG recordings

Additionally, single MUAPs were recorded from the thenar muscle group by conventional single-channel surface-EMG in two healthy subjects (both left hand) with surface disk electrodes of 10 mm diameter, initially, in a muscle belly-tendon montage. During these recordings the position of the active electrode was systematically shifted over the muscle belly aligned with the short axis of the high-density grid to achieve optimal recordings. The additional time needed to improve signal amplitude with conventional recordings was determined. The set-up consisted of a Viking IV EMG-apparatus (Nicolet Biomedical, Inc., Madison, Wisconsin) connected to the excitability software as previously described.[30]

Excitability testing of single MUAPs

After selecting a single-channel surface-EMG signal, the excitability-testing protocol for single MUAPs was applied. First, the current (pulse width, 1 ms) was set to a value at which the single MUAP showed its typical all-or-none responses. Then, a target amplitude was set slightly lower than the single MUAP amplitude, so that when it was exceeded a response was detected. The excitability program then used this target amplitude in tracking the threshold by varying the current (pulse width 1 ms) to keep the percentage of stimuli which activate the single MUAP at approximately 50%. The current required for this is called the unconditioned threshold current. The protocol comprised four excitability tests (strength-duration, threshold electrotonus, current-threshold, and recovery cycle). In the strength duration (SD) test, the relation between stimulus charge (stimulus intensity x stimulus duration) and stimulus duration (with durations of 0.2, 0.4, 0.6, 0.8, and 1.0ms) was assessed. In the threshold electrotonus (TE), the threshold changes were tracked when applying a conditioning stimulus preceding the test pulse of varying duration up to 100 ms to depolarize (at +40% of the unconditioned target current threshold) and hyperpolarize (at -40% of the unconditioned target current threshold) the single motor axon. To assess the current-threshold relation (I/V), the threshold changes were tracked after applying a 200ms conditioning current varying from +50% depolarizing to -100% hyperpolarizing. In the final test, the recovery cycle (RC), the threshold changes were tracked at various intervals between 2 and 200 ms after a supramaximal conditioning stimulus eliciting the single MUAP. Throughout the excitability tests, the acquisition software allowed visual feedback from the high-density surface-EMG signals, which enabled the operator to evaluate the quality of tracking the single MUAP under study in real-time. The 126 surface-EMG signals were stored allowing further offline post-processing in Matlab (R2014b: The MathWorks, Natick, Massachusetts, USA) with decomposition software (described in detail elsewhere[23,25]), which was slightly adjusted to facilitate single MU analysis.

Quantifying spatiotemporal properties of single MUAPs

To determine the benefit of selecting a single-channel surface-EMG signal, we quantified the spatial specificity of the single MUAPs by calculating the coverage of their spatio-temporal profiles on the recording grid. Therefore, we calculated the root-mean-square (RMS) amplitude map, in a window of 20 ms, of an averaged single MUAP, obtained from up to 20 responses during the strength-duration test (Fig 3E). The coverage was defined as the ratio between the number of channels that exceeds 50% of the maximum RMS amplitude divided by the total number of channels. Theoretically, if the spatiotemporal profile of a single MUAP has the same shape and size on all channels (e.g. an MU located relatively deeply in the muscle), coverage will be 100% and there is no advantage in selecting a single-channel surface-EMG signal. On the other hand, if a single MUAP only appears on a single channel (e.g. a small-sized superficially located MU), coverage will be 0.8% (1 / 126). In this case, the spatial information provides the greatest value, as it enables the precise selection of the single-channel that corresponds to the spatial-specific location of the MU in the muscle. Thus, the higher the spatial specificity of a single MUAP, the lower the coverage, and the greater the advantage obtained by using topographical information provided by high-density surface-EMG. With the topographical information also muscular properties, such as the muscle fiber conduction velocity (MFCV), becomes available. Studying the axonal and muscular function of a single MU simultaneously may be useful in fatigue-related studies.[31] Therefore, also the MFCV was assessed from the spatiotemporal profile of the single MUAPs using a slightly adjusted, previously described cross-correlation method.[32,33]

Statistical analysis

Statistical tests were performed in Matlab (R2014b: The MathWorks, Natick, Massachusetts, USA). A p-value of <0.05 was considered statistically significant. To relate excitability measures, Spearman's correlation was used. The Kolmogorov-Smirnov method was used to assess normality. As the results proved to be not normally distributed, data are presented as median with 5th and 95th percentiles.

RESULTS

Excitability recordings were successfully performed in a total of 14 single human motor axons. In three of the ten subjects, excitability tests were performed in more than 1 single motor axon. The median absolute unconditioned threshold current of the single MUAPs was 2.4 mA (1.5 mA – 7.9 mA). To determine the stability of the unconditioned threshold current, the averaged threshold currents of the first and last three minutes of

9

the recordings were compared. No significant differences were observed (last – first; -0.06 mA; IQR: -0.43 mA – 0.01 mA, p = 0.14, n = 14). Stability was also assessed by determining the fluctuations (in 5th – 95th percentiles) around the normalized unconditioned thresholds. These fluctuations ranged between 96% (IQR: 91% - 97%, n = 14) and 104% (IQR: 103% - 115%, n = 14) throughout the recordings. Therefore, it shows the ability to perform stable recordings within single MUs could be performed. The absolute MUAP size obtained from the selected single-channel surface-EMG signals was 187 μV (73 μV – 517 μV). The median recording duration was 44 min (40 min – 57 min).

Before excitability testing, an optimal single-channel had to be selected, which differed for every single MU as illustrated for the right hand in Figure 1, thereby demonstrating the advantage of the additional spatial information obtained by high-density recordings. The single MUAPs had a high spatial specificity on the muscle expressed by their low median coverage on the grid of 6.6 % (1.9 % - 13.7 %). This confirmed that the additional spatial information was of considerable value, and that by selecting a single-channel, it was possible to obtain a high selectivity for the investigated single MUAPs. Another factor which helped in the recognition of single MUAPs was that they occasionally elicited an F-wave (Fig. 2). Since all F-waves of a single MUAP are similar, the match between single MUAP and its F-wave illustrates that tracking was performed on a single MUAP.[25]

An example of selecting an optimal single-channel is illustrated in Figure 3. Figure 3A shows a spatiotemporal profile of a single MUAP, which was used for excitability testing. During the excitability recordings, another single MUAP with a lower threshold was frequently active, which was also used for excitability testing in a subsequent recording (Fig. 3B). Hence, they were often both active at the same time, resulting in their summed response (Fig. 3C). Despite their simultaneous activity, the high spatial specificity facilitated isolating the single MUAPs by selecting single-channel surface-EMG signals (Fig. 3D from the gray boxes in Fig. 3C). Thus, with the two selected optimal channels, a balance was found between minimizing the interference of the other single MUAP, and maximizing the surface-EMG signal of the studied single MUAP, improving signal-to-noise ratio. As the high-density recordings readily obtained the spatiotemporal profiles of the two single MUAPs, manually selection of the optimal single-channel sufficed. Figure 3E shows another illustration of the spatial specificity of the single MUAP with the root-mean-square (RMS) amplitude map which was used to calculate the coverage (coverage = 4%, white dashed square). The threshold currents of the single MUAP from Figure 3A were tracked throughout the excitability recordings shown in Figure 4A. In Figure 4B, the activity of the single MUAP is shown during the strength-duration excitability recordings with the typical all-or-none responses.
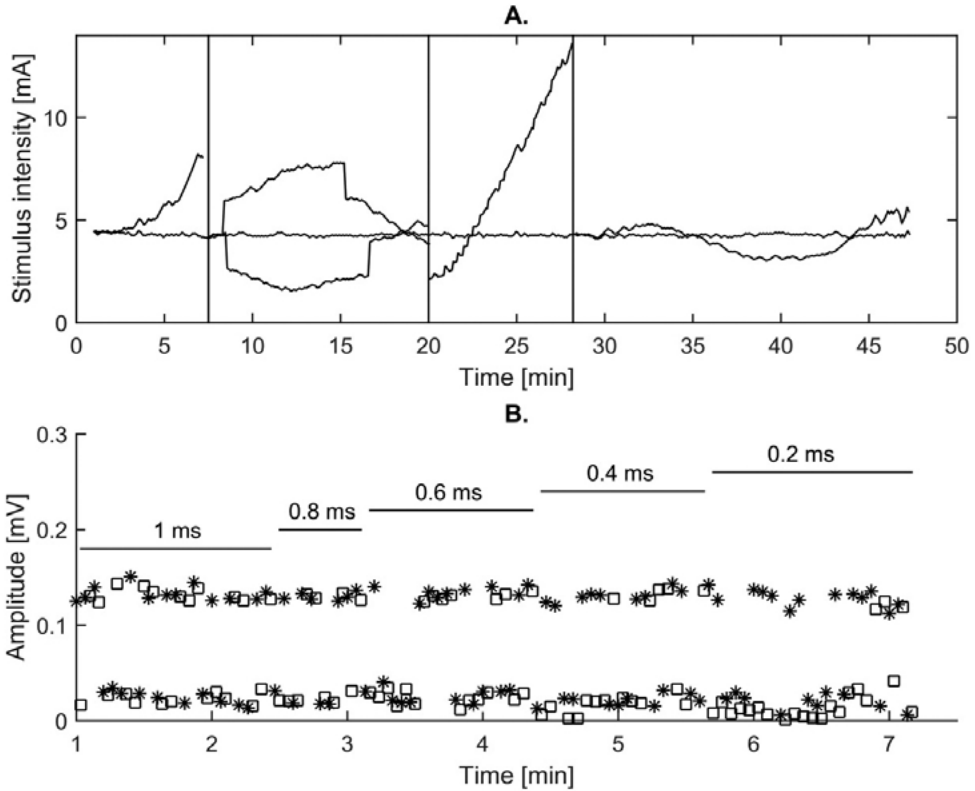
Figure 4. Excitability indices of a single MUAP.

Figure 4 legend. (A) The test stimulus threshold (thin horizontal black line) of a single MUAP, together with the changes in threshold during strength-duration (SD), threshold electrotonus (TE), current/voltage (I/V) relationship and recovery cycle (RC). (B) Zoomed part from (A) showing the all-or-none activity of the single MUAP during the SD test. The illustrated responses are from the test stimuli (stars), and stimuli with durations of 0.2ms, 0.4ms, 0.6ms, 0.8ms, and 1.0ms (squares). Same single MUAP as in Figure 3A.

Once a single MUAP and its optimal single-channel surface-EMG signal had been selected, the excitability tests could be performed without any significant issues. It was only in the recovery cycle, at short intervals, that threshold tracking was prone to interference by the activity of other single MUAPs. This has been encountered previously in excitability tests with single-channel surface-EMG recordings applying a full excitability protocol[14]. In this study, the occasional presence of F-waves, which coincide with intervals during the recovery cycle, had minor effect on tracking. In Figure 5, the excitability curves are shown for all 14 single human motor axons. Table 1 presents the descriptive characteristics of multiple excitability measures. A significant correlation was found between the strength-duration time con-

stant (SDTC) and rheobase (r = -0.80, p < 0.001). In line with Weiss's law, rheobase decreased when SDTC became longer. [2,10] The conventional single-channel surface-EMG recordings in the two healthy subjects required additional time and effort in the attempts to improve the optimal location and to detect isolated all-or-none responses of single MUAPs. Despite systematically shifting of the active electrode over the muscle to improve signal amplitude, which took approximately 15 min per subject, no accurate judgment could be made on the spatial selectivity without topographical information of the single MUAPs. When multiple single MUAPs were active due to overlapping thresholds, it became difficult to delineate an improved signal amplitude of a single MUAP under study from the altered signal amplitudes of other single MUAPs. Eventually, the strength-duration test was applied in one MUAP per subject (SDTC = 0.401 ms, rheobase = 1.5 mA; SDTC = 0.480 ms, rheobase = 2.4 mA).

Figure 5. Excitability recordings of all 14 single motor units.
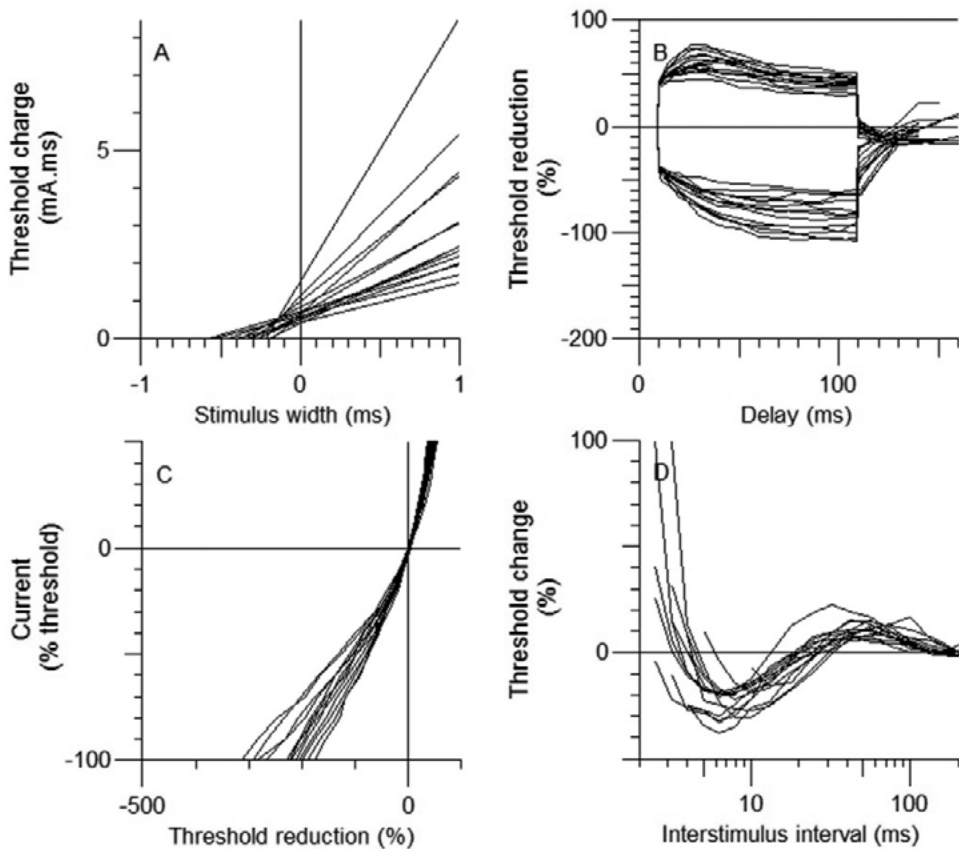

Figure 5 legend. (A) strength-duration relationship plotted as charge vs. stimulus duration, (B) threshold electrotonus, (C) current/voltage relationship, and (D) recovery cycle.

Table 1. Excitability and single MUAP properties obtained from 14 single motor units from ten healthy subjects.

Measures	Median (5th – 95th percentile)
SDTC (ms)	0.307 (0.177 – 0.571)
Rheobase (mA)	2.0 (1.1 – 6.5)
TEd90-100ms (%)	40.9 (29.4 – 50.4)
TEh90-100ms (%)	-82.9 (-106.4 - -60.9)
Resting I/V slope (-)	0.83 (0.63 – 1.04)
Minimum I/V slope (-)	0.34 (0.22 – 0.43)
Refractory period (ms)*	4.09 (3.24 – 5.89)
Superexcitability (%)	-19.0 (-34.6 – -13.9)
Subexcitability (%)	9.6 (5.5 – 18.9)
MUAP size (µV)	187 (73 – 517)
Coverage (%)	6.6 (1.9 - 13.7)
MFCV (m/sec)**	3.9 (3.0 – 5.9)

SDTC, strength-duration time constant; TEd90 – 100ms, depolarizing threshold electronus at 90 – 100ms; TEh90 – 100ms, hyperpolarizing threshold electronus at 90 – 100ms, I/V = current/voltage. * In five MUAPs, the refractory period was not recorded. (N = 9). ** In five MUAPs MFCV could not be reliably obtained (N = 9).

Mean skin temperature at the stimulation site during the excitability recordings was 30.5°C (26.9°C – 33.8°C). In 64% of the MUAPs (9 out of 14) the MFCV could be derived reliably. The median MFCV was 3.9 m/sec (3.0 m/sec – 5.9 m/sec, n = 9).

9

DISCUSSION

We have described a novel approach to studying excitability in single MUAPs using high-density surface-EMG. By selecting an optimal single-channel surface-EMG signal, a high specificity for single MUAPs was obtained, which helps in the isolation of single MUAP responses required for reliable excitability testing. To date, excitability studies in single MUAPs have relied solely on information from single-channel surface-EMG.[10,11,12,14] High-density surface-EMG have been shown to improve the identification of single MUAPs and avoid suboptimal electrode placement, as the grid covers a significant part of the muscle. Applying high-density surface-EMG with excitability testing allows optimal use of both electrophysiological techniques for reliable assessment of excitability in single human motor axons.

Generally, the excitability properties of single MUAPs in this study are comparable to the previous findings in healthy subjects[10,14] (only the latter author applied a full excitability protocol in single MUAPs). The relatively short SDTC has also been observed before[10], where it was shown to be shorter for single MUAPs than for target CMAPs of 30% of its maximum amplitude. In another study, however, no difference was found in SDTC of single MUAPs and target CMAPs of 40% of its maximum amplitude.[14] SDTC reflects the small capacity of the nodal membrane and also the degree of persistent sodium current. Although we cannot directly compare the SDTC of single MUAPs with target CMAPs in our study, the relatively short SDTC does not indicate an increase in persistent sodium current for the sampled single MUAPs. Furthermore, in our study, the hyperpolarizing threshold electrotonus in single MUAPs was less pronounced than what one might expect in excitability tests with target CMAPs. It was suggested that this phenomenon was related to a larger current through the hyperpolarizing-activated cyclic nucleotide-gated (HCN) channels in low-threshold recruited single MUAPs.[14]

In excitability testing with single-channel surface-EMG, it is common to apply a large electrode over the skin resulting in averaging of the surface potential compared to that of high-density surface-EMG recordings[35]. Our approach is, therefore, probably more sensitive to detecting small-sized, low-threshold MUs,[25] where the investigated MUs may not only originate from the thenar muscles, but also from the lumbrical muscles. Although this may generate bias towards small-sized low-threshold MUs, large-sized MUs were also recorded, and, independent of the intrinsic threshold property (low or high), the proximity of the stimulus electrode on the skin to the axon also determines, to a significant extent, which single MUs are activated.[1] As such, the latter also influences selectivity of which single MUs are activated. Therefore, it is important to mark stimulation sites to reduce variability, which also aid in their redetection in subsequent sessions.

To determine the benefit of selecting a single-channel surface-EMG from the high-density grid, the spatial specificity was quantified by determining the coverage for every single MUAP. The low coverage of single MUAPs on the grid supports the advantage of selecting a single-channel surface-EMG signal to obtain a high selectivity for single MUAPs. This aspect should also be evaluated in the context of the interference of other MUAPs. In addition, the locations of the selected single-channels on the grid had a large spread supporting the benefit of having additional spatial information of the single MUAPs (Fig. 1). Furthermore, conventional single-channel surface-EMG required more time to identify single MUAPs and to improve signal amplitude by shifting the electrode over the muscle.[36] Even then, it remained ambiguous whether optimal spatial selectivity was obtained due to the absence of topographical information. High-density surface-EMG was more convenient as, once the electrode array was positioned over the muscle, a single-channel could be selected. Therefore, excitability recordings from single

MUAPs in subjects without marked motor unit loss requires high-density surface-EMG, because other single MUAPs may interfere with threshold tracking. Nevertheless, single-channel recordings of single surface MUAPs can be useful in other settings as well as in assessing excitability in patients with marked motor unit loss and a limited number of easily identifiable single MUAPs. Although not systematically determined, selecting a single-channel probably improves the signal-to-noise ratio, since the increase in amplitude size outweighs the reduction in noise by the use of a large electrode. In this first concept design, we decided to use a single-channel to minimize the number of procedures for the operator and to avoid extra operations when transferring the surface-EMG signal to the excitability set-up.

An inherent aspect of excitability tests of single MUAPs is that, due to the probabilistic nature of the threshold of single MUAPs, a longer recording duration is required than with target CMAPs. Nevertheless, depending on the clinical question posed, shortened excitability protocols can be applied,[37,38] which significantly reduce recording time. With unconditioned stimuli, a single MU threshold can be clearly separated from that of other MUs due to the absence of interference. This may, however, not hold true when applying conditioned stimuli. Although this is the case irrespective of the applied method, our approach can partly solve this issue, as it offers a higher specificity for a single MU.

CONCLUSION

We have shown that studying excitability of single MUAPs by high-density surface-EMG is feasible. We have demonstrated that single MUAPs can be more reliably recognized, thus making it easier to apply excitability tests. It is, therefore, a suitable method for reliably assessing excitability in single MUAPs without any requirement for specific conditions, such as enlarged MUAPs due to collateral sprouting or marked MU loss. Although studying the same MUAP longitudinally is challenging, especially under pathophysiological conditions, successful longitudinal studies have been performed in ALS using single-channel surface-EMG recordings. [39,40] With the additional discriminative power of high-density surface-EMG to identify the same MU, this will likely become more accurate. As such, our new approach has the potential to monitor excitability changes within single MUs over time, as high-density surface-EMG enables re-identification of single MUs in subsequent sessions.[18] To ensure that changes in single MUs can be ascribed to pathophysiological excitability changes, further studies, such as assessing variability of single MU's properties, and standardization of the set-up is required. Once realized, this new approach will enable changes in MUs due to pathology or therapeutic interventions, to be revealed, making it a promising tool for future studies in neuromuscular disorders.

9

REFERENCES

1. Bergmans J. The physiology of single human nerve fibres. Vander. 1970;University of Louvain.

2. Bostock H. The strength-duration relationship for excitation of myelinated nerve: computed dependence on membrane parameters. J Physiol. 1983;341:59-74.

3. Raymond SA. Effects of nerve impulses on threshold of frog sciatic nerve fibres. J Physiol. 1979;290:273-303.

4. Weigl P, Bostock H, Franz P, Martius P, Muller W, Grafe P. Threshold tracking provides a rapid indication of ischaemic resistance in motor axons of diabetic subjects. Electroencephalogr Clin Neurophysiol. 1989;73:369-371.

5. Baker M, Bostock H. Depolarization changes the mechanism of accommodation in rat and human motor axons. J Physiol. 1989;411:545-561.

6. Bostock H, Baker M. Evidence for two types of potassium channel in human motor axons in vivo. Brain Res. 1988;462:354-358.

7. Bostock H, Baker M, Grafe P, Reid G. Changes in excitability and accommodation of human motor axons following brief periods of ischaemia. J Physiol. 1991;441:513-535.

8. Bostock H, Baker M, Reid G. Changes in excitability of human motor axons underlying post-ischaemic fasciculations: evidence for two stable states. J Physiol. 1991;441:537-557.

9. Bostock H, Bergmans J. Post-tetanic excitability changes and ectopic discharges in a human motor axon. Brain. 1994;117 (Pt 5):913-928.

10. Mogyoros I, Kiernan MC, Burke D. Strength-duration properties of human peripheral nerve. Brain. 1996;119 (Pt 2):439-447.

11. Bostock H, Lin CS, Howells J, Trevillion L, Jankelowitz S, Burke D. After-effects of near-threshold stimulation in single human motor axons. J Physiol. 2005;564:931-940.

12. Burke D, Howells J, Trevillion L, McNulty PA, Jankelowitz SK, Kiernan MC. Threshold behaviour of human axons explored using subthreshold perturbations to membrane potential. J Physiol. 2009;587:491-504.

13. Hales JP, Lin CS, Bostock H. Variations in excitability of single human motor axons, related to stochastic properties of nodal sodium channels. J Physiol. 2004;559:953-964.

14. Trevillion L, Howells J, Bostock H, Burke D. Properties of low-threshold motor axons in the human median nerve. J Physiol. 2010;588:2503-2515.

15. Bostock H, Cikurel K, Burke D. Threshold tracking techniques in the study of human peripheral nerve. Muscle Nerve. 1998;21:137-158.

16. Kiernan MC, Burke D, Andersen KV, Bostock H. Multiple measures of axonal excitability: a new approach in clinical testing. Muscle Nerve. 2000;23:399-409.

17. Franssen H, Straver DC. Pathophysiology of immune-mediated demyelinating neuropathies--Part II: Neurology. Muscle Nerve. 2014;49:4-20.

18. Maathuis EM, Drenthen J, van Dijk JP, Visser GH, Blok JH. Motor unit tracking with high-density surface EMG. J Electromyogr Kinesiol. 2008;18:920-930.

19. Blok JH, van Dijk JP, Drost G, Zwarts MJ, Stegeman DF. A high-density multichannel surface electromyography system for the characterization of single motor units. Rev Sci Instrum. 2002;73:1887-1897.

20. Holobar A, Farina D, Gazzoni M, Merletti R, Zazula D. Estimating motor unit discharge patterns from high-density surface electromyogram. Clin Neurophysiol. 2009;120:551-562.

21. Lapatki BG, Van Dijk JP, Jonas IE, Zwarts MJ, Stegeman DF. A thin, flexible multielectrode grid for high-density surface EMG. J Appl Physiol (1985). 2004;96:327-336.

22. Stegeman DF, Kleine BU, Lapatki BG, Van Dijk JP. High-density Surface EMG: Techniques and Applications at a Motor Unit Level. Biocybern Biomed Eng. 2012;32:3-27.

23. Blok JH, Van Dijk JP, Zwarts MJ, Stegeman DF. Motor unit action potential topography and its use in motor unit number estimation. Muscle Nerve. 2005;32:280-291.

24. Farina D, Negro F, Gazzoni M, Enoka RM. Detecting the unique representation of motor-unit action potentials in the surface electromyogram. J Neurophysiol. 2008;100:1223-1233.

25. van Dijk JP, Blok JH, Lapatki BG, van Schaik IN, Zwarts MJ, Stegeman DF. Motor unit number estimation using high-density surface electromyography. Clin Neurophysiol. 2008;119:33-42.

26. Maathuis EM, Drenthen J, van Doorn PA, Visser GH, Blok JH. Multiplet discharges after electrical stimulation: new evidence for distal excitability changes in motor neuron disease. Amyotroph Lateral Scler. 2012;13:514-520.

27. Sleutjes BT, Gligorijevic I, Montfoort I, van Doorn PA, Visser GH, Blok JH. Identifying fasciculation potentials in motor neuron disease: A matter of probability. Muscle Nerve. 2016;53:227-233.

28. Sleutjes BT, Maathuis EM, van Doorn PA, Blok JH, Visser GH. Electrically evoked multiplet discharges are associated with more marked clinical deterioration in motor neuron disease. Muscle Nerve. 2016;53:222-226.

29. Zhou P, Li X, Jahanmiri-Nezhad F, Rymer WZ, Barkhaus PE. Duration of observation required in detecting fasciculation potentials in amyotrophic lateral sclerosis using high-density surface EMG. J Neuroeng Rehabil. 2012;9:78.

9

30. Kovalchuk MO, Franssen H, Van Schelven LJ, Sleutjes BTHM. Comparing excitability at 37°C versus at 20°C: Differences between motor and sensory axons. Muscle Nerve. 2018 Apr;57(4):574-580.

31. Boerio D, Lefaucheur JP, Bassez G, Hogrel JY. Central and peripheral components of exercise-related fatigability in myotonic dystrophy type 1. Acta Neurol Scand. 2012;125:38-46.

32. Drost G, Stegeman DF, Schillings ML, Horemans HL, Janssen HM, Massa M, et al. Motor unit characteristics in healthy subjects and those with postpoliomyelitis syndrome: a high-density surface EMG study. Muscle Nerve. 2004;30:269-276.

33. Houtman CJ, Stegeman DF, Van Dijk JP, Zwarts MJ. Changes in muscle fiber conduction velocity indicate recruitment of distinct motor unit populations. J Appl Physiol (1985). 2003;95:1045-1054.

34. Bostock H, Sears TA, Sherratt RM. The spatial distribution of excitability and membrane current in normal and demyelinated mammalian nerve fibres. J Physiol. 1983;341:41-58.

35. van Dijk JP, Lowery MM, Lapatki BG, Stegeman DF. Evidence of potential averaging over the finite surface of a bioelectric surface electrode. Ann Biomed Eng. 2009;37:1141-1151.

36. Doherty TJ, Brown WF. A method for the longitudinal study of human thenar motor units. Muscle Nerve. 1994;17:1029-1036.

37. Bostock H, Burke D, Hales JP. Differences in behaviour of sensory and motor axons following release of ischaemia. Brain. 1994b;117 (Pt 2):225-234.

38. Vagg R, Mogyoros I, Kiernan MC, Burke D. Activity-dependent hyperpolarization of human motor axons produced by natural activity. J Physiol. 1998;507 (Pt 3):919-925.

39. Chan KM, Stashuk DW, Brown WF. A longitudinal study of the pathophysiological changes in single human thenar motor units in amyotrophic lateral sclerosis. Muscle Nerve. 1998;21:1714-1723.

40. Gooch CL, Harati Y. Longitudinal tracking of the same single motor unit in amyotrophic lateral sclerosis. Muscle Nerve. 1997;20:511-513.

10

Warming nerves for excitability testing

MARIA O. KOVALCHUK
HESSEL FRANSSEN
FÉLINE E.V. SCHEIJMANS
LEONARD J. VAN SCHELVEN
LEONARD H. VAN DEN BERG
BOUDEWIJN T.H.M. SLEUTJES

ABSTRACT

Objective. To find the best method of warming the median nerve prior to excitability testing to a standard temperature.

Methods. In 5 healthy subjects, the forearm and hand were warmed for 1 hour to 37ºC by infrared lamp, water blanket, or water bath. Recordings were performed before and during warming every 10 minutes. Excitability indices were fitted by exponential relations, thereby calculating the time needed to reach 95% of their asymptotic end value.

Results. Distal motor latency, refractory period, and superexcitability at 10 ms changed exponentially with time. Warming by water bath took the shortest time (24 minutes); this was followed by warming by infrared lamp (34 minutes) and water blanket (35 minutes). Discussion. Warming by water bath is the quickest way. The other methods took only moderately more time. Future studies need to specify both warming method and warming time prior to excitability testing.

INTRODUCTION

Excitability testing is a non-invasive method to assess changes in resting membrane potential and activity of axolemmal voltage-gated ion channels at one site of a peripheral nerve[1-3]. The method has provided relevant information on pathophysiology of single motor axons and subsets of motor or sensory axons in peripheral nervous system disorders, including diabetic neuropathy, neuropathy in renal failure, multifocal motor neuropathy, chronic inflammatory demyelinative neuropathy, and amyotrophic lateral sclerosis[4-14]. Methods to perform excitability testing have been continuously improved to better assess the involvement of ion channels[13,15,16] as well as activity of the sodium-potassium pump[17,18] in healthy and diseased nerves.

Since a number of excitability indices depend on temperature[19-21], a simple, fast and inexpensive method to control temperature is needed when investigating axon pathophysiology in nerve disorders or to assess effects of trial medication on peripheral nerve excitability. Several studies showed that it is not necessary to perform near-nerve temperature to determine if nerve temperature is brought close to a desired value. When a limb is warmed long enough in a medium of the desired temperature, the temperature of the nerve to be investigated approaches the temperature of the medium[22-24]. According to this principle, we investigated different methods of warming the median nerve, and assessed the effects on selected excitability indices.

METHODS

Subjects

We recruited 5 subjects (4 men and 1 woman, mean age 31.8 years, range 31-34) from the neuromuscular department staff of the University Medical Center Utrecht. None of the subjects had a history of neurological symptoms or used medication. Informed consent was obtained from all subjects. The investigation was done in accordance of the Declaration of Helsinki and was approved by the Medical Ethics Committee of the University Medical Center Utrecht.

Warming methods

We investigated 3 methods for warming the arm: infrared lamp, water blanket and water bath. Per subject, each of these methods was applied on a different day. On each day 7 recordings per method were performed, one baseline excitability test followed by 6

10

excitability tests during warming every 10 minutes (for warming by infrared lamp and water blanket) or every 16 minutes (for warming by water bath) (Supplementary figure 1). Warming time was 60 minutes in order to ensure that, with each method, nerve temperature approached 37°C[23]. The infrared lamp (Dräger Babytherm 8004/8010, Lübeck, Germany) was placed 85 cm above the forearm and hand. It was set at 37°C and connected to a feedback system using a temperature-sensor (268-411800 NATUS Flexible Surface Temp Prob) placed near the stimulation site at the wrist. To avoid the lamp switching off due to the sensor reaching 37°C before the skin reached 37°C, an isolating patch (Heat Reflecting Patch, Ohmeda Medical, Laurel, MD, USA) was placed over the sensor. The water blanket (Maxi-therm Lite Infant blanket, Cincinnati Sub-zero, Cincinnati, OH, USA) was wrapped around the forearm, wrist, and palm. It was connected to a heating circulator (Norm-O-Temp water system, CSZ Cincinnati Sub-zero, Cincinnati, OH, USA) that heated water to 37°C and pumped it through the blanket. The water bath in which the forearm and hand were placed was equipped with a thermostat valve through which water of 37°C flowed as soon as a water thermometer detected a water temperature drop of 1.0°C. For the water bath, warming had to be interrupted for excitability testing. The recording electrodes remained in situ during warming in water and were isolated from the water by Tegaderm (Transparent Film Roll, 3M health care, Germany) and band aid spray (Cavilon, 3M health care, Germany). The stimulating electrodes were taken off during warming in water and their site was marked by water-resistant ink; they were quickly replaced by new ones before the next excitability testing. Skin temperature was continuously monitored via a temperature sensor (0.1 °C accuracy) placed near the stimulating electrode on the wrist.

Supplementary figure 1.
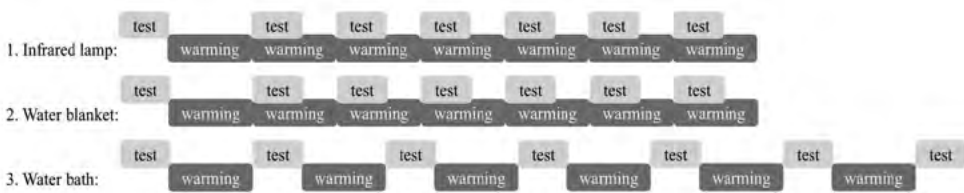
Excitability

The median nerve was stimulated via non-polarizable electrodes (Red Dot, 3M Healthcare, Germany) with the cathode at the wrist and the anode 10cmmore proximal on the radial side of the forearm. The thenar compound muscle action potential (CMAP) was recorded by 1.0 cm diameter disk skin electrodes (Disposable Disk Electrodes, Natus Neurology, Middleton, WI, USA) with the active electrode over the abductor pollicis

brevis muscle belly (7 cm from the stimulus cathode) and the reference electrode on the metacarpophalangeal joint.

The set-up consisted of a Viking IV EMG apparatus (Nicolet Biomedical, Inc., Madison, Wisconsin, USA) for CMAP recording, connected with a computer (Analog to digital converter PCI-6221, National Instruments, Austin, TX, USA) running QtracS software (version 19/06/2015, Institute of Neurology, London, UK), and an isolated bipolar constant current stimulator (DS5, Digitimer, model D185-HB4, Welwyn Garden City, Hertfordshire, UK) producing conditioning and test stimuli. Test stimuli of 1.0 ms duration assessed threshold for a target CMAP of 40% of its maximal amplitude by proportional threshold tracking. Conditioning stimuli were constant currents that either slightly depolarized or hyperpolarized the resting membrane potential, or induced nerve action potentials.

A shortened excitability test was designed which could be performed within 5 minutes in order to accurately track changes during warming. A test comprised (i) stimulus-response curve (relation between the current of a 1.0 ms duration stimulus and the amplitude of the induced CMAP), (ii) strength-duration test (relation between stimulus currents that elicited the target CMAP for stimulus durations of 1.0 ms, 0.8 ms, 0.6 ms, 0.4 ms, and 0.2 ms), which is automatically converted into the linear stimulus charge (stimulus current x stimulus duration) vs. stimulus duration (Qt) relation, (iii) I/V relation (relation between the magnitude of a 200 ms duration conditioning current varying from 50% depolarizing to 100% hyperpolarizing and the threshold at its end), and (iv) recovery cycle (the threshold fluctuations induced 2-10 ms after a 1.0 ms duration supramaximal conditioning stimulus). The following variables were obtained: strength duration time constant (SDTC; absolute value of the x-intercept of the Qt relation), rheobase (slope of the Qt relation), resting I/V slope (slope between 10% depolarizing and 10% hyperpolarizing conditioning stimuli), minimal I/V slope, refractory period (time between conditioning stimulus and return of threshold to baseline), peak superexcitability and time to peak superexcitability (most negative threshold value), and superexcitability at 10 ms. The maximum CMAP amplitude was obtained from the shortened recovery cycle. Throughout excitability testing distal motor latency (DML) was measured every 1.6 seconds. DML was defined as the point where the CMAP deviated from the baseline by 10% of its baseline-to-peak amplitude.

10

ANALYSIS

With a sudden change in environmental temperature, the temperature of a limb will slowly change towards the environmental temperature. The changing temperature and electrophysiological variables over time have been approximated by a decaying exponential function[23,24] (Supplementary figure 2):

$$y = y_{end} + (y_{start} - y_{end}).e^{-t/\tau}$$

where y_{start} is the initial value of the variable, y_{end} the asymptote of the variable, (t) the warming-time and (τ) the time-constant, defined as the time-point at which variable (y) has reached 63% of the difference between the initial value (y_{start}) and its asymptotic value (y_{end}). For each subject, variable, and warming method, we calculated the warming times needed to reach the time constant and 95% of the end value ($t_{95\%}$). Additionally, using a non-linear mixed effects model, we determined the warming time needed to reach the time constant and 95% of the end value ($t_{95\%}$) as composite over all subjects per warming method. Because the asymptotic value of a variable can only be reached after an infinite time of warming we assumed that the 95% end value is relevant to determine the warming time in clinical practice as was also shown for nerve conduction variables in a previous study[23]. For the water bath recordings, the time period outside the bath was omitted for the analysis. Exponential fitting was done by the Curve Fitting and the Statistical Toolbox within Matlab (The Mathworks, Natick, MA, version R2014b). As peak superexcitability occurred between recorded thresholds, cardinal spline interpolation was applied to compute its value[25]. Statistical analysis was performed in Matlab. $P < 0.05$ was considered statistically significant different. The Kolmogorov-Smirnov test was used to assess normality. As the data proved to be not normally distributed, the Wilcoxon signed rank test was applied to compare values at baseline and final recording to assess if variables were significantly affected by temperature by means of the three warming methods. The data is presented as median and interquartile range (IQR).

Supplementary figure 2.
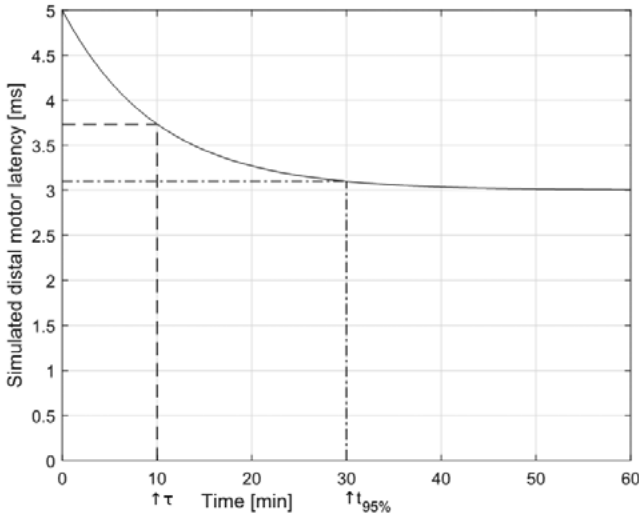
RESULTS

All 105 excitability recordings were successfully performed in the five subjects. Compared to the median values at baseline over all three methods, the final recordings after warming showed a decrease in DML (from 4.71 ms to 4.21 ms; p < 0.001), shortening of the refractory period (from 3.56 ms to 2.92 ms; p < 0.001), less negative (less prominent) peak superexcitability (from -28.9% to -22.6%; p<0.001), shortening of time to peak superexcitability (from 6.34 ms to 4.81 ms; p< 0.001), less negative superexcitability at 10 ms (from -19.2 % to -4.0%; p < 0.001), and a decrease in resting I/V slope (from 0.61 to 0.59; p = 0.002). No significant differences were found for the strength-duration time constant (from 0.44 ms to 0.45 ms; p = 0.92), rheobase (from 3.06 mA to 3.05 mA; p = 0.60), minimal I/V-slope (from 0.19 to 0.19; p = 0.89), and the maximum CMAP amplitude (from 10.5 mV to 10.0 mV; p = 0.09).

Of the variables that significantly changed during warming, visual assessment indicated that DML, refractory period and superexcitability at 10 ms changed exponentially (Fig. 1). Hence, exponential fitting was performed on these three variables. Only in subject 1 were clear exponential changes observed for peak superexcitability during warming in all three methods. In this subject no clear changes were observed for the refractory period during warming in the water bath so fitting was not possible. In subject 2 superexcitability at 10 ms did not follow an exponential increase during warming by infrared lamp and water blanket. Due to warming, superexcitability at 10 ms increased to positive values in 2 subjects (Table 1, Fig. 2).

10

Figure 1. Distal motor latency, refractory period and superexcitability at 10 ms in three subjects during different warming procedures.
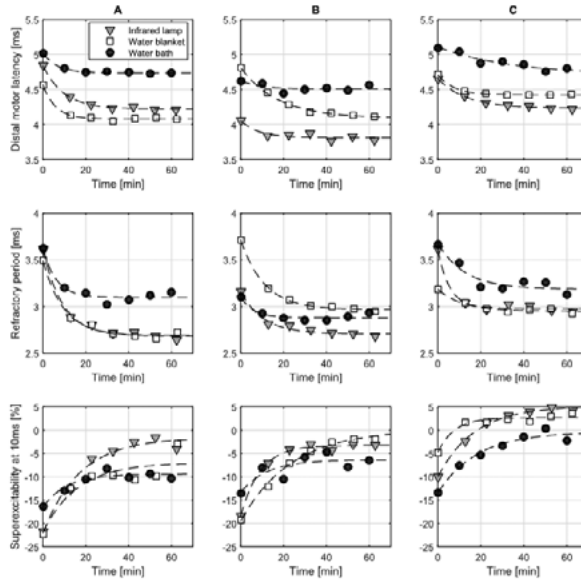

Figure 1 legend. (A) subject 3, (B) subject 4, and (C) subject 5. Distal motor latency (top), refractory period (middle), and superexcitability at 10 ms (bottom) are illustrated during warming by infrared lamp (triangles), water blanket (squares), and water bath (circles). Exponential fits are given by dashed lines.

Table 1. Recorded starting values, recorded end values, and fitted 95% end values of distal motor latency, refractory period, and superexcitability at 10ms.

Subject	Methods	Distal motor latency (ms)			Refractory period (ms)			Superexcitability at 10ms (%)		
		Recorded		Fitted	Recorded		Fitted	Recorded		Fitted
		Start	End	95% end-value	Start	End	95% end-value	Start	End	95% end-value
1	Infrared	4.53	4.24	4.19	3.54	2.92	2.98	-27.79	-7.96	-8.84
	Blanket	4.57	4.17	4.20	3.41	2.91	2.95	-20.01	-4.63	-5.83
	Bath	4.71	4.5	4.53	3.84	3.95	-	-14.89	-1.79	-2.39
2	Infrared	5.84	4.18	3.98	5.27	2.29	2.26	-29.56	-16.81	-
	Blanket	4.88	3.87	3.79	3.56	2.28	2.31	-34.69	-11.90	-
	Bath	4.43	4.01	4.06	3.05	2.42	2.49	-31.57	-17.35	-17.99
3	Infrared	4.84	4.21	4.25	3.62	2.64	2.73	-21.72	-3.97	-2.66
	Blanket	4.57	4.08	4.10	3.50	2.72	2.73	-22.27	-2.94	-7.75
	Bath	5.02	4.73	4.75	3.62	3.15	3.12	-16.38	-10.32	-9.78
4	Infrared	4.06	3.78	3.82	3.16	2.68	2.73	-18.41	-3.17	-3.99
	Blanket	4.81	4.11	4.13	3.72	2.95	3.00	-19.22	-1.82	-0.84
	Bath	4.62	4.57	4.52	3.10	2.93	2.89	-13.53	-6.40	-6.67
5	Infrared	4.66	4.22	4.25	3.61	2.95	3.01	-9.96	4.30*	4.42
	Blanket	4.71	4.43	4.44	3.19	2.93	2.96	-4.82	3.69*	2.34
	Bath	5.10	4.80	4.73	3.67	3.13	3.21	-13.48	-2.18	-1.01

* Note that due to warming the threshold change for superexcitability at 10 ms may become positive.

Figure 2. Recovery cycles in subject 5 during warming with water blanket.
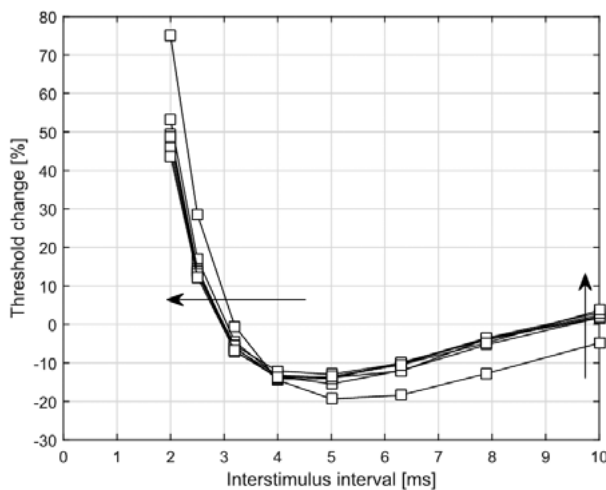

Figure 2 legend. Horizontal arrow: shortening of the refractory period during warming. Vertical arrow: increase in thresholds at interstimulus interval of 10 ms during warming.

Table 2 shows the time needed for DML, refractory period and superexcitability at 10 ms to reach their time constant (τ) and $t_{95\%}$ per warming method, per subject and as composite over all subjects. The median values of $t_{95\%}$ over the 5 subjects were: (i) for DML: 36 minutes (IQR 29-57) for the infrared lamp, 36 minutes (IQR 22-61) for the water blanket and 20 minutes (IQR 16-44) for the water bath; (ii) for refractory period: 28 minutes (IQR 25-41) for the infrared lamp, 34 minutes (IQR 29-40) for the water blanket and 19 minutes (IQR 14-29) for the water bath; (iii) superexcitability at 10 ms: 45 minutes (IQR 33-52) for the infrared lamp, 37 minutes (IQR 24-60) for the water blanket and 33 minutes (IQR 30-42) for the water bath. The median value of $t_{95\%}$ over all three variables was fastest for the water bath (24 minutes) and slower for the infrared lamp (34 minutes) and water blanket (35 minutes). The differences between the fastest and slowest methods were moderate with 16 minutes for DML, 15 minutes for refractory period and 12 minutes for superexcitability at 10 ms. As composite over all subjects, the water bath showed the shortest time constant for DML, refractory period and superexcitability at 10 ms compared to the infrared lamp and the water blanket (Table 2).

Skin temperature

There were no correlations between baseline skin temperature before warming and the time constants for DML (r = -0.48; p=0.07), refractory period (r = -0.19; p=0.51), and superexcitability at 10 ms (r = -0.43; p = 0.14). Skin temperature and DML, skin temperature and refractory period, and distal motor latency and refractory period were all linearly related; this was not the case for skin temperature and superexcitability at 10 ms (Fig. 3). Median baseline skin temperature over all three methods and 5 subjects was 32.3°C (IQR30.3 - 32.8 °C). After 60 minutes of warming, it was 36.6°C (IQR 33.5– 36.8°C) with a median increase of 3.8°C (IQR2.5- 5.4°C).

Table 2. Warming time, expressed by time constant (τ) and the time needed to reach 95% of the end value ($t_{95\%}$) for the different warming methods.

Subject	Methods	Baseline skin temperature* (ºC)	Distal motor latency		Refractory period		Superexcitability at 10 ms	
			τ (min)	$t_{95\%}$ (min)	τ (min)	$t_{95\%}$ (min)	τ (min)	$t_{95\%}$ (min)
1	Infrared	32.3	12	36	9	27	13	39
	Blanket	33.2	12	36	10	29	8	25
	Bath	32.5	6	17	-	-	10	32
2	Infrared	28.6	34	103	23	68	-	-
	Blanket	29.6	29	87	18	56	-	-
	Bath	29.8	4	11	3	10	7	22
3	Infrared	30.6	10	30	9	28	17	52
	Blanket	33.2	6	18	10	29	16	48
	Bath	32.8	7	20	6	19	11	33
4	Infrared	32.8	9	26	11	32	9	27
	Blanket	30.2	17	52	11	34	24	71
	Bath	32.3	8	25	6	18	12	37
5	Infrared	32.3	14	42	5	17	17	51
	Blanket	34.2	7	23	12	35	8	23
	Bath	30.8	33	100	13	39	18	55
Composite	Infrared	-	18	55	14	43	14	42
	Blanket	-	15	45	13	38	15	46
	Bath	-	8	23	8	23	10	31

* Baseline skin temperature was taken before start of warming.

10

Figure 3. Temperature sensitive variables: mutual relations and relations with skin temperature.
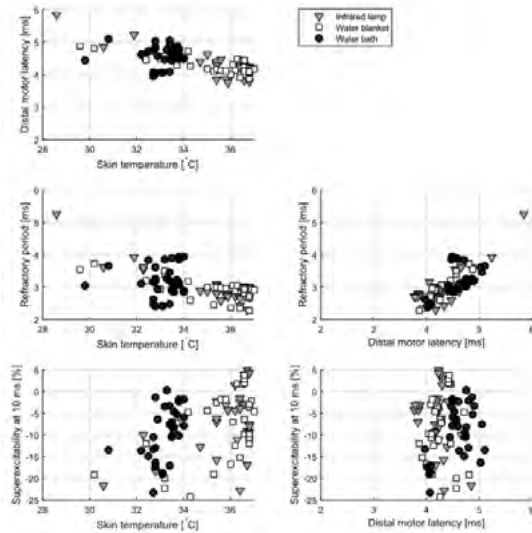

Figure 3 legend. Variables were obtained from the complete set of excitability recordings obtained for each warming method.

DISCUSSION

The present study investigated the warming time in an environment at 37°C that was needed for DML and selected excitability indices of the median nerve at the wrist to approach 95% of the asymptotic end value at that environmental temperature. The warming time for those variables was fastest for the water bath with moderately more time for the infrared lamp and water blanket. The time constants for DML were comparable to previous observations when using a water bath to warm the nerve[23]. Although a linear relation between DML and skin temperature was also previously found,[22] a more complex response to warming was observed for excitability indices. This may be due to the varying contribution of ion channels and pumps underlying these indices, where they may also respond differently to temperature changes[20,21].

The relationship between temperature and compound signals measured in clinical neurophysiology is complicated. At lower temperatures, temporal dispersion between single nerve fiber action potentials increases (due to differential slowing of Na-channel opening between fibers) and single nerve and muscle fiber action potential amplitudes both increase (due to

longer open-time of Na-channels). Because increased temporal dispersion tends to decrease compound potential amplitude, whereas increased single-fiber action potential amplitude tends to increase it, these two processes have opposing effects on compound potential amplitude[29,30]. These opposing effects together with the studied temperature range may underlie the non-significant trend observed towards decrease in compound signal in our study.

In single myelinated nerve fibers, conduction velocity increases linearly with near-nerve temperature in the range of 20 to 40°C[26-28]. The time to bring a single nerve fiber to the temperature of the medium in which it is embedded is short because of the small volume of the nerve fiber. On the other hand, during the process of warming a limb, both conduction velocity and DML were shown to change slowly over time according to exponential relations[23,24]. This is because limb nerves are surrounded by muscle, fat, connective tissue and skin, each of which has a considerably larger volume than the nerve so that it requires many tens of minutes to bring a cold limb to a higher temperature. Furthermore, the muscle tissue surrounding the nerve is more rapidly warmed than cooled because it is richly supplied by blood. This results in hysteresis between warming and cooling: it takes less time (shorter time constant) to warm a limb from 30°C to 37°C than to cool it back from 37°C to 30°C[24]. This indicates that skin temperature cannot be used as a surrogate marker for nerve temperature when experiments with temperature are performed.

Long-time warming at 37°C by infrared lamp, water blanket or water bath are each suitable to warm the median nerve at the wrist prior to excitability testing. There is a moderate difference between the methods considering the necessary warming time with the water bath requiring the least amount of time, which could be of a clinical advantage for test reliability. Yet, with respect to the time required to reach stable indices, it must be noted that efficiency of heat transfer from source to target (nerve) may differ between the warming methods. Therefore, the method of warming and the time warmed prior to the recordings should be specified. It should be further noted that, irrespective of the warming method, the efficiency of warming the nerve may also be influenced by pathological conditions where arterial circulation is affected, changes in tissue properties (e.g. edema or callus) or in peripheral nerve disorders. To determine how specific disease conditions affect the necessary warming time will require additional studies. As the recordings were performed on different days, some variation may be present in the absolute values of the indices associated with electrode repositioning and starting nerve temperature, independent of the time required to reach stable indices for the warming methods. Warming by water blanket for long lasting excitability testing has some practical advantages, due to the possibility of maintaining a homogenous environmental temperature during the recordings, easiness in installation, mobility of the setup and moderate expenses. It must be emphasized that these results apply for testing nerves at the wrist at 37°C and that they are not necessarily applicable to deeper lying nerves as these may need longer warming times.

10

REFERENCES

1. Bostock H, Cikurel K, Burke D. Threshold tracking techniques in the study of human peripheral nerve. Muscle Nerve 1998;21:137–158.

2. Burke D, Kiernan MC, Bostock H. Excitability of human axons. ClinNeurophysiol 2001;112:1575-1585.

3. Kiernan MC, Burke D, Andersen KV, Bostock H. Multiple measures of axonal excitability: a new approach in clinical testing. Muscle Nerve 2000; 23:399-409.

4. Bostock H, Sharief MK, Reid G, Murray NM. Axonal ion channel dysfunction in amyotrophic lateral sclerosis. Brain 1995;118:217-225.

5. Cappelen-SmithC, Kuwabara S, Lin CS, Mogyoros I, Burke D. Membrane properties in chronic inflammatory demyelinating neuropathy. Brain 2001; 124:2439-2447.

6. Cappelen-Smith C, Kuwabara S, Lin CS, Burke D. Abnormalities of axonal excitability are not generalized in early multifocal motor neuropathy. Muscle Nerve 2002;26:769–776.

7. Howells J, Matamala JM, Park SB, Garg N, Vucic S, Bostock H, et al. In vivo evidence for reduced ion channel expression in motor axons of patients with amyotrophic lateral sclerosis. J Physiol 2018;596:5379 - 5396.

8. Kanai K, Kuwabara S, Misawa S, Tamura N, Ogawara K, Nakata M, et al. Altered axonal excitability properties in amyotrophic lateral sclerosis: impaired potassium channel function related to disease stage. Brain 2006;129: 953 - 962.

9. Kiernan MC, Guglielmi JM, Kaji R, Murray NMF, Bostock H. Evidence for axonal membrane hyperpolarization in multifocal motor neuropathy with conduction block. Brain 2002;125:664 – 675.

10. Krishnan AV, Kiernan MC. Altered excitability properties in established diabetic neuropathy. Brain 2005;128:1178 – 1187.

11. Krishnan AV, Phoon RKS, Pussell BA, Charlesworth JA, Kiernan MC. Sensory nerve excitability and neuropathy in end-stage kidney disease. J Neurol Neurosurg Psychiatry 2006;77: 548-551.

12. Krishnan AV, Lin CS, Kiernan MC. Activity-dependent excitability changes suggest Na+/K+ pump dysfunction in diabetic neuropathy. Brain 2008;131:1209-1216.

13. Misawa S, Kuwabara S, Kanai K, Tamura N, Nakata M, Ogawara K, et al. Nodal persistent Na+ currents in human diabetic nerves estimated by the technique of latent addition. Clin Neurophysiol 2006;117:815–820.

14. Misawa S. Pathophysiology of neuropathic pain: Na+ channel and hyperexcitability of primary afferents. Brain Nerve 2012;64:1249-1253.

15. Bostock H, Rothwell JC. Latent addition in motor and sensory fibres of human peripheral nerve. J Physiol 1997;498:277-294.

16. Tomlinson S, Burke D, Hanna M, Koltzenburg M, Bostock H. In vivo assessment of HCN channel current (I(h)) in human motor axons. Muscle Nerve 2010;41:247-256.

17. Hageman S, Kovalchuk MO, Sleutjes BTHM, van Schelven LJ, van den Berg LH, Franssen H. Sodium-potassium pump assessment by submaximal electrical nerve stimulation. Clin Neurophysiol 2018;129:809-814.

18. Kiernan MC, Bostock H. Effects of membrane polarization and ischaemia on the excitability properties of human motor axons. Brain 2000;123:2542-2551.

19. Franssen H, Gebbink TA, Wokke JH, van den Berg LH, van Schelven LJ. Is cold paresis related to axonal depolarization? J Peripher Nerv Syst 2010;15:227-237.

20. Kiernan MC, Cikurel K, Bostock H. Effects of temperature on the excitability properties of human motor axons. Brain 2001;124:816-825.

21. Kovalchuk MO, Franssen H, van Schelven LH, Sleutjes BTHM. Comparing excitability at 37°C with 20°C: differences between motor and sensory axons. Muscle Nerve 2018;57:574-580.

22. Drenthen J, Blok JH, Dudok van Heel EBM, Visser GH. Limb temperature and nerve conduction velocity during warming with hot water blankets. J Clin Neurophysiol 2008;25:104-110.

23. Franssen H, Wieneke GH. Nerve conduction and temperature: necessary warming time. MuscleNerve 1994;17:336-344.

24. Geerlings AHC, Mechelse K. Temperature and nerve conduction velocity, some practical problems. Electromyogr Clin Neurophysiol 1985;25:253-259.

25. Khan M, Ohno Y. Compression of temporal video data by Catmull-Rom Spline and quadratic Bézier Curve fitting. 16th international conference in Central Europe on computer graphics, visualization and computer vision. Available at: http://wscg.zcu.cz/DL/wscg_DL.htm. Czech Republic, February 4-7, 2008.

26. Low PA, McLeod JG. Refractory period, conduction of trains of impulses, and effect of temperature on conduction in chronic hypertrophic neuropathy. J Neurol Neurosurg Psychiatry 1977;40:434-447.

27. Paintal AS. Effects of temperature on conduction in single vagal and saphenous myelinated nerve fibres of the cat. J Physiol 1965;180:20–49.

28. Raminsky M. The effects of temperature on conduction in demyelinated single nerve fibers. Arch Neurol 1973;28:287-292.

29. Rutten GJM, Gaasbeek RDA, Franssen H. Decrease in nerve temperature: a model for increased temporal dispersion. Electroencephalogr Clin Neurophysiol 1998;109: 15 – 23.

30. Stegeman DF, Weerd de JPC. Modelling compound action potentials of peripheral nerves in situ. II. A study of the influence of temperature. Electroencephalogr Clin Neurophysiol 1982; 54: 516 - 529.

10

11

General discussion

Amyotrophic lateral sclerosis (ALS) is the most common motor neuron disease (MND), characterized by upper and lower motor neuron loss, resulting in muscle weakness, respiratory failure and severe decrease of life expectancy.[1] Potentially treatable disorders, such as multifocal motor neuropathy (MMN), mimicking ALS or other MNDs, should be distinguished.[2] Overlap of MNDs and immune-mediated disorders of the peripheral nervous system has been discussed.[3] MMN is a chronic inflammatory neuropathy presented with slowly progressive, asymmetric limb weakness and normal life expectancy.[4] The distinctive features of MMN are the selective motor fiber involvement, phenomena of conduction block and cold paresis, presence of antibodies against GM1 ganglioside.[5-7] The favorable response to immunoglobulins; serum anti-GM1 antibodies in about half of the patients, possibly bringing to the complement associated disruption of the node of Ranvier complex; similarities with acute motor axonal neuropathy, support the immune-mediated pathogenesis of MMN.[8-10] Much has been done to explore each of the above features, but the exact pathological mechanisms are still unknown.

The role of membrane properties in motor neuron disorders is not fully elucidated. Highlighting excitability abnormalities of the axon would support their importance in the pathogenesis and disease progression of ALS and MMN, offering novel treatment approaches.

Delineating biophysical differences between motor and sensory axon is essential to explain the selectivity of fiber involvement in peripheral nerve disorders and their vulnerability to pathological conditions in lower MNDs and peripheral neuropathies.[11,12] Although motor nerve selectivity in MMN could be explained by differences in antigenic properties of GM1-gangliosides between motor and sensory axons, the fact that antigenic distinctions were only found for the intramembranous ceramide portion of GM1, and not the extracellular antigenic sugar portion, makes this hypothesis debatable.[12-16] Difference in active or passive membrane properties of motor and sensory fibers could also contribute in the selective nerve impairment. In *chapter 2* we assess the effect of temperature on excitability properties of healthy motor and sensory nerves. Compared to motor axons, more complicated changes than depolarization, take place in the sensory axons. These changes may possibly reflect a combination of decreased slow potassium conductance, decreased hyperpolarization-activated current and changes in resting membrane potential. The decrease of current-voltage slope observed in sensory axons due to cooling, may be partially explained by the gating kinetics of different subtypes of the HCN-channels expressed in motor and sensory axons, being of relevance for motor nerves selective damage and their vulnerability to cooling in MMN.[17-19]

Performing motor and sensory excitability testing in MMN patients extended our knowledge on the discrepancies between motor and sensory fibers, showing no similarities in

the abnormalities trend of membrane properties due to MMN (*chapter 4*). Sophisticated mathematical modeling points towards increased Barrett-Barrett conductance in motor fibers and increase in internodal fast potassium conductance in sensory fibers, suggesting myelin sheath or paranodal seal involvement in motor and paranodal detachment in sensory fibers. Direct comparison of motor and sensory excitability parameters within the same nerve in both healthy and diseased subjects was exclusively applied, putting more weight on our findings.

Selective motor involvement in MMN results in clinical and neurophysiological impairment, such as conduction block – failure of action potential propagation, which exact location *in vivo* is difficult to define. However, conduction block could be simulated by means of computational model. Combining the McIntyre model[20] and experimental mammalian and human nerve excitability studies, an extended longitudinal myelinated axon model has been elaborated (*chapter 3*). In this model we introduced several types of morphological impairment close to the node of Ranvier. The impact of perinodal changes on conduction in motor and sensory axons has been quantitatively studied. Simulations of increasing nodal sodium channel dysfunction and paranodal myelin detachment induced progressive conduction slowing. A boundary of block emerged when the two mechanisms interacted – reducing sodium channel conductance and paranodal periaxonal resistance. This boundary shifted in opposite directions for a smaller affected region and nodal widening. Sensory axons were more resistant to block than motor axons. These differences could contribute to the predominance of motor deficit in MMN.

Extended longitudinal myelinated axon model together with the modeling results from *chapter 4* add to our knowledge on the structural damage of the nerves in MMN, mainly based on scarce pathological studies, revealing both demyelination and axonal damage.[21-23]

Excitability measurements at different target compound muscle action potential (CMAP) levels in MMN have not been previously reported (*chapter 5*). The ion channel activity and recruitment pattern of different diameter axons could yield specific pattern of motor involvement along the disease course in MMN. Our recordings showed the largest discrepancies between 20% and 60% threshold levels: nine out of thirteen recorded excitability parameters showed significant difference of $p \leq 0.01$. Between 20% and 40%, and 40% and 60% thresholds five of the excitability parameters differed significantly. Our findings suggest that subtypes of motor axons could be more vulnerable to develop axon damage along the course of MMN. Due to the complexity of motor unit involvement even in healthy nerves, data obtained from diseased motor fibers should be interpreted carefully.[24-25]

11

In ALS, a motor neuron loss disorder, axons ultimately degenerate along the disease progression. Increased membrane excitability was previously shown in both peripheral and central motor neurons in ALS.[26-28] Non-invasive investigation of the axonal excitability may be a reliable biomarker of motor neuron damage in ALS. In order to validate excitability testing as a biomarker of hyperexcitability we investigated median nerve at the wrist of 18 patients with ALS (*chapter 6*). Excitability testing showed to produce repeatable results in patients with ALS, both within and between visits, for all 18 excitability variables except accommodation half-time. No correlation between disability scale, ALSFRS-R, and excitability variables, was found.

This study was combined with the assessment of treatment effect of riluzole and retigabine on excitability parameters in a randomized, double-blind, 3-way cross-over, placebo-controlled study. No effect on excitability was produced by riluzole, unlike to retigabine, reversing hyperexcitability by significantly decreasing strength-duration time-constant (9.2%) and refractoriness at 2ms (10.2 percentage points) compared to placebo, justifying long-term studies evaluating impact on disease progression and survival.

Peripheral nerve excitability testing showed to be useful, quick, non-invasive biomarker to test for potential treatments for ALS, and measure treatment efficacy.

Immunoglobulin (Ig) is the only approved medication in MMN.[8] Immune-mediated mechanism is probably not unique to explain the improvement of muscle strength. We performed excitability testing in 42 MMN patients prior to the maintenance immunoglobulin infusion and on the peak of clinical effect following Ig administration to record changes in excitability. Within subject analysis showed statistically significant decrease in TEdpeak following Ig infusion (p=0.04) (*chapter 7*). Although, based on previous studies,[29-30] influence on persistent sodium current could be expected, rather than on slow potassium conductance, our finding supports the idea that immunoglobulin produces very moderate changes in axonal membrane properties of MMN patients.

The electrogenic sodium-potassium pump is crucial in maintaining resting membrane potential: per cycle 3 sodium ions are removed from the axon for only 2 potassium ions brought into the axon resulting in lack of positive charges inside the axolemma and negative value of resting membrane potential. Altered activity of the axonal sodium-potassium pump was reported in few peripheral nerve disorders and ALS.[29,31-33] However, proper technique assessing the activity of sodium-potassium pump has not been implemented. In *chapter 8* we show that submaximal electrical stimulation is a suitable and reliable alternative to maximal voluntary contraction (MVC) for investigating sodium-potassium pump function. Both techniques induce axonal hyperpolarization, but, contrary to MVC, submaximal electrical stimulation was not painful and it resulted in reproduci-

ble threshold increases. Applying submaximal electrical stimulation could clarify previously reported guess whether sodium-potassium pump activity is impaired at the site of conduction block and/or at adjacent to conduction block in MMN.[32]

Excitability in single human motor axons was first studied by Joseph Bergmans.[34] Since then the methodology of acquiring axonal excitability variables significantly improved. However, until now such data was only obtained from single-channel surface EMG, which is still challenging in terms of identifying single motor unit action potential (MUAP).[35-37] The excitability of a single MUAP provides a more precise information on the pathophysiological events compared to the data recorded from compound muscle action potential.[38] In *chapter 9* we describe new technique of high-density surface-EMG[39] which was successfully applied in 10 healthy subjects. A 9 x 14 array of densely spaced electrodes attached to the skin over the thenar muscle group was used to obtain a single-channel surface-EMG signal and perform excitability testing in MUAP. The recorded excitability variables are comparable to previous studies. The median recording duration was 44 min (40 min – 57 min). The method showed to be reliable in the study of ion channel function in single motor axons not requiring specific conditions, such as prominent motor unit loss or enlarged MUAPs due to collateral sprouting.

Strong evidence of proper nerve temperature required when performing nerve conduction studies was earlier reported.[40-42] Since excitability parameters are temperature dependent, an optimal technique is required to bring the nerve to a desired temperature (*chapter 10*). In terms of rapidity and stability of the temperature of the medium of the median nerve at the wrist, we compared three warming techniques – water bath, infrared lamp and water blankets. Based on the time needed for distal motor latency, refractory period, and superexcitability at 10 ms to approach 95 % of the asymptotic end value ($t_{95\%}$) at that environmental temperature, we compared this value for each of the methods. All three methods showed to be suitable to perform proper excitability testing of the median nerve at the wrist with the median value of $t_{95\%}$ over all three variables fastest for the water bath (24 minutes) and slower for the infrared lamp (34 minutes) and water blanket (35 minutes).

Our research highlights the importance of assessing changes in resting membrane potential and activity of axolemmal voltage-gated ion channels in motor neuron disorders and peripheral nerve diseases.

11

REFERENCES

1. van Es MA, Hardiman O, Chio A, et al. Amyotrophic lateral sclerosis. Lancet 2017;390:2084-2098.

2. Hardiman O, Al-Chalabi A, Chio A, et al. Amyotrophic lateral sclerosis. Nat Rev Dis Primers. 2017 Oct 20;3:17085.

3. Vlam L, Piepers S, Sutedja NA, et al. Association of IgM monoclonal gammopathy with progressive muscular atrophy and multifocal motor neuropathy: a case-control study. J Neurol. 2015 Mar;262(3):666-73.

4. Umapathi T, Hughes RA, Nobile-Orazio E, Léger JM. Immunosuppressant and immunomodulatory treatments for multifocal motor neuropathy. Cochrane Database Syst Rev. 2009 Jan 21;(1):CD003217.

5. Nobile-Orazio E, Cappellari A, Priori A. Multifocal motor neuropathy: current concepts and controversies. Muscle Nerve 2005;31:663– 80.

6. Olney RK, Lewis RA, Putnam TD, Campellone JVJ. Consensus criteria for the diagnosis of multifocal motor neuropathy. Muscle Ne rve (2003) 27:117–121.

7. Vlam L, van der Pol WL, Cats EA, Straver DC, Piepers S, et al. Multifocal motor neuropathy: diagnosis, pathogenesis and treatment strategies. Nat Rev Neurol. 2011 Nov 22;8(1):48-58.

8. Léger JM, Chassande B, Musset L, et al. Intravenous immunoglobulin therapy in multifocal motor neuropathy: a double-blind, placebo-controlled study. Brain. 2001;124:145–153.

9. Yuki N. Acute motor axonal neuropathy and multifocal motor neuropathy: more in common than not. Muscle Nerve. 2013 Nov;48(5):693-5.

10. Susuki K, Yuki N, Schafer DP, et al. Dysfunction of nodes of Ranvier: a mechanism for anti-ganglioside antibody-mediated neuropathies. Exp Neurol 2012; 233:534-542.

11. Straver DC, van Asseldonk JT, Notermans NC, et al. Cold paresis in multifocal motor neuropathy. J Neurol. 2011 Feb;258(2):212-7.

12. Franssen H, Straver DC. Pathophysiology of immune-mediated demyelinating neuropathies--Part II: Neurology. Muscle Nerve. 2014 Jan;49(1):4-20.

13. Ogawa-Goto K, Funamoto N, Abe T, Nagashima K., et al. Different ceramide compositions of gangliosides between human motor and sensory nerves. J Neurochem 1990;55:1486–1493.

14. Bostock H, Burke D, Hales JP. Differences in behaviour of sensory and motor axons following release of ischaemia. Brain 1994;117:225-34.

15. Kiernan MC, Mogyoros I, Burke D. Differences in the recovery of excitability in sensory and motor axons of human median nerve. Brain 1996 Aug;119:1099-105.

16. Kiernan MC, Lin CS, Burke D. Differences in activity-dependent hyperpolarization in human sensory and motor axons. J Physiol. 2004 Jul 1;558(Pt 1):341-9.

17. Franssen H, Wieneke GH, Wokke JH. The influence of temperature on conduction block. Muscle Nerve. 1999 Feb;22(2):166-73.

18. R. Kaji. Physiology of conduction block in multifocal motor neuropathy and other demyelinating neuropathies. Muscle Nerve 2003;27:285-96.

19. Howells J, Czesnik D, Trevillion L, Burke D. Excitability and the safety margin in human axons during hyperthermia. J Physiol 2013 Jun 15;591(12):3063-80.

20. McIntyre CC, Richardson AG, and Grill WM. Modeling the excitability of mammalian nerve fibers: influence of afterpotentials on the recovery cycle. J Neurophysiol 87: 995-1006, 2002.

21. Corbo M, Abouzahr MK, Latov N, Iannaccone S, Quattrini A, Nemni R, et al. Motor nerve biopsy studies in motor neuropathy and motor neuron disease. Muscle Nerve. 1997 Jan;20(1):15-21.

22. Kaji R, Oka N, Tsuji T, Mezaki T, Nishio T, Akiguchi I, et al. Pathological findings at the site of conduction block in multifocal motor neuropathy. Ann Neurol. 1993 Feb;33(2):152-8.

23. Taylor BV, Dyck PJ, Engelstad J, et al. Multifocal motor neuropathy: pathologic alterations at the site of conduction block. J Neuropathol Exp Neurol. 2004 Feb;63(2):129-37.

24. Thomas CK, Nelson G, Than L, Zijdewind I. Motor unit activation order during electrically evoked contractions of paralyzed or partially paralyzed muscles. Muscle Nerve. 2002 Jun;25(6):797-804.

25. Kayagil TA, Grimes JP, Grill WM. Mechanisms underlying reversal of motor unit activation order in electrically evoked contractions after spinal cord injury. Muscle Nerve. 2008;37:210 –218.

26. Kanai, K. et al. Altered axonal excitability properties in amyotrophic lateral sclerosis: impaired potassium channel function related to disease stage. Brain 129, 953-62 (2006).

27. Park SB, Kiernan MC ,Vucic S. Axonal Excitability in Amyotrophic Lateral Sclerosis: Axonal Excitability in ALS. Neurotherapeutics 14, 78-90 (2017).

28. Kanai K., Shibuya K, Sato Y, et al. Motor axonal excitability properties are strong predictors for survival in amyotrophic lateral sclerosis. J Neurol Neurosurg Psychiatry 83, 734-8 (2012).

11

29. Lin CS, Krishnan AV, Park SB, Kiernan MC. Modulatory effects on axonal function after intravenous immunoglobulin therapy in chronic inflammatory demyelinating polyneuropathy. Arch Neurol. 2011 Jul;68(7):862-9.

30. Boërio D, Créange A, Hogrel JY, et al. Nerve excitability changes after intravenous immunoglobulin infusions in multifocal motor neuropathy and chronic inflammatory demyelinating neuropathy. J Neurol Sci. 2010;292(1-2):63-71.

31. Krishnan AV, Lin CSY, Kiernan MC. Activity-dependent excitability changes suggest Na+/K+ pump dysfunction in diabetic neuropathy. Brain 2008;131:1209-16.

32. Kiernan MC, Guglielmi JM, Kaji R, et al. Evidence for axonal membrane hyperpolarization in multifocal motor neuropathy with conduction block. Brain. 2002 Mar;125(Pt 3):664-75.

33. Vucic S, Krishnan AV, Kiernan MC. Fatigue and activity dependent changes in axonal excitability in amyotrophic lateral sclerosis. J Neurol Neurosurg Psychiatry 2007;78:1202-8.

34. Bergmans J. The physiology of single human nerve fibres. Vander. 1970;University of Louvain.

35. Bostock H, Lin CS, Howells J, Trevillion L, Jankelowitz S, Burke D. After-effects of near-threshold stimulation in single human motor axons. J Physiol. 2005;564:931-940.

36. Mogyoros I, Kiernan MC, Burke D. Strength-duration properties of human peripheral nerve. Brain. 1996;119 (Pt 2):439-447.

37. Maathuis EM, Drenthen J, van Doorn PA, et al. Multiplet discharges after electrical stimulation: new evidence for distal excitability changes in motor neuron disease. Amyotroph Lateral Scler. 2012 Oct;13(6):514-20.

38. van Dijk JP, Blok JH, Lapatki BG, et al. Motor unit number estimation using high-density surface electromyography. Clin Neurophysiol. 2008;119:33-42.

39. Trevillion L, Howells J, Bostock H, Burke D. Properties of low-threshold motor axons in the human median nerve. J Physiol. 2010;588:2503-2515.

40. Geerlings AHC, Mechelse K. Temperature and nerve conduction velocity, some practical problems. Electromyogr Clin Neurophysiol 1985;25:253-259.

41. Franssen H, Wieneke GH. Nerve conduction and temperature: necessary warming time. MuscleNerve 1994;17:336-344.

42. Drenthen J, Blok JH, Dudok van Heel EBM, Visser GH. Limb temperature and nerve conduction velocity during warming with hot water blankets. J Clin Neurophysiol 2008;25:104-110.

ADDENDA

SUMMARY

In this thesis two disorders of motor neurons are discussed: amyotrophic lateral sclerosis (ALS) and multifocal motor neuropathy (MMN). ALS is characterized by progressive weakness of limb, trunk and bulbar muscles resulting in death within a few years after onset. In ALS, both upper and lower motor neurons degenerate due to genetic or unknown reasons. No effective treatment is available. MMN is characterized by slowly progressive and asymmetric weakness and atrophy of limb muscles with arms and hands being more affected than legs. Life expectancy in MMN is normal. In MMN lower motor neurons in peripheral nerves are affected due to degeneration or multifocal loss of their myelin sheath. MMN is considered an immune-mediated neuropathy since in approximately half of the patients serum antibodies against ganglioside GM1 are found and since administration of immunoglobulins induces improvement of muscle strength. The improvement is only temporary (weeks to months) so that repeated administration is needed. Despite treatment, muscle strength and loss of motor axons slowly progresses.

Chapter 1 describes the method used in this thesis to record axonal membrane properties in peripheral nerves of ALS and MMN patients. This method, known as excitability testing, is used to assess changes in activity of voltage-gated ion channels in the axon membrane of a group of motor or sensory axons at one site of a peripheral nerve. Excitability testing involves delivering a complex set of submaximal electrical stimuli to a nerve and recording the resulting change in excitation threshold for a motor or sensory response of fixed size. By varying the stimulus properties, different types of ion channels can be assessed, and, indirectly, the activity of the sodium-potassium pumps in the axolemma.

The thesis addresses the following questions: (i) can motor vulnerability in MMN be explained by differences in axolemmal properties between motor and sensory axons, (ii) is advanced mathematical modeling of human myelinated axons helpful in unrevealling pathophysiological mechanisms, (iii) can excitability testing reveal pathophysiological mechanisms in MMN or ALS, (iv) can excitability testing be improved by developing novel methods, (v) can effects of treatment be monitored by excitability testing?

Chapter 2 describes changes in excitability properties of healthy motor and sensory axons following cooling of the nerve. This showed that cooling induced changes in axon membrane properties that differed between motor and sensory axons. This finding may be relevant to explain the pure motor involvement and cold paresis in MMN.

Chapter 3 describes a novel and advanced computational model of the human myelinated axon. By simulating several types of morphological impairment close to the node of Ranvier, we found that motor axons were more vulnerable to develop conduction block than sensory axons. This may further help to understand the selective motor involvement in MMN.

Chapter 4 presents motor and sensory excitability data obtained from the median nerve at the wrist in 20 MMN patients. In all patients the median nerve was affected by conduction block or slowing. Motor excitability was markedly abnormal and sensory excitability varied from

Addenda

normal to mildly abnormal. Modeling of the excitability data by the conventional Bostock model was consistent with myelin sheath dysfunction for motor and paranodal detachment for sensory axons. The abnormality in sensory axons possibly represents the early phase of what occurs in motor axons.

Chapter 5 describes excitability abnormalities in three different motor axon types (distinguished by their threshold for excitation) of MMN patients. This showed different excitability abnormalities for each of the three groups, suggesting that different motor axons within one nerve may be affected by different mechanisms.

Chapter 6 describes a randomized, double-blind, 3-way cross-over, placebo-controlled study in ALS patients. We assessed the effect of riluzole (the current registered treatment for ALS) and retigabine, a potassium-channel activator, on excitability. We found that a single dose of retigabine has a greater effect on axonal membrane properties than a single dose of riluzole. Excitability testing proved to be predictive of clinical outcome and a very useful, non-invasive, biomarker to test for potential treatments for ALS.

Chapter 7 describes the minimal to moderate effects on motor axon membrane properties of immunoglobulin treatment in MMN patients.

Chapter 8 describes a novel method to directly assess sodium-potassium pump function by excitability testing. Instead of activating the pump by supramaximal electrical stimulation (which is too painful for application in patients) or by maximal voluntary muscle contraction (which is unreliable) we used submaximal electrical stimulation to activate the pump. This resulted in a non-painful and reliable test which is suitable to investigate if pump activity is compromised in ALS and MMN patients.

Chapter 9 describes a novel method to assess excitability in single motor axons rather than a group of motor axons. By using high-density surface-EMG and defining threshold as the stimulus current which elicits a specific response of one motor unit on high-density surface EMG in 50% of trials we were able to record typical excitability responses in normal subjects. This method may be used to better delineate abnormalities in ALS and MMN patients since it avoids averaging out effects that are inherent to studying groups of axons.

Chapter 10 describes our search for the best method to warm a nerve to 37°C prior to excitability testing of the median nerve at the wrist. Warming a nerve to a fixed temperature is important since excitability variables, especially refractoriness, are sensitive to nerve temperature. The results showed that the quickest way to reach the desired nerve temperature was warming by water bath, followed by warming by warm water blankets and warming by infrared heater.

This thesis demonstrated the significance and usefulness of implementing nerve excitability testing in scientific and clinical research of motor neuron disorders as it offers the possibility to assess protein function in the axolemma.

SUMMARY IN DUTCH (NEDERLANDSE SAMENVATTING)

Dit proefschrift beschrijft twee aandoeningen van motorische neuronen: amyotrofische lateraal sclerose (ALS) en multifocale motorische neuropathie (MMN). ALS wordt gekenmerkt door progressieve zwakte van arm-, been-, romp-, gelaats- en ademhalingsspieren. ALS leidt tot de dood binnen enkele jaren. Bij ALS gaan centrale en perifere motorische neuronen verloren door een genetische of andere, onbekende, oorzaken. Er is geen effectieve behandeling bekend, maar riluzole kan de levensduur iets verlengen. Bij MMN treedt langzaam progressieve, asymmetrische spierzwakte van armen en benen op die meer uitgesproken is bij armen en handen. De levensverwachting bij MMN is normaal. Bij MMN gaan perifere motorische neuronen verloren en is er multifocale demyelinisatie van deze neuronen. MMN wordt beschouwd als een immuun-gemedieerde neuropathie omdat bij de helft van de patiënten serum antilichamen tegen ganglioside GM1 worden gevonden en omdat de spierzwakte verbetert na het geven van immunoglobulinen. Deze verbetering is slechts tijdelijk (weken tot maanden) zodat deze kuren steeds moeten worden herhaald. Ondanks deze behandeling verergert de spoierzwakte geleidelijk in de loop der jaren.

Hoofdstuk 1 beschrijft de methode die in dit proefschrift gebruikt werd om perifere zenuwen bij ALS en MMN patiënten te onderzoeken. Met deze methode, excitability-testing genoemd, kunnen veranderingen in de activiteit van voltage-gated ionkanalen in het axonmembraan van een groep motorische of sensibele axonen op een plaats van een perifere zenuw worden onderzocht. Bij excitability testing worden complexe electrische stimuli aan een zenuw gegeven en worden de daardoor geinduceerde veranderingen in stimulusdrempel (threshold) voor het opwekken van een vaste motorische of sensibele responsie gemeten. Met bepaalde stimulus eigenschappen kunnen specifieke groepen ionkanalen geactiveerd en daardoor gemeten worden. Ook kan de activiteit van natrium-kalium pompen gemeten worden.

Dit proefschrift behandelt de volgende vragen: (i) kan de selectieve motorische betrokkenheid bij MMN verklaard worden door verschillen in axonmembraaneigenschappen tussen motorische en sensibele axonen, (ii) is geavanceerde computer-simulatie van een humaan gemyeliniseerd axon nuttig om pathofysiologische mechanismen bij MMN te onderzoeken, (iii) kan excitability testing pathofysiologische veranderingen bij MMN aantonen, (iv) kan excitability testing verbeterd worden met nieuwe methoden, (v) kunnen behandeleffecten gemonitord worden met excitability testing?

Hoofdstuk 2 beschrijft veranderingen in excitability bij gezonde motorische en sensibele axonen na afkoeling van de zenuw. De door afkoeling geinduceerde veranderingen verschilden tussen motorische en sensibele axonen. Deze bevinding kan helpen om de sterke verlamming bij koude die bij MMN patiënten kan optreden te verklaren.

Hoofdstuk 3 beschrijft een nieuw ontwikkeld en geavanceerd mathematisch model van een humaan gemyeliniseerd axon. Door verschillende morfologische veranderingen rond de knoop van Ranvier te modeleren vonden we dat motorische axonen gevoeliger waren voor het ontwikkelen van geleidingsblokkade dan sensibele axonen. Dit helpt om de selectieve motorische uitval bij MMN beter te leren begrijpen.

Addenda

Hoofdstuk 4 beschrijft motorische en sensibele excitability data van 20 MMN patiënten. Bij alle patiënten werd de n. medianus bij de pols onderzocht en bij allen was er een motorische geleidingsstoornis van de nervus medianus. Motorische excitability was sterk afwijkend en sensibele excitability normaal tot licht afwijkend. Conventioneel mathematisch modeleren volgens de Bostock methode suggereerde demyelinisatie van motorische axonen en loslaten van de myelineschede bij sensibele axonen. Mogelijk representeren de afwijkingen bij sensibele axonen het eerste stadium van de bij motorische axonen gevonden demyelinisatie.

Hoofdstuk 5 beschrijft excitability afwijkingen van drie verschillende typen motorische axonen (op basis van prikkeldrempel en, mogelijk, axondiameter) bij MMN patiënten. Bij ieder van de drie groepen werden verschillende afwijkingen gevonden, hetgeen er mogelijk op wijst dat, binnen een zenuw, verschillende pathofysiologische mechanismen een rol spelen.

Hoofdstuk 6 beschrijft een gerandomiseerde, dubbel-blinde, 3-way cross-over, placebo-gecontroleerde studie bij ALS patiënten. Het effect op excitability werd gemeten van: (i) riluzole (de huidige therapie voor ALS) en (ii) retigabine, een kalium-ionkanaal activator. Retigabine had meer effect op excitability dan riluzole; bovendien toonde excitability testing de door retigabine geinduceerde verandering in kaliumkanaal activiteit goed aan. Excitability testing bleek ook een betrouwbare biomarker te zijn om behandeling bij ALS te testen.

Hoofdstuk 7 beschrijft dat immunoglobuline behandeling bij MMN slechts minimale tot matige veranderingen van excitability variabelen induceert.

Hoofdstuk 8 beschrijft een nieuwe methode om natrium-kalium pomp activiteit te meten met excitability testing. In plaats van de pomp te activeren met supramaximale hoogfrequente elektrische stimulatie (te pijnlijk voor patiënten) of de pomp te activeren met maximale willekeurige spieraanspanning (te onbetrouwbaar) kozen we ervoor de pomp te activeren met submaximale hoogfrequente electrische stimulatie. Deze methode bleek niet pijnlijk te zijn en een betrouwbare gegevens op te leveren. Deze methode kan dus worden toegepast bij ALS en MMN patiënten teneinde na te gaan of de pomp dysfunctioneert.

Hoofdstuk 9 beschrijft een nieuwe methode om excitability te meten aan een motorisch axon (in plaats van een groep axonen). Hierbij wordt high-density surface-EMG gemeten om een specifieke motor unit responsie te identificeren. De stimulusdrempel (threshold) wordt gedefinieerd als de stroomsterkte waarbij een specifieke motor unit in 50% van de trials aanslaat. Met deze methode konden dezelfde excitability responsies worden gemeten die ook met de conventionele methode worden gemeten. Deze nieuwe methode is derhalve geschikt om afwijkingen bij ALS en MMN patients beter te beschrijven omdat de uitmiddelingseffecten die optreden bij conventionele excitability testing van een groep axonen vermeden worden.

Hoofdstuk 10 beschrijft een onderzoek naar de beste methode om een zenuw op te warmen tot 37°C voordat excitability van de nervus medianus bij de pols wordt getest. Opwarmen is van belang omdat excitability variabelen temperatuursafhankelijk zijn; dit geldt vooral voor de recovery cycle. De resultaten lieten zien dat opwarmen in water de de snelste methode was om de gewenste zenuwtemperatuur te bereiken, gevolgd door opwarmen met een warmwaterdeken en opwarmen met infrarood lamp.

Dit proefschrift toont aan dat excitability testing nuttig is voor wetenschappelijk en klinisch onderzoek van aandoeningen van motorische neuronen.

ACKNOWLEDGEMENTS (DANKWOORD) (БЛАГОДАРНОСТЬ)

Coincidences do exist. Otherwise, how could it happen, that simply willing to get acquainted with the set-up of the neuromuscular department, I came to the PhD defense day in the Academiegebouw at Domplein 29?

This was in December 2011, when I first came to the Neuromusculaire Ziekten (NMZ) department of UMC Utrecht, but my astonishment started, when during our email correspondence, professor Hessel Franssen kindly invited me to stay with his family while I am in the Netherlands. During my short visit he and his wife were so hospitable to show me lovely, typical Dutch, surroundings of Amsterdam, and the capital itself.

Next year, when I came for two- months EMG training, and Hessel "infected" me with the grandioses perspectives of nerve excitability, I was still far from the idea of making a PhD research. Even when we received a one-year grant from the European Federation of neurological societies (EFNS) for the "Disease mechanisms in multifocal motor neuropathy" project, I saw it only as a short (but great) scientific and personal experience. Only few months later, when I was asked if I regard PhD as an option, I realized a new life horizon. By this proposal, from my opinion, Hessel showed to be even more risky, than professor Leonard van den Berg, the engine of progress in the motor neuron and neuropathy field. Leonard asked me thrice, when interviewing, if I am definite about quitting my beloved mother land and family for several years. Despite all fears, it went well. Not to overestimate the way both Hessel and Leonard, were aiding me. Every day side by side with Hessel was full of scientific, musical, cultural, linguistic, humoristic events, with the clue elements - signal boxes and British series. Leonard was what we say - *редко, но метко* - we met once in a while, but even few minutes dialogue brought me self-assurance and optimism. I should emphasize how much inspiration and team feeling brought me onderzoeksbespreking!

Since I dived into real PhD duties the circle of my gratitude significantly enlarged, as on every step someone new was there to help.

Leonard van Schelven, who's contribution is hard to evaluate. While we were only three of us - true excitability enthusiasts together with Hessel and me, - *elke donderdag om 17 uur* was a special challenge for me. Sometimes I was grateful Leonard had a very strict timing, otherwise master class on medical physics would last that long, so that I would stop understanding it. This was hard, but so much pleasure to touch a wonderful backstage of science. Apart high skies, innumerous number of methodological issues have been solved by Leonard and his colleagues from the Department of Medical Technology and Clinical Physics.

Addenda

Since Boudewijn Sleutjes joined our excitability locomotive, the train goes so quickly, it cannot slow down four years later. Where would knowledge on axonal membrane properties be without Boudewijn's great ideas in modeling, novel methodology, original practical approaches, his scrupulosity, decisiveness, strictness to the working process and punctuality? Dear Boudewijn, I am truly grateful for your professional and personal support. Thank you for all the brainstorming and fun we had all along this excitability project!

My main companion in excitability testing, Jesper Raaijman, not only we shared long-lasting threshold electrotonus recordings, but you was the one on whom I could rely in practical aspects of our research. Patients communication, EMG and QTRAC set-up, excitability recordings, repeating temperature and pump experiments, all the practical pitfalls we've gone through are hard to recall, but always with smile. I am so proud to see how much you are evolving nowadays in your profession! And thanks for bringing my bike to the Central Station at the hottest summer day ever, fixed in the Netherlands!

Current research project, elaborated by Hessel, and assisted by so many people, wouldn't come true without a special interest of Jean-Marc Léger, chair of the EFNS Training and education Committee, to the nerve excitability in MMN. Coincidently (?), Jean-Marc played a crucial role in my personal life - first by taking me out of Moscow and later on by inviting me to attend *Les Journées internationales de la Société Française de Neurologie* in Paris.

Two very special persons are inseparable from the field of nerve excitability and each sub-project of my thesis - Joseph Bergmans and Hugh Bostock. I wish to stand up when naming those. True scientists, exclusively educated and broad in knowledge and interests, they are the parents of nerve excitability science as it is nowadays.

My personal communication and mail correspondence with Joseph revealed an example of stoicism *(Là aussi, après un passé difficile, le présent et le futur sont beaux !)* and life curiosity *(énorme joie de vivre et cette curiosité pour tout ce qui l'entourait)* in all aspects - scientific, cultural, floristic and daily life.

Can I ever forget the enjoy of having a discussion on Japanese 櫻, Nâzım Hikmet's poetry, or اهز ديدح architectural style in Chicheley with Joseph Bergmans, or arguing on potassium channels and the joy of climbing Swiss mountains at the Nobelstraat café with Hugh Bostock..?!

Beste paranimf, Stephan Goedee, to my appearance, the Netherlands and UMC Utrecht are not trully valid in your absence. So much medical and personal moments shared together! What shall I say...BEDANKT! For the books, music, training, patients, ideas and...teasing!

Дорогая Женя, dear paranymph, Evgeniya Druzhinina, this was a true joy to organize an unofficial exchange program between Utrecht and Moscow to discover nerve ultrasound experience and cultural background.

Supervising students, who performed excitability projects in terms of their fellowships, was a very special experience to me. That's how I met Susanne van den Brink, Steven Hageman, Anne-France Pirson, Féline Scheijmans, Nariç Durmus. Together we performed exciting research, each contributing to this thesis, and shared great moments in discussing personal

interests and achievements. Even after starting their own PhDs, Steven and Féline kept in touch, assisting us now and then.

Alexander and Jessica, your sincere interest to my PhD thesis, your personal support and decisiveness in learning me Dutch, hold a very special place in my heart. Not to forget that together with Stephan, Michael, Perry, Ingrid and other neurologists you made this project happen by diagnosing multifocal motor neuropathy.

Mysterious Ludo van der Pol, strict Michael van Es, and brave Jan Veldink, your single presence in the NMZ boosted my scientific motivation!

Beste dames, NMZ secretaresses! Mariette, Paulie, Charlotte, Nelly, Kimberley and Kimberley, Henriette, where would I be without your kind and vivid hearts, offering personal compassion and helping me with patients' logistics?

Dear Nicolette Notermans and Marina Blom thank you for providing special conditions to perform the experiments on excitability.

Bert, Nizare, Nico you were so kind to solve practical issues along the project.

No need to explain how precious are statistics in science. Dear Ruben and Stavros, your valuable advices were essential for interpreting our results.

My guardian angel, Annemarie, hard to name all the circumstances where you offered me your kindest assistance!

I appreciate and deeply thank all my healthy participants! You are heroes to be so patient and share your time for dozens of excitability testings. It was also a pleasure to work with MMN and ALS patients, enthusiastic, friendly and talkative, ready to participate in the research.

Gabriel Rinkel, Gerda Kuiper, Maureen de Leeuw, Irene Jonkers, employees of the Divisie Hersenen, dear co-authors, thank you all for your individual contributions.

Fortunate was I to get acquainted with James Howells (Australia), Michel van Putten (the Netherlands), Peter van den Bergh (Belgium), Martin Koltzenburg (United Kingdom), Christian Krarup, Mihai Moldovan and Hatice Tankisi from Denmark, Satoshi Kuwabara (Japan) who were open and positive in giving feedback on our project.

Staying out from the Netherlands during my last year of PhD turned out to be a new challenge, which was enormously alleviated by Nadah Dekker. My true hero! So much power and wisdom in you, translated to tranquility you generously share with the environment - random people, garden, cuisine, family. I got a big piece of this pacifying cake of yours!

Dear mom and dad, my brother Svatoslav (sure you are watching me from some seventh sky), grandmother Elena and Kaleria, grandfather Vladimir and Ivan, I wouldn't be where I am without your achievements and life troubles. My beloved Anatoly, happy we shared this PhD, you was a silent witness during late night and early morning work, and an active one (as you are right now, calling me to inflate the balloon, while final adjustments are done).

Addenda

Viktor Borisovich and Svetlana Nikolaevna, Anna, Ekaterina, Valeria, Viktoria, Evgeniy, Miloš, Svetlana, Anna, Anjela and Evgeniya, Sergey, Dmitriy, Yaroslav, dear schoolmates, your moral support and trust in me were of a great motivation! Kirill and Natalya, what an unexpected surprise to have you at the end of the project, helping with the thesis book!

It all started by coincidence, when my supervisor Sergey Nikitin, once emailed professor Hessel Franssen to consult some Russian VIP. It feels bizarre to be that lucky!

Lucky to work on a such *bouleversant* scientific topic in a brilliant University Medical Center of Utrecht, meet outstanding, kind people, to live in a great environment, where fields are green and rabbits run away from your bike when traveling home, lucky to experience Dutch traditions and attend Concertgebouw concerts, to improve languages and broaden life views.

Turning back I see a rock behind - the PhD research, surrounded my insignificant illusions and troubles of life.

This was a truly great journey, alike Kon-Tiki expedition crossing the Pacific ocean; with storms and sunny breaks - scientific achievements and hypothesis falls, educational meetings and acquaintances, emotional Scottish dances and hot Spanish siestas, finally offering a great satisfaction of overcoming yourself and bringing the scientific knowledge to a new horizon.

LIST OF PUBLICATIONS

1. Sleutjes BTHM, Kovalchuk MO, Durmus N, Buitenweg JR, van Putten MJAM, van den Berg LH, Franssen H. Simulating perinodal changes observed in immune-mediated neuropathies: impact on conduction in a model of myelinated motor and sensory axons. J Neurophysiol. 2019 Sep 1;122(3):1036-1049. doi: 10.1152/jn.00326.2019.

2. Kovalchuk MO, Franssen H, Scheijmans FEV, Van Schelven LJ, Van Den Berg LH, Sleutjes BTHM. Warming nerves for excitability testing. Muscle Nerve. 2019 Sep;60(3):279-285. doi: 10.1002/mus.26621.

3. Sleutjes BTHM, Drenthen J, Boskovic E, van Schelven LJ, Kovalchuk MO, Lumens PGE, van den Berg LH, Franssen H. Excitability tests using high-density surface-EMG: A novel approach to studying single motor units. Clin Neurophysiol. 2018 Aug;129(8):1634-1641. doi: 10.1016/j.clinph.2018.04.754.

4. Kovalchuk MO, Heuberger JAAC, Sleutjes BTHM, Ziagkos D, van den Berg LH, Ferguson TA, Franssen H, Groeneveld GJ. Acute Effects of Riluzole and Retigabine on Axonal Excitability in Patients With Amyotrophic Lateral Sclerosis: A Randomized, Double-Blind, Placebo-Controlled, Crossover Trial. Clin PharmacolTher. 2018 Dec;104(6):1136-1145. doi: 10.1002/cpt.1096.

5. Hageman S, Kovalchuk MO, Sleutjes BTHM, van Schelven LJ, van den Berg LH, Franssen H. Sodium-potassium pump assessment by submaximal electrical nerve stimulation. Clin Neurophysiol. 2018 Apr;129(4):809-814. doi: 10.1016/j.clinph.2018.01.016.

6. Kovalchuk MO, Franssen H, Van Schelven LJ, Sleutjes BTHM. Comparing excitability at 37°C versus at 20°C: Differences between motor and sensory axons. Muscle Nerve. 2018 Apr;57(4):574-580. doi: 10.1002/mus.25960.

7. Nikitin SS, Kovalchuk MO, Proskurina EA, Khoroshaya IV. First Case of Late-Onset Glycogen Storage Disease Type II in Russia with a Novel Mutation. J Neuromuscul Dis. 2015;2(s1):S26.

8. Nikitin SS, Kurbatov SA, Bredelev VA, Kovalchuk MO. Alarming signs and symptoms in the early diagnostics of late onset Pompe disease: super omnia clinica. Zh Nevrol Psikhiatr Im S S Korsakova. 2015;115(12):19-24. doi: 10.17116/jnevro201511511219-24.

9. Diukova GM, Toropina GG, Kovalchuk MO, Semenov RV, Troshneva A. Headaches of tension and psychogenic headaches: assessment of the treatment with venlafaxine. Zh Nevrol Psikhiatr Im S S Korsakova. 2010;110(3):37-41.

10. Pogromov AP, Diukova GM, Kovalchuk MO, Strokov IA, Akhmedzhanova LT, Generozov EV, Markin SS. Familial transthyretin amyloidosis. Klin Med (Mosk). 2009;87(11):67-71.

11. Strokov IA, Diukova GM, Pogromov AP, Generozov EV, Zhadin PM, Kovalchuk MO. Familial amyloid neuropathy associated with the Cys114 mutation of the transthyretin gene in a Russian family. Zh Nevrol Psikhiatr Im S S Korsakova. 2007;107(9):67-72.

Addenda

CURRICULUM VITAE

Maria Kovalchuk was born in Moscow, Russia, 5th of October 1984. She graduated in 2008 from I.M. Sechenov Moscow Medical Academy, scientific faculty with the diploma of medical doctor. During university studies she participated in the lab protocols on neuroimmunochemistry of the V.P. Serbsky State Research Center for social and forensic psychiatry. During her medical studies she accomplished clinical study on the TTR Cys 114 mutation of familial amyloid polyneuropathy in a pair of monozygotic twins. In 2010 she finished her neurology residentship in I.M. Sechenov Moscow Medical Academy, followed by clinical work as a neurologist in the general hospital in Moscow. She got acquainted with excitability technique in 2012 during the department-co-department fellowship, granted by the European Federation of Neurological societies (EFNS), under the supervision of Dr. Hessel Franssen. From August 2014 Maria starts to collect excitability data in healthy subjects in terms of the scientific fellowship on disease mechanisms in multifocal motor neuropathy, sponsored by EFNS, performed in the neuromuscular department of University Medical Center of Utrecht (supervisor – Dr. H. Franssen). Later the research evolved into the current PhD project, supported by the Prinses Beatrix Spierfonds.